Wave Propagation in Solids with Finite Deformation and Finite Strain

By

Deeptesh Selvaraj

Submitted to the Department of Mechanical Engineering and the
Graduate Faculty of the University of Kansas
in partial fulfillment of the requirements for the degree of
Master of Science

Prof. Karan S. Surana, Chairperson

Committee members

Prof. Peter TenPas

Prof. Robert Sorem

Date defended: _____

The Thesis Committee for Deeptesh Selvaraj certifies
that this is the approved version of the following thesis :

Wave Propagation in Solids with Finite
Deformation and Finite Strain

Prof. Karan S. Surana, Chairperson

Date approved: _____

Abstract

This work investigates one dimensional wave propagation in thermoelastic and thermoviscoelastic solids with and without memory. The work considers the solid matter to be compressible with finite deformation and finite strain. The mathematical model utilizes Contravariant second Piola-Kirchhoff stress and Green's strain as work conjugate pair in the conservation and balance laws. For thermoviscoelastic solids the second Piola-Kirchhoff stress is decomposed into equilibrium and deviatoric stress. The constitutive theory for deviatoric stress is expressed in terms of Greens's strain tensor. The thermodynamic pressure in the constitutive theory for equilibrium second Piola-Kirchhoff stress is defined as a function of density using the published experimental data for rubber. In case of thermoelastic solids the constitutive theories consists of total second Piola-Kirchhoff stress as a function of Green's strain tensor. The mathematical model consisting of conservation, balance laws and the constitutive theories are first presented in R^3, then explicitly given in R^1 followed by the dimensionless form in R^1. The nonlinear partial differential equation describing 1D wave propagation for finite deformation and finite strain are numerically solved using space-time finite element method based on space-time residual functional in which the local approximation function for a space-time element are p-version hierarchical with higher order global differentiability in space and time. For an increment of time the solution is computed for a space-time strip and then time marched to obtain the evolution for desired value of time. The solutions computed in the present work are compared with recently published work in which the thermodynamic pressure is approximated by mean normal stress.

Acknowledgements

I would like to thank and express my sincere gratitude to my adviser and committee chair, Dr. Karan S. Surana for his constant support and invaluable guidance. Professor Surana's exhaustive knowledge and enthusiasm for the subject has helped me immensely in successful completion of this work. I would also like to thank Dr. Peter W. Tenpas and Dr. Robert M. Sorem for taking time to serve on my thesis committee and for the guidance offered during my Graduate Teaching Assistant (GTA) assignment.

I would also like to thank the Department of Mechanical Engineering and the Department of Physics and Astronomy for providing me financial assistance during my gradaute studies. The computational infrastructure and the computational resources provided by the Computational Mechanics Laboratory (CML) of the Department of Mechanical Engineering of the University of Kansas is also acknowledged.

Above all, I would like to thank my mother G.Umamageshwari for being a source of inspiration to me.

Contents

List of Figures

Chapter 1

Literature Review and Scope of Work

1.1 Introduction

In the recent paper Surana et al [1] presented comprehensive review of the published work pertinent in context with present work. In the following this literature review of reference [1] is included for completeness. In reference [3] conservation and balance laws are considered and some aspects of the constitutive theories are also discussed with the main objective of obtaining simplified mathematical models with various assumptions that would permit theoretical or semianalytical solutions. Many specialized forms of the 1D and 2D wave equations and their possible solutions are discussed. Reference [4] considers solids under high-pressure shock compression. This book presents many aspects of mechanics, physics, and chemistry in such deformation. Plasticity or irreversible deformation processes are a central point of focus in this reference. The material in the book is largely devoted to experiments, design of experiments, and analysis of experimental data. Experimentally focused work on "nonlinear phenomena in the propagation of elastic waves in solids" is also presented in reference [5]. The authors consider Green's strain and many applications to different and unique materials. Precise mathematical models used and the constitutive theories considered and their derivations are not given. In reference [6], the authors consider a one degree of freedom oscillator subjected to an external force and a restoring viscoelastic force

with memory based on a phenomenological approach. Such models are not valid in the thermodynamic sense and their extension to R^2 and R^3 is not possible [2]. Finite amplitude waves in isotropic elastic plates are considered by Lima and Hamilton [7]. A perturbation technique with semianalytical solution is used to obtain the solutions of the governing equation of equilibrium in Lagrangian description. Periodic harmonic solutions are presented. In reference [8], thermoelastic small-amplitude wave propagation in nonlinear elastic media is considered. Helmholtz free energy density is expressed as a nonlinear function of the principal stretches and is used to derive the constitutive equation for stress. For thermoelastic material based on reference [2], this approach of deriving constitutive theory is unfounded. This approach is applied to layered structures. Lima and Hamilton [9] presented a study of finite amplitude waves in isotropic elastic waveguides with arbitrary cross-sectional area using perturbation and modal analysis techniques to obtain the solutions of nonlinear equations of motion for harmonic motion. The second Piola-Kirchhoff stress tensor is expressed as a quadratic function of the Green's strain tensor using a special form given in references [10, 11]. A study of nonlinear deformation waves in solids and dispersion due to microstructures using Mindlin type model is considered in reference [12]. Finite volume method is used to study propagation and interaction of one dimensional waves. Nonlinear transient thermal stresses and elastic wave propagation studies in thick temperature-gradient dependent FGM cylinder using a second-order point-collocation method are presented in reference [13]. In reference [14], numerical simulations of linear and nonlinear waves in hypoelastic solids is presented using conservation element and solution element method (CESE). These investigations are hypothetical as the constitutive theories for hypoelastic solids are hypothetical since these constitutive theories can not describe the constitution of solids. Numerical simulation of nonlinear elastic wave propagation in piecewise homogeneous media are considered in reference [15]. Wave reflection, transmission, and interaction of waves are not clearly demonstrated primarily due to complexity of the properties of the domain. Vibrations and wave propagation in thick FGM cylinders with temperature dependent material properties is investigated in reference [16]. A nodal discontinuous Galerkin finite element method is considered for nonlinear elastic wave propagation in reference [17]. Nonlinear

transient stress wave propagation in thick FGM cylinder using a unified generalized thermoelasticity theory is considered in reference [18]. Nonlinear constitutive model for axisymmetric bending of annular graphene-like nanoplates with gradient elasticity enhancement effects is considered in reference [19]. In reference [20], nonlinear semianalytical finite-element algorithm for the analysis of internal resonance conditions in complex wave guides is considered. Linear stress waves in elastic medium for infinitesimal deformation linear elasticity have been studied by Surana et al [21]. In [1] authors consider 1D wave propagation in thermoelastic and thermoviscoelastic solids with and without memory for finite deformation and finite strain. In this work the thermodynamic pressure is approximated by mean normal stress. Comprehensive numerical studies are presented for ramp and pulse loadings.

From the brief literature review presented here we note the following. (*i*) The mathematical models resulting from conservation and balance laws are not explicitly defined and stated in most cases. (*ii*) The constitutive theories for thermoelastic and thermoviscoelastic materials with and without memory and the basis for their derivations are mostly absent. In many instances phenomenological approach is used. (*iii*) A mix of various space-time decoupled methods based on finite volume, finite element approaches for discretization in space followed by some time integration scheme are used to obtain evolutions described by the IVPs. In many instances semi-analytical approaches are considered for highy simplified mathematical models that lack the desired physics. (*iv*) In the model problems considered and the numerical studies presented for them, the complexity of the physics of the model problem rarely permits the assesment of the importance of nonlinearity when compared to the corresponding solutions from the linear models. (*v*) The issue of time accuracy of numerical solutions is never addressed in any of the references. This is of utmost significance as only with the correct time evolution can we assess the importance and significance of the nonlinear wave propagation.

1.2 Considerations in the Present Study and the Scope of Study

The current work considers 1D wave propagation in thermoelastic and thermoviscoelastic solids with and without memory for finite deformation and finite strain as in reference [1], but the thermodynamic pressure approximated by mean normal stress in [1] is replaced by actual equation of state for soft rubber [35]. Thermodynamic pressure is expressed as a fifth degree algebraic polynomial in density using experimental data in [35]. Dependence of the thermodynamic pressure on temperature is not considered as the boundaries are considered to be insulated, hence the only entropy production is due to dissipation that results in very small temperature rise, not sufficient to influence thermodynamic pressure. The main objective of this work is to study 1D wave propagation in solid media in which compressibility is accounted for in a consistent manner through actual equation of state and show comparisons with results in reference [1] in which the equation of state is approximated.

Chapter 2

Mathematical Models and Computational Method

The conservation and balance laws for solids with finite deformation and finite strain have been derived and can be found in reference [1]. It is shown that consideration of finite deformation and finite strain requires use of contravariant second Piola-Kirchhoff stress ($\boldsymbol{\sigma}^{[0]}$) and its work conjugate Green's Strain tensor ($\boldsymbol{\varepsilon}_{[0]}$) in the derivation of conservation and balance laws. In case of thermoelastic solids the energy equation is a heat conduction equation and the constitutive theory for total second Piola-Kirchhoff stress tensor is derived in terms of Green's strain tensor. For thermoelastic solids the mechanical rate of work does not result in rate of entropy production. In case of the thermoviscoelastic solids with or without memory the rate of mechanical work results in rate of entropy production. This requires decomposition of second Piola-Kirchhoff stress tensor into equilibrium second Piola-Kirchhoff stress tensor ($[{}_{\boldsymbol{e}}\boldsymbol{\sigma}^{[0]}]$) and the deviatoric second Piola-Kirchhoff stress tensor ($[{}_{\boldsymbol{d}}\boldsymbol{\sigma}^{[0]}]$). The constitutive theory for deviatoric second Piola-Kirchhoff stress tensor is derived in terms of $[\boldsymbol{\varepsilon}_{[0]}]$ and the rate of $\boldsymbol{\varepsilon}_{[0]}$ i.e, $\boldsymbol{\varepsilon}_{[1]}$ while the constitutive theory for $[{}_{\boldsymbol{e}}\boldsymbol{\sigma}^{[0]}]$ requires thermodynamic pressure using equation of state. For thermoviscoelastic solids with memory also we perform stress decomposition of $[\boldsymbol{\sigma}^{[0]}]$ into $[{}_{\boldsymbol{e}}\boldsymbol{\sigma}^{[0]}]$ and $[{}_{\boldsymbol{d}}\boldsymbol{\sigma}^{[0]}]$. The Constitutive theory for $[{}_{\boldsymbol{d}}\boldsymbol{\sigma}^{[0]}]$ is a rate equation that requires use of $[{}_{\boldsymbol{d}}\boldsymbol{\sigma}^{[0]}]$, $[{}_{\boldsymbol{d}}\boldsymbol{\sigma}^{[1]}]$, $[\boldsymbol{\varepsilon}_{[0]}]$ and $[\boldsymbol{\varepsilon}_{[1]}]$. $[{}_{\boldsymbol{d}}\boldsymbol{\sigma}^{[1]}]$ and

$[\boldsymbol{\varepsilon}_{[1]}]$ are rates or material derivative of $[{}_{\boldsymbol{d}}\boldsymbol{\sigma}^{[0]}]$ and $[\boldsymbol{\varepsilon}_{[0]}]$. The constitutive theory for $[{}_{\boldsymbol{e}}\boldsymbol{\sigma}^{[0]}]$ remains same as in case of thermoviscoelastic solids without memory. Fourier heat conduction law with constant thermal conductivity is used in all cases.

2.1 Mathematical Models in $\mathbf{R}^3$

Following [1], we can write the following for the conservation and balance laws and the constitutive theories (assuming absence of sources and sinks) in Lagrangian description. TE and TVE refer to thermoelastic and thermoviscoelastic materials. Following [1], we can write the following for the conservation and balance laws and the constitutive theories (assuming absence of sources and sinks) in Lagrangian description. TE and TVE refer to thermoelastic and thermoviscoelastic materials.

Continuity:
$$\rho_0 = |J|\rho(\boldsymbol{x},t) \tag{2.1}$$

Linear momenta:
$$\rho_0\{\ddot{u}\} - ([J][\sigma^{[0]}]^T)\{\nabla\} = 0 \tag{2.2}$$

Angular momenta:
$$[\sigma^{[0]}] = [\sigma^{[0]}]^T \tag{2.3}$$

where,
$$[J] = \left[\frac{\partial \bar{x}}{\partial x}\right]; \quad \{v\} = \{\dot{u}\}$$

Energy equation:

$$\left.\begin{array}{ll} \rho_0 \frac{\partial e}{\partial t} + \{\nabla\}^T\{q\} = 0; & \text{TE} \\ \rho_0 \frac{\partial e}{\partial t} + \{\nabla\}^T\{q\} - tr([\sigma^{[0]}]^T[\dot{\varepsilon}_{[0]}]^T) = 0; & \text{TVE with and without memory} \end{array}\right\} \tag{2.4}$$

Constitutive theories:

$$\left.\begin{aligned} [\sigma^{[0]}] &= 2\mu[\varepsilon_{[0]}] + \lambda(tr[\varepsilon_{[0]}])[I]; \qquad \text{TE} \\ \left[\sigma^{[0]}\right] &= [{}_e\sigma^{[0]}] + [{}_d\sigma^{[0]}]; \qquad \text{TVE with and without memory} \end{aligned}\right\} \tag{2.5}$$

where

$$[{}_e\sigma^{[0]}] = -p(\rho,\theta)|J|[J]^T[J]^{-1} \tag{2.6}$$

$$\left.\begin{aligned} &\left[{}_d\sigma^{[0]}\right] = 2\underset{\sim}{\mu}[\varepsilon_{[0]}] + \underset{\sim}{\lambda}(tr[\varepsilon_{[0]}])[I] + 2\underset{\sim}{\mu}_1[\boldsymbol{\varepsilon}_{[1]}] + \underset{\sim}{\lambda}_1(tr[\boldsymbol{\varepsilon}_{[1]}])[I]; \quad \text{TVE, no memory} \\ &\left[{}_d\sigma^{[0]}\right] + \lambda_1\left[{}_d\sigma^{[1]}\right] = \\ &\qquad 2\mu_1[\varepsilon_{[0]}] + \lambda_1(tr[\varepsilon_{[0]}])[I] + 2\underline{\mu}_1[\boldsymbol{\varepsilon}_{[1]}] + \underline{\lambda}_1(tr[\boldsymbol{\varepsilon}_{[1]}])[I]; \quad \text{TVE, with memory} \end{aligned}\right\} \tag{2.7}$$

In which ρ and ρ_o are densities in the current and reference configuration, x and $\bar{x}$ are material point co-ordinates in reference and current configuration, $\boldsymbol{v}$ are velocities, [J] is Jacobian of deformation, ∇ is gradient vector, $\boldsymbol{u}$ and $\dot{\boldsymbol{u}}$ are displacements and their material derivative and e is specific internal energy, q is heat vector, μ and λ are material constants for thermoelastic solid, $\underset{\sim}{\mu}$, $\underset{\sim}{\lambda}$, $\underset{\sim}{\mu}_1$, $\underset{\sim}{\lambda}_1$ are material co-efficients for thermoviscoelastic solid without memory and λ_1, μ_1, $\underline{\mu}_1$, $\underline{\lambda}_1$, are material co-efficients for thermoelastic solid with memory, λ_1 is relaxation time for thermoviscoelastic solid with memory, k is co-efficients of thermalconductivity and θ is absolute temperature, $p(\rho,\theta)$ is the thermodynamic pressure and is assumed to be positive when compressive. Thermodynamic pressure is generally a function of ρ and θ.

Equation of State:

Equation of state defines thermodynamic pressure p as a function of density ρ and temperature θ. In the present 1D numerical studies the rod is assumed completely insulated, hence the temperature change is purely due to dissipation i.e, rate of entropy generation is due to rate of work, thus may not be significant to influence thermodynamic pressure. In the present work we consider the

following for equation of state [35]

$$p = \tilde{c}_0 + \tilde{c}_1\rho + \tilde{c}_2(\rho)^2 + \tilde{c}_3(\rho)^3 + \tilde{c}_4(\rho)^4 + \tilde{c}_5(\rho)^5 \tag{2.8}$$

which is a fifth degree polynomial in ρ. This relationship is a curve fit to the experimental data for hard rubber [35]. In equation (2.8) quatities have their usual dimensions. In all numerical studies we refer to the thermodynamic pressure p in (2.8) by abreviation TP. In the experimental work, hard rubber was tested in tension yielding pressure values upto $3 \times 10^7\ N/m^2$ that results in almost 80% reduction in density (as shown in figure 2.1). In the numerical studies presented in this paper the p versus ρ equation of state (2.8) is also used in compression. Figure 2.1 also shows p versus ρ graph in compression obtatined using (2.8). In many applications involving hard rubber or such

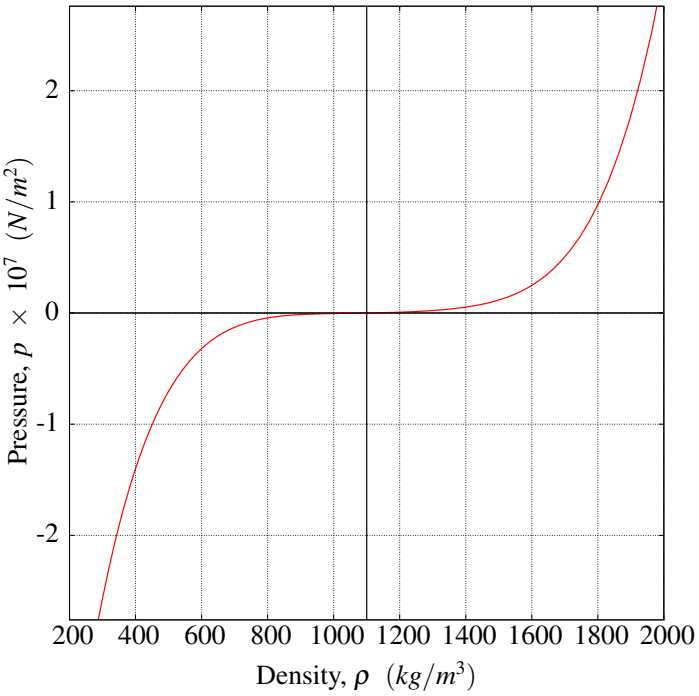

Figure 2.1: Pressure versus Density

other solids, $p = p(\rho)$ or $p = p(\rho, \theta)$ may require elaborate experimental work to determine. In such cases mean normal stress (mechanical pressure) is used as an approximation to the equation

of state. That is we use the following [2],

$$p = \frac{1}{3}\sigma_{ii}^{(0)}; \qquad \text{Mechanical pressure (MP)} \tag{2.9}$$

with $\boldsymbol{\sigma^{(0)}}$ being contravariant cauchy stress. Using

$$\left[{}_d\sigma^{(0)}\right] = \left[\sigma^{(0)}\right] - p\,[I] \tag{2.10}$$

equation (2.9) reduces to

$${}_d\sigma_{ii}^{(0)} = 0 \tag{2.11}$$

quation (2.9) is obviously an approximation to the actual equation of state. More specifically it is based on incompressibilty assumption. Thus comparing results using (2.8) and (2.9) will be meaningful to determine deviation in result caused due to assumption of (2.9) for thermodynamic pressure. We refer to equation of state (2.9) in numerical studies by "MP" mechanical pressure.

2.2 Mathematical Models in $\mathbf{R}^1$

The mathematical models in R^1 is directly deduced from the mathematical model in R^3, but keeping in mind that in R^1 the other two dimension do not exist. Secondly the mathematical model in R^1 presented here incorporates some factors with values of 1 or 0 inorder to conveniently use the same mathematical model for infinitesimal deformation and strain as well as for finite deformation and finite strain. The conservation and balance laws in R^1 can be written as (in the absence of body forces and other sources and sinks) we assume the system (rod) to be insulated. Hence when we consider the thermoelastic matter, the energy equation is not required.

Continuity: $$\rho_0 = \left(1 + f\frac{\partial u}{\partial x}\right)\rho(\boldsymbol{x},t) \tag{2.12}$$

Linear momenta: $$\rho_0\frac{\partial^2 u}{\partial t^2} - \frac{\partial}{\partial x}\left((1 + f\frac{\partial u}{\partial x})\sigma_{xx}^{[0]}\right) = 0 \tag{2.13}$$

Energy Equation: $$\rho c_{p_0}\frac{\partial \theta}{\partial t} + \frac{\partial q}{\partial x} - {}_d\sigma_{xx}^{[0]}\left(\dot{\varepsilon}_{[0]}\right)_{xx} = 0 \tag{2.14}$$

Constitutive theories:

Thermoelastic ; $$\sigma_{xx}^{[0]} = E(\varepsilon_{[0]})_{xx} \tag{2.15}$$

TVE with or without memory ; $$\sigma_{xx}^{[0]} = ({}_e\sigma_{xx}^{[0]} + {}_d\,\sigma_{xx}^{[0]}) \tag{2.16}$$

TVE with or without memory ; $${}_e\sigma_{xx}^{[0]} = -p(\rho)\left(1 + f\frac{\partial u}{\partial x}\right) \tag{2.17}$$

TVE, no memory ; $${}_d\sigma_{xx}^{[0]} = {}^d\underset{\sim}{E}(\varepsilon_{[0]})_{xx} + {}^d\underset{\sim}{c}(\dot{\varepsilon}_{[0]})_{xx} \tag{2.18}$$

TVE, with memory ; $${}_d\sigma_{xx}^{[0]} + \lambda\frac{\partial {}_d\sigma_{xx}^{[0]}}{\partial t} = {}^d\underset{\sim}{E}(\varepsilon_{[0]})_{xx} + {}^d\underset{\sim}{c}(\dot{\varepsilon}_{[0]})_{xx} \tag{2.19}$$

TVE with and without memory ; $$q = -k\frac{\partial \theta}{\partial x} \tag{2.20}$$

in which, $$(\varepsilon_{[0]})_{xx} = \frac{\partial u}{\partial x} + f\frac{1}{2}\left(\frac{\partial u}{\partial x}\right)^2 \tag{2.21}$$

$$\left(\dot{\varepsilon}_{[0]}\right)_{xx} = \frac{\partial (\varepsilon_{[0]})_{xx}}{\partial t} \tag{2.22}$$

and $$J = 1 + f\frac{\partial u}{\partial x} \quad ; \quad \text{Jacobian of deformation} \tag{2.23}$$

In the energy equation. we have used $e(x,t) = c_{p_0}\theta(x,t)$. The factor f takes on values of zero for small deformation and small strain and a value of one for finite deformation and finite strain. Equation of state remains the same for thermodynamic pressure (TP) and mechanical pressure (MP) as described by (2.8) and (2.9) respectively

Remarks:

The mathematical model of thermoelastic solids ((2.12), (2.13) and (2.15)) can also be expressed using ${}_d\sigma_{xx}^{[0]}$,

$$ {}_d\sigma_{xx}^{[0]} = \sigma_{xx}^{[0]} - \frac{\sigma_{xx}^{[0]}}{3} = \frac{2}{3}\sigma_{xx}^{[0]} \tag{2.24} $$

or

$$ \sigma_{xx}^{[0]} = \frac{3}{2}{}_d\sigma_{xx}^{[0]} \tag{2.25} $$

using 2.25 in 2.13 and 2.15 we obtain,

$$ \rho_0 = \left(f\frac{\partial u}{\partial x} + 1 \right) \rho(x,t) \tag{2.26} $$

$$ \rho_0 \frac{\partial^2 u}{\partial t^2} - \frac{3}{2}\frac{\partial}{\partial x}\left((1 + f\frac{\partial u}{\partial x}\ ) {}_d\sigma_{xx}^{[0]} \right) = 0 \tag{2.27} $$

$$ {}_d\sigma_{xx}^{[0]} = \frac{2}{3}E(\varepsilon_{[0]})_{xx} \tag{2.28} $$

However, we note for Thermoviscoelastic solids with and without memory (2.24) does not hold as in this case

$$ {}_d\sigma_{xx}^{[0]} = \sigma_{xx}^{[0]} - {}_e\sigma_{xx}^{[0]} \tag{2.29} $$

and ${}_e\sigma_{xx}^{[0]}$ is given by (2.17) that requires thermodynamic pressure $p(\rho)$.

2.3 Dimensionless forms of Mathematical Models in $\mathbf{R}^1$

We present the dimensionless forms of the mathematical models given in sections 2.2 by choosing appropriate reference quantities. We consider the mathematical models derived in sections 2.2 and introduce hat ($\hat{}$) i.e. x changes to $\hat{x}$, t to $\hat{t}$, θ to $\hat{\theta}$, etc. This implies that all quantities with hat have their usual dimensions or units in terms of force ($\hat{F}$), length ($\hat{L}$), and time ($\hat{t}$). Next we choose

a reference value of force (F_0), length (L_0), and time (t_0) which would yield dimensionless force (F), length (L), and time (t), the quantities without hat $(\hat{})$, as $F = \frac{\hat{F}}{F_0}$, $L = \frac{\hat{L}}{L_0}$, and $t = \frac{\hat{t}}{t_0}$. This is a general process of non-dimensionalizing. Additionally, we may have to choose other reference quantities too, for example, θ_0 for temperature $\hat{\theta}$ so that we can obtain dimensionless temperature $\theta = \frac{\hat{\theta}}{\theta_0}$. For wave propagation the reference speed of sound is a good choice for reference velocity (v_0). If we choose L_0 as reference length then with v_0 and L_0, reference time $t_0 = \frac{L_0}{v_0}$, i.e. t_0 can not be independent of L_0 and v_0. We consider the following reference quantities, the resulting dimensionless variables, and the dimensionless parameters.

$$\left.\begin{gathered}
x = \frac{\hat{x}}{L_0}, \quad \rho_0 = \frac{\hat{\rho}}{\tilde{\rho}_0}, \quad c_{p0} = \frac{\hat{c}_p}{\tilde{c}_{p0}}, \quad u = \frac{\hat{u}}{L_0}, \quad k = \frac{\hat{k}}{k_0} \\
{}_d\boldsymbol{\sigma}_{xx}^{[0]} = \frac{{}_d\hat{\sigma}_{xx}^{[0]}}{\tau_0}, \quad {}_e\boldsymbol{\sigma}_{xx}^{[0]} = \frac{{}_e\hat{\sigma}_{xx}^{[0]}}{\tau_0}, \quad \boldsymbol{\sigma}_{xx}^{[0]} = \frac{\hat{\sigma}_{xx}^{[0]}}{\tau_0}, \\
E = \frac{\hat{E}}{E_0}, \quad v_0 = \sqrt{\frac{E_0}{\tilde{\rho}_0}} \quad \text{(reference speed of sound)} \\
\tau_0 = E_0 = \tilde{\rho}_0 v_0^2 \quad \text{(characteristic kinetic energy)} \\
t_0 = \frac{L_0}{v_0}, \quad \theta = \frac{\hat{\theta}}{\theta_0} \\
\tilde{\rho}_0 \ \text{ and } \ \tilde{c}_{p_0} \ \text{ are reference values of density and specific heat} \\
{}^d\underset{\sim}{\hat{E}} = \frac{{}^d\underset{\sim}{E}}{E_0} \qquad ; \quad p = \frac{\hat{p}}{\tau_0}
\end{gathered}\right\} \tag{2.30}$$

Using (2.30) , mathematical models in ((2.1) to (2.29)) can be nondimensionalized. The dimensionless form of these are given in the following,

Continuity: $$\rho_0 = \left(1 + f\frac{\partial u}{\partial x}\right)\rho(\boldsymbol{x},t) \tag{2.31}$$

Linear momenta: $$\rho_0\frac{\partial^2 u}{\partial t^2} - \left(\frac{\tau_0}{(\tilde{\rho}_0 v_0^2)}\right)\frac{\partial}{\partial x}\left((1+f\frac{\partial u}{\partial x})\sigma_{xx}^{[0]}\right) = 0 \tag{2.32}$$

Energy Equation: $$\rho_0 c_{p_0}\frac{\partial \theta}{\partial t} + \left(\frac{k_0 t_0}{\tilde{\rho}_0 L_0^2 \tilde{c}_{p0}}\right)\frac{\partial q}{\partial x} - \left(\frac{\tau_0}{\tilde{\rho}_0 \tilde{c}_{p0}\theta_0}\right){}_d\sigma_{xx}^{[0]}\left(\dot{\varepsilon}_{[0]}\right)_{xx} = 0 \tag{2.33}$$

Constitutive theories: $$\sigma_{xx}^{[0]} = E(\varepsilon_{[0]})_{xx} \quad ; \quad \text{Thermoelastic} \tag{2.34}$$

$$\sigma_{xx}^{[0]} = ({}_e\sigma_{xx}^{[0]} + {}_d\sigma_{xx}^{[0]}) \quad ; \quad \text{TVE with or without memory} \tag{2.35}$$

$${}_e\sigma_{xx}^{[0]} = -p(\rho)\left(1 + f\frac{\partial u}{\partial x}\right); \quad \text{TVE with or without memory} \tag{2.36}$$

$${}_d\sigma_{xx}^{[0]} = \left(\frac{E_0}{\tau_0}\right){}^d\underset{\sim}{E}(\varepsilon_{[0]})_{xx} + {}^d\underset{\sim}{C}(\dot{\varepsilon}_{[0]})_{xx} \;\; ; {}^d\underset{\sim}{C} = \left(\frac{{}^d\hat{\underset{\sim}{C}}}{\tau_0 t_0}\right); \quad \text{TVE, no memory} \tag{2.37}$$

$${}_d\sigma_{xx}^{[0]} + De\frac{\partial\, {}_d\sigma_{xx}^{[0]}}{\partial t} = \left(\frac{E_0}{\tau_0}\right){}^d\underset{\sim}{E}(\varepsilon_{[0]})_{xx} + {}^d\underset{\sim}{C}(\dot{\varepsilon}_{[0]})_{xx} \quad ; \quad \text{TVE, with memory} \tag{2.38}$$

$$q = -k\frac{\partial \theta}{\partial x} \quad ; \quad \text{TVE with and without memory} \tag{2.39}$$

$$p = c_0 + c_1\rho + c_2(\rho)^2 + c_3(\rho)^3 + c_4(\rho)^4 + c_5(\rho)^5 \quad \text{TVE with or without memory} \tag{2.40}$$

In which,

$$\left.\begin{aligned} D_e = \frac{\lambda}{t_0} \quad , \quad c_0 = \left(\frac{\tilde{c}_0}{\tau_0}\right) \quad , \quad c_1 = \left(\frac{\tilde{c}_1\tilde{\rho}_0}{\tau_0}\right) \quad , \quad c_2 = \left(\frac{\tilde{c}_2{\tilde{\rho}_0}^2}{\tau_0}\right) \\ c_3 = \left(\frac{\tilde{c}_3{\tilde{\rho}_0}^3}{\tau_0}\right) \quad , \quad c_4 = \left(\frac{\tilde{c}_4{\tilde{\rho}_0}^4}{\tau_0}\right) \quad , \quad c_5 = \left(\frac{\tilde{c}_5{\tilde{\rho}_0}^5}{\tau_0}\right) \end{aligned}\right\} \tag{2.41}$$

Figure 2.2 shows a graph of dimensionless p versus dimensionless ρ that precisely corresponds

to p versus ρ graph of figure 2.1 in which p and ρ have their usual dimensions. Once again here also the p versus ρ in compression is generated using (2.40)

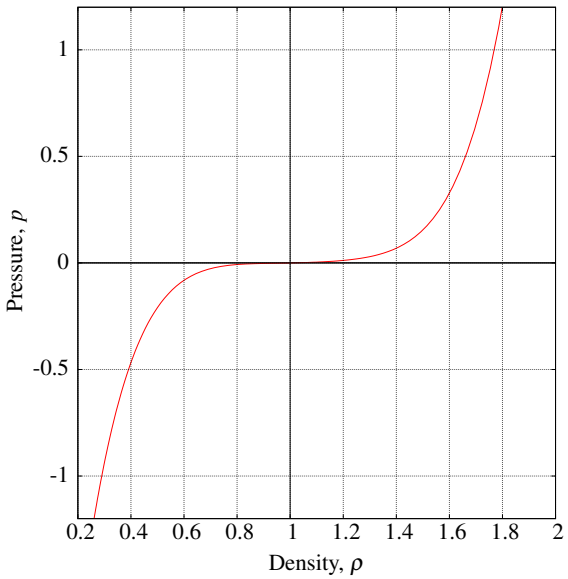

Figure 2.2: Dimensionless Pressure versus Density

2.4 Computational Framework for Numerical Simulation of Evolution

For the sake of simplicity, we consider mathematical models in R^1 describing one-dimensional wave propagation in thermoelastic and thermoviscoelastic media with and without memory. This choice is due to simplicity of physics so that the significant and subtle features of linear and non-linear wave propagation can be clearly demonstrated. Thus the mathematical models in section 2.2 (R^1) contain x and t as independent coordinates. All three mathematical modes in section 2.2 can be arranged in the following compact form.

$$\boldsymbol{A\phi} - \boldsymbol{f} = 0 \quad \forall\, (x,t) \;\in\; \Omega_{xt} = \Omega_x \times \Omega_t = (0,L) \times (0,\tau) \tag{2.42}$$

or

$$\sum_{j}^{m} A_{ij}\phi_j - f_i = 0; \quad i = 1,2,\cdots,m \quad \forall\,(x,t)\ \in\ \Omega_{xt} \tag{2.43}$$

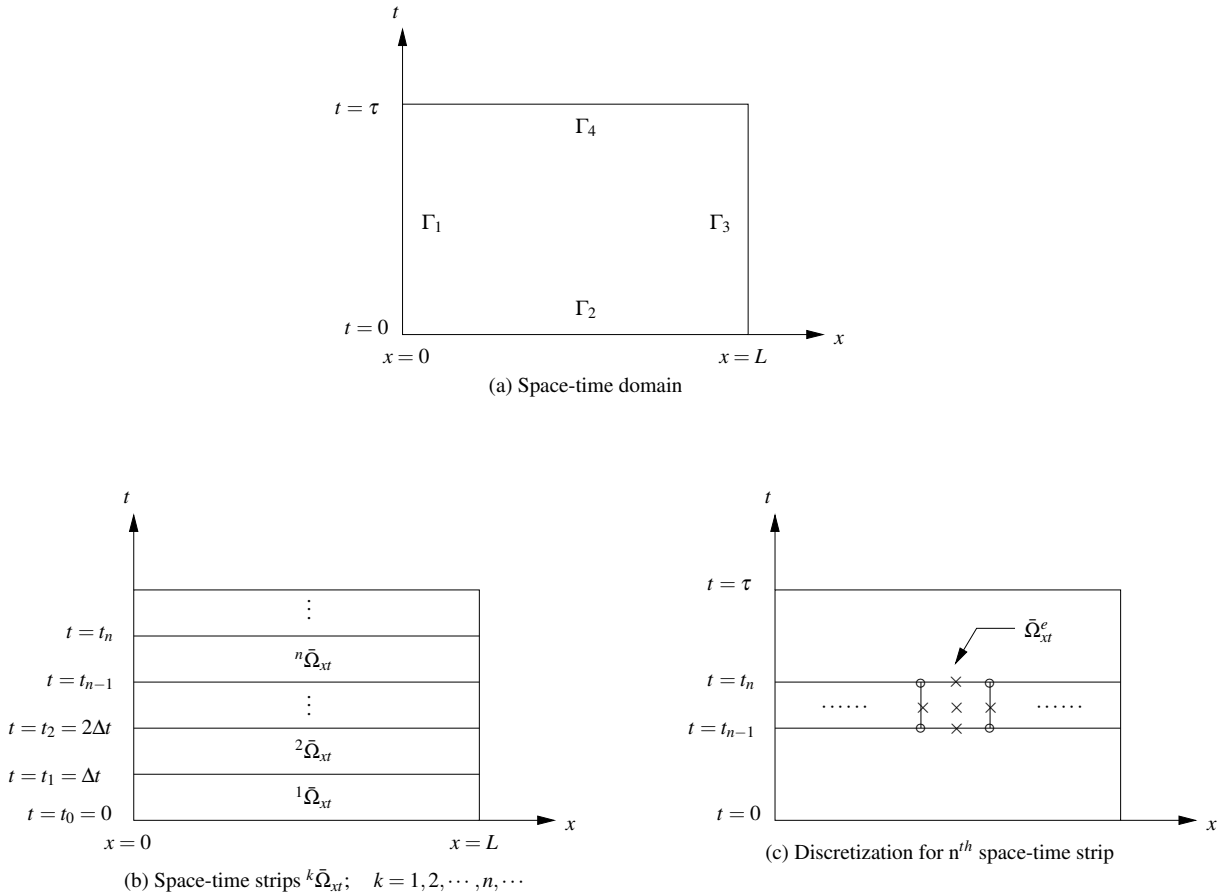

Figure 2.3: Space-Time Domain, Space-Time Strips, and Discretization for nth Space-Time Strip. (a) Space-time domain; (b) Space-Time strips ${}^{k}\overline{\Omega}^{T}_{xt}$; k=1,2,$\cdots$,n,$\cdots$; (c) Discretization for n^{th} space-time strip.

Equations (2.42) or (2.43) are a system of m partial differential equations. In (2.42), matrix $\boldsymbol{A}$ contains the differential operators, $\boldsymbol{\phi}$ is a vector of dependent variables, and $\boldsymbol{f}$ is a vector containing nonhomogeneous terms. In (2.42), Ω_{xt} is the open space-time domain such that $\bar{\Omega}_{xt} = \Omega_{xt} \bigcup \Gamma$, $\bar{\Omega}_{xt}$ being closure of Ω_{xt} and Γ being the closed boundary of Ω_{xt}. Additionally, the following holds (figure 2.3), $\bar{\Omega}_x = \Omega_x \bigcup \Gamma_x$ and $\bar{\Omega}_t = \Omega_t \bigcup \Gamma_t$ such that $\Gamma = \Gamma_x \bigcup \Gamma_t$. For simplicity, we consider

$\Gamma = \bigcup_{i=1}^{4} \Gamma_i$ as shown in figure 2.3(a). Figure 2.3(b) shows a subdivision of the space-time domain $\bar{\Omega}_{xt}$ into space-time strips such that

$$\bar{\Omega}_{xt} = \bigcup_{n} {}^{n}\bar{\Omega}_{xt} \quad \forall\ (x,t)\ \in\ {}^{n}\bar{\Omega}_{xt} = \bar{\Omega}_x \times {}^{n}\bar{\Omega}_t = [0,L] \times [t_{n-1}, t_n] \tag{2.44}$$

The nth space-time strip, with domain ${}^{n}\bar{\Omega}_{xt}$, is from time t_{n-1} to t_n over the spatial domain $[0,L]$. The time interval Δt for the strips need not be uniform (but assumed so here for simplicity). Consider the nth space-time strip ${}^{n}\bar{\Omega}_{xt}$ and its discretization ${}^{n}\bar{\Omega}^{T}_{xt}$ into space-time elements

$${}^{n}\bar{\Omega}^{T}_{xt} = \bigcup_{e} \bar{\Omega}^{e}_{xt} \tag{2.45}$$

in which $\bar{\Omega}^{e}_{xt}$ is the space-time domain of a space-time element, e (figure 2.3(c)), a nine node space-time p-version element. Consider the nth space-time strip with its space-time domain ${}^{n}\bar{\Omega}_{xt}$ and its discretization ${}^{n}\bar{\Omega}^{T}_{xt}$. Let ${}^{n}_{i}\phi_h;\ i = 1,2,\cdots,m$ be the approximations of $\phi_i;\ i = 1,2,\cdots,m$ over ${}^{n}\bar{\Omega}^{T}_{xt}$ and let ${}^{n}_{i}\phi^{e}_{h}$ be the local approximation of ϕ_i over a space-time element $\bar{\Omega}^{e}_{xt}$ such that

$${}^{n}_{i}\phi_h = \bigcup_{e} ({}^{n}_{i}\phi^{e}_{h});\ i = 1,2,\cdots,m \tag{2.46}$$

If we substitute ${}^{n}_{j}\phi_h$ in (2.43), then we obtain the residual functions (equations), $E_i = i = 1,2,\cdots,m$, for the nth space-time strip.

$$E_i = A_{ij}({}^{n}_{j}\phi_h) - f_i;\ i = 1,2,\cdots,m \tag{2.47}$$

On the other hand, if we substitute ${}^{n}_{i}\phi^{e}_{h}$ in (2.43), we obtain residual equations, E^{e}_{i}, for a space-time element e.

$$E^{e}_{i} = A_{ij}({}^{n}_{i}\phi^{e}_{h}) - f_i;\ i = 1,2,\cdots,m \tag{2.48}$$

We consider the space-time finite element method based on residual functional (space-time least squares method). See references [22]- [31] for more details. Let ${}^nI$ be the residual functional for the discretization of the nth space-time strip defined by the sum of the scalar products of E_i with itself over ${}^n\bar{\Omega}_{xt}^T$.

$$ {}^nI = \sum_{i=1}^{m} (E_i, E_i)_{{}^n\bar{\Omega}_{xt}^T} \tag{2.49} $$

Since $(E_i, E_i)_{{}^n\bar{\Omega}_{xt}^T}$ is a functional, (2.49) can be written in terms of the sum of element residuals, i.e.

$$ {}^nI = \sum_{i} (E_i, E_i)_{{}^n\bar{\Omega}_{xt}^T} = \sum_{e} \left(\sum_{i} (E_i^e, E_i^e)_{\bar{\Omega}_{xt}^e} \right) = \sum_{e} I^e \tag{2.50} $$

Based on the calculus of variations [22], an extremum of the functional ${}^nI$ is also a solution of the associated Euler's equations (partial differential equations in the mathematical models). An extremum of ${}^nI$ requires that we set its first variation, $\delta({}^nI)$, to zero, a necessary condition, provided ${}^nI$ is differentiable in its arguments.

$$ \delta({}^nI) = \sum_{e} \delta I^e = 2 \sum_{e} \left(\sum_{i} (E_i^e, \delta E_i^e)_{\bar{\Omega}_{xt}^e} \right) = 2 \sum_{e} \{g^e\} = 2\{g\} = 0 \tag{2.51} $$

Thus, $\{g\} = 0$ is a necessary condition for an extremum of functional ${}^nI$. The sufficient condition, or extremum principle, is given by

$$ \delta^2({}^nI) = 2 \sum_{e} \left(\sum_{i} \left((\delta E_i^e, \delta E_i^e)_{\bar{\Omega}_{xt}^e} + (E_i^e, \delta^2 E_i^e)_{\bar{\Omega}_{xt}^e} \right) \right) \tag{2.52} $$

In ((2.52), $\delta^2({}^nI) \; > 0, = 0, < 0$, ensures a minimum, a saddle point, or a maximum, respectively, of ${}^nI$ for the solution ${}_i^n\phi_h$ obtained from (2.51)). Equation (2.52)) is clearly not an extremum principle. Following [22]- [31], we approximate (2.52) to obtain a unique extremum principle.

$$ \delta^2({}^nI) \cong 2 \sum_{e} \left(\sum_{i} (\delta E_i^e, \delta E_i^e)_{\bar{\Omega}_{xt}^e} \right) > 0 \tag{2.53} $$

This is a unique extremum principle (see reference [22] for details). Since some of the equations in the mathematical model are nonlinear, some E_i^e are nonlinear functions of the depen-

dent variables. That is $\{g\}$ in (2.51) is a nonlinear function. Consider the local approximations ${}^{n}_{i}\phi^{e}_{n} \in V_n \subset H^{k,p}(\bar{\Omega}^{e}_{xt})$ in which $k = (k_1, k_2)$, k_1 and k_2 being the orders of the scalar product space $H^{k,p}(\bar{\Omega}^{e}_{xt})$ in space and time. Consider the local approximations of ϕ_i over $\bar{\Omega}^{e}_{xt}$

$$ {}^{n}_{i}\phi^{e}_{h} = [N^i]\{{}_i\delta^e\};\ i = 1, 2, \cdots, m \tag{2.54} $$

in which $[N^i]$ are space-time local approximation functions and $\{{}_i\delta^e\}$ are nodal degrees of freedom for a dependent variable ϕ_i. Let $\{\delta^e\}^T = [\{{}_1\delta^e\}^T,\ \{{}_2\delta^e\}^T,\ \cdots,\{{}_m\delta^e\}^T]$ be the total degrees of freedom for all of the dependent variables ϕ_i for an element, e. Therefore, the total degrees of freedom $\{\delta\}$ for the discretization ${}^{n}\bar{\Omega}^{T}_{xt}$ can be written as

$$ \{\delta\} = \bigcup_{e} \{\delta^e\} \tag{2.55} $$

With (2.54) and (2.55), $\{g\}$ in (2.51) is a nonlinear function of $\{\delta\}$, hence the necessary condition $\{g\} = 0$ must be satisfied iteratively. We consider Newton's linear method. Let $\{\delta_0\}$ be an assumed solution (a starting solution), then

$$ \{g(\{\delta_0\})\} \neq 0 \tag{2.56} $$

Let $\{\Delta\delta\}$ be a change in $\{\delta_0\}$ such that

$$ \{g(\{\delta_0\} + \{\Delta\delta\})\} = 0 \tag{2.57} $$

We expand $\{g\}$ in (2.57) in a Taylor series about $\{\delta_0\}$ and retain only up to linear terms in $\{\Delta\delta\}$.

$$ \{g(\{\delta_0\} + \{\Delta\delta\})\} \cong \{g(\{\delta_0\})\} + \left.\frac{\partial\{g\}}{\partial\{\delta\}}\right|_{\{\delta_0\}} \{\Delta\delta\} = 0 \tag{2.58} $$

Then

$$ \{\Delta\delta\} = -\left[\frac{\partial\{g\}}{\partial\{\delta\}}\right]^{-1}_{\{\delta_0\}} \{g(\{\delta_0\})\} \tag{2.59} $$

An improved solution, $\{\delta\}$, is obtained using

$$\{\delta\} = \{\delta_0\} + \alpha\{\Delta\delta\};\ 0 \le \alpha \le 2 \quad \text{such that } {}^{n}I(\{\delta\}) \le {}^{n}I(\{\delta_0\}) \tag{2.60}$$

Use of α in (2.60) is called line search [22]- [31]. Using $\{\delta\}$ in (2.60), we check if the absolute value of each component of $\{g(\{\delta\})\}$ is less than or equal to Δ, (generally 10^{-6} or lower) a preset tolerance for computed zero. If this condition is satisfied by $\{\delta\}$ in (2.60), then we have a converged solution $\{\delta\}$ from Newton's linear method, otherwise we set $\{\delta_0\}$ to be $\{\delta\}$ and repeat (another iteration) the calculations described above. It is worth noting that

$$\frac{\partial\{g\}}{\partial\{\delta\}} = \frac{1}{2}\delta^2 I \tag{2.61}$$

which when approximated using (2.53)) gives a positive definite coefficient matrix due to the fact that $\delta^2 I > 0$. Thus, we can rewrite (2.59) as

$$\{\Delta\delta\} = -\frac{1}{2}[\delta^2 I]^{-1}_{\{\delta_0\}}\{g(\{\delta_0\})\} \tag{2.62}$$

$$\delta^2 I = \sum_e \left(\sum_i (\delta E_i^e, \delta E_i^e)_{\bar{\Omega}^e_{xt}} \right) = \sum_e [K^e] \tag{2.63}$$

in which $[K^e]$ is the element coefficient matrix and $[\delta^2 I]$ in (2.60)) are the assembled element equations for the discretization ${}^{n}\bar{\Omega}^T_{xt}$. Likewise, the following holds

$$\{g\} = \sum_e \{g^e\}; \quad \{g^e\} = \sum_i (E_i^e, \delta E_i^e) \tag{2.64}$$

2.4.1 Time Marching Procedure: Computations of Evolution

We initiate computations with the first space-time strip shown in figure 2.4 with boundary conditions on two boundaries and initial conditions at time $t = 0$, the boundary at $t = \Delta t$ being the

open boundary where nothing is known about the solution. With proper choice of discretization, p-level, and minimally conforming space choice [22]- [31], the integrated sum of squares of the residuals ${}^1I$ for the first space-time strip are achieved to be less than or equal to $O(10^{-6})$. With the minimally conforming choice of k, the orders k_1 and k_2 of the approximation space in space and time, the space-time integrals are Riemann over ${}^n\bar{\Omega}_{xt}^T$, hence ${}^1I$ of the order of $O(10^{-6})$ or lower indicates that the GDEs are satisfied accurately in the pointwise sense over ${}^1\bar{\Omega}_{xt}^T$ [22]- [31]. Upon obtaining an accurate solution for ${}^1\bar{\Omega}_{xt}^T$ the computations are initiated for ${}^2\bar{\Omega}_{xt}^T$ keeping the same p-levels, same values of k, and the same discretization as used for ${}^1\bar{\Omega}_{xt}^T$. For the second space-time strip, ${}^2\bar{\Omega}_{xt}^T$, ICs at $t = \Delta t$ are from the computed solution at $t = \Delta t$ for ${}^1\bar{\Omega}_{xt}^T$. This process is continued till the desired time $t = \tau$ is reached. The benefits of space-time coupled finite element process based on residual functional and the computations of evolutions using space-time strip with time marching are well documented in references [22]- [31].

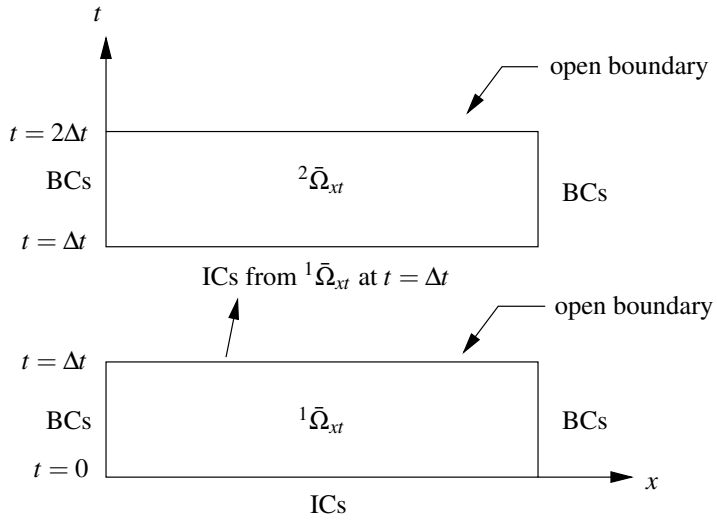

Figure 2.4: First Two Space-Time Strips with BCs and ICs

Chapter 3

Numerical Studies

We consider one dimensional axial wave propagation in thermoelastic solid and thermoviscoelastic solid with and without memory. In all three mathematical models (section 2.3) Green's strain tensor is used as a measure of finite strain and the second Piola-Kirchhoff stress tensor as energy conjugate stress measure. Figure 3.1(a) shows a schematic of the dimensionless rod of length one unit. The right end of the rod (at $x = 1.0$) is subjected to two different types of loadings.

3.1 Loadings

We consider two different types of loadings at $x = 1.0$.

Pulse Loading (L1) at $x = 1$:

This loading consists of a stress pulse $\sigma_{xx}^{[0]}(t)$ of maximum amplitude $\pm\sigma_1$, positive for tensile loading and negative for compressive loading applied over a time interval of $2\Delta t$. In figure 3.1(b), $\sigma_{xx}^{[0]}(t)$ is continuous with continuous first time derivative for $0 \leq t \leq 2\Delta t$, zero for $t \geq 2\Delta t$ and is defined using the following.

$$\left.\begin{aligned}
&\text{at} \quad t=0;\ \sigma_{xx}^{[0]}(t)=0,\ \frac{\partial \sigma_{xx}^{[0]}}{\partial t}=0 \\
&\text{at} \quad t=\Delta t;\ \sigma_{xx}^{[0]}(t)=\pm\sigma_1,\ \frac{\partial \sigma_{xx}^{[0]}}{\partial t}=0 \\
&\text{at} \quad t=2\Delta t;\ \sigma_{xx}^{[0]}(t)=0,\ \frac{\partial \sigma_{xx}^{[0]}}{\partial t}=0 \\
&\text{for} \quad t\geq 2\Delta t;\ \sigma_{xx}^{[0]}(t)=0
\end{aligned}\right\} \tag{3.1}$$

The stress pulse $\sigma_{xx}^{[0]}(t)$ described by 3.1 has support of $2\Delta t$ with maximum amplitude of $\pm\sigma_1$ at $t=\Delta t$ such that for $0\leq t\leq 2\Delta t$ $\sigma_{xx}^{[0]}(t)$ is a cubic function of time t and $\sigma_{xx}^{[0]}(t)=0$ for $t\geq 2\Delta t$.

Ramp Loading (L2) at $x=1$:

This loading consists of stress $\sigma_{xx}^{[0]}(t)$ defined as a ramp function over a time interval of Δt with maximum value of $\pm\sigma_1$. Positive and negative signs correspond to tension and compression respectively. The ramp $\sigma_{xx}^{[0]}(t)$ is continuous with continuous first derivative for (cubis function) $0\leq t\leq \Delta t$ and remains $\pm\sigma_1$ for $t\geq \Delta t$.

$$\left.\begin{aligned}
&\text{at} \quad t=0;\ \sigma_{xx}^{[0]}(t)=0,\ \frac{\partial \sigma_{xx}^{[0]}}{\partial t}=0 \\
&\text{at} \quad t=\Delta t;\ \sigma_{xx}^{[0]}(t)=\pm\sigma_1,\ \frac{\partial \sigma_{xx}^{[0]}}{\partial t}=0 \\
&\text{for} \quad t\geq \Delta t;\ \sigma_{xx}^{[0]}(t)=\pm\sigma_1
\end{aligned}\right\} \tag{3.2}$$

Figure 3.1(c) shows a schematic of this loading.

3.2 Material Coefficients, Reference Quantities and Dimensionless Parameters

Details of the choices of reference quantities, material coefficients and dimensionless parameters for TE and TVE solids with and without memory are given in the following.

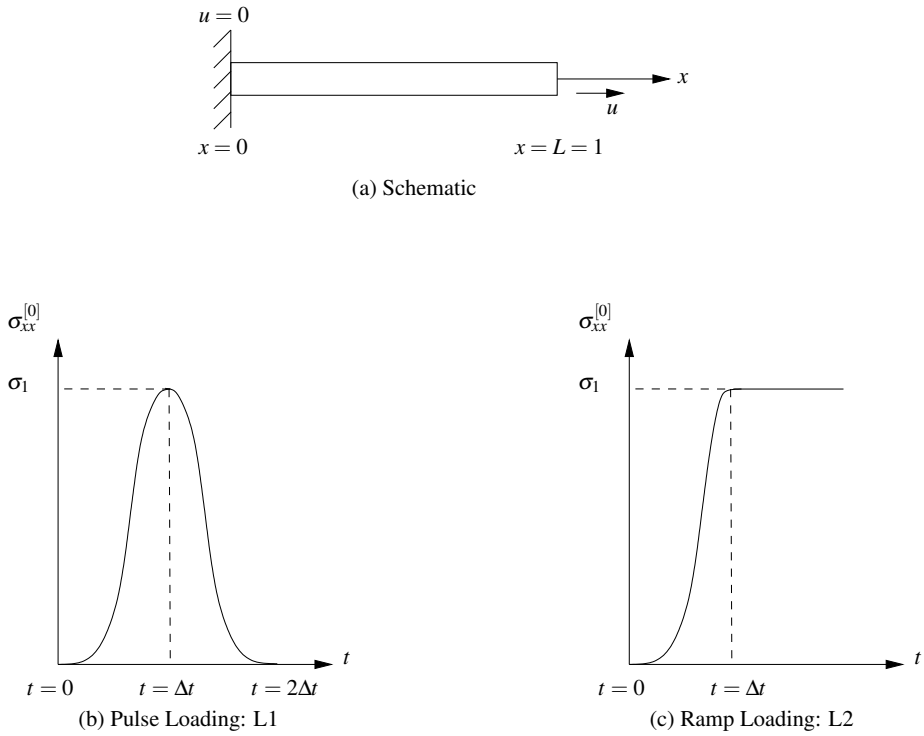

(a) Schematic

(b) Pulse Loading: L1

(c) Ramp Loading: L2

Figure 3.1: Schematic of 1D rod, Pulse, and Ramp loading

Thermoelastic Solid Continua (TE)

We consider hard rubber [35] for which we have the following assuming it to be purely elastic,

$\hat{\rho_0} = 1100\ kg/m^3$, $\hat{E} = 2.3 \times 10^7\ N/m^2$

we choose $\tilde{\rho_0} = \hat{\rho_0}$; hence $\rho_0 = \frac{\hat{\rho_0}}{\tilde{\rho_0}} = 1$

$E_0 = \hat{E}$; hence $E = \frac{\hat{E}}{\tilde{E}} = 1$

$L_0 = 1$

reference speed of sound $v_0 = \sqrt{E_0/\tilde{\rho_0}} = 144.5\ \ m/s$

reference time $t_0 = \frac{l_0}{v_0} = 0.007s$

$\tilde{\rho_0}$ is reference density

Thermoviscoelastic Solid Without Memory (TVE)

$\hat{\rho_0} = 1100\ kg/m^3$, $\hat{E} = 2.3 \times 10^7\ N/m^2$

$\tilde{\rho_0} = \hat{\rho_0}$; hence $\rho_0 = \frac{\hat{\rho_0}}{\tilde{\rho_0}} = 1$

$v_0 = \sqrt{E_0/\tilde{\rho_0}} = 144.5\ m/s$

$t_0 = \frac{l_0}{v_0} = 0.007s$

θ_0 = 300k , $\hat{c}_{p_0}$ =1380 $\frac{J}{kg \cdot K}$

$\tilde{c}_{p_0}$= $\hat{c}_{p_0}$, hence $c_{p_0} = \hat{c}_{p_0}/\tilde{c}_{p_0}$

$\hat{k}_0$=0.16 $\frac{w}{mk}$, $\tilde{k}_0$=0.16 $\frac{w}{mk}$, hence $k_0 = \frac{\hat{k}_0}{\tilde{k}_0}$

The coefficients used in the equation of state (thermodynamic pressure) in (2.40) are given in the following

$\tilde{c_0} = -48.989328, \quad \tilde{c_1} = 230.489344, \quad \tilde{c_2} = -435.159055$

$\tilde{c_3} = 412.2533551, \quad \tilde{c_4} = -196.29911, \quad \tilde{c_5} = 37.704793$

Thermoviscoelastic Solid With Memory (TVEM)

The details of material coefficients, referemce quantities and dimensionless quatities given for TVE solid without memory hold here. In addition we have deborah number $De=\lambda/t_0$. Values of De are given with numerical studies.

3.3 Considerations of material coefficients, Thermodynamic pressure and Mechanical pressure

We assume that the slope of dimensionless $\sigma_{xx}^{[0]}$ versus $\varepsilon_{[0]}$ is constant and the modulus of elasticity E relating the two that has a dimensionless value of one. Thus, in case of thermoelastic solids we can use E=1 in the constitutive theory. In case of thermoviscoelastic solids with and without memory the constitutive theory considers deviatoric second Piola Kirchhoff stress and Green's strain. In addition the equilibrium stress is related to thermodynamic pressure. In the present work we assume that $\sigma_{xx}^{[0]}$ vs $(\varepsilon_{[0]})_{xx}$ behavior assumed for TE solid remains the same for

TVE solid with and without memory i,e

$$\sigma_{xx}^{[0]} = E\ \varepsilon_{[0]} \tag{3.3}$$

holds for TVE and TVEM in dimensionless form in which E=1. Recall that from continuity

$$\rho(x,t) = \rho_0/(1+\partial u/\partial x) \tag{3.4}$$

$$(\varepsilon_{[0]})_{xx} = \frac{\partial u}{\partial x} + \frac{1}{2}\left(\frac{\partial u}{\partial x}\right)^2 \tag{3.5}$$

$$p = p(\rho) \tag{3.6}$$

$${}_d\sigma_{xx}^{[0]} = \sigma_{xx}^{[0]} - {}_e\sigma_{xx}^{[0]} \tag{3.7}$$

$${}_e\sigma_{xx}^{[0]} = -p(\rho)(1+\frac{\partial u}{\partial x}) \tag{3.8}$$

In the following behaviors of $(\varepsilon_{[0]})_{xx}$ versus $\partial u/\partial x$, ρ versus $\partial u/\partial x$, p versus ρ (in tension), ${}_e\sigma_{xx}^{[0]}$ versus $(\varepsilon_{[0]})_{xx}$, ${}_d\sigma_{xx}^{[0]}$ versus $(\varepsilon_{[0]})_{xx}$ in the entire range of $(\varepsilon_{[0]})_{xx}$ as well as in the linear range are presented. A range of $\partial u/\partial x$ corresponding to ρ that corresponds to valid range of $p(\rho)$ in tension $(2\times 10^7 N/m^2)$ in the experiment is choosen.

1. For this range of $\partial u/\partial x$, $(\varepsilon_{[0]})_{xx}$ is calculated using (3.5). A graph of $(\varepsilon_{[0]})_{xx}$ versus $\partial u/\partial x$ is shown in figure 3.2(a).

2. Density ρ is calculated using (3.4) for this range of $\partial u/\partial x$. A plot of ρ versus $\partial u/\partial x$ is as shown in 3.2(b).

3. Thermodynamic pressure $p(\rho)$ is calculated for this range of ρ (in (2)). A plot of $p(\rho)$ versus ρ is as shown in figure 3.2(c) (in tension only).

4. Equilibrium second Piola-Kirchhoff stress ${}_e\sigma_{xx}^{[0]}$ is calculated using (3.8). A graph of ${}_e\sigma_{xx}^{[0]}$ versus $(\varepsilon_{[0]})_{xx}$ as shown in figure 3.2(d)

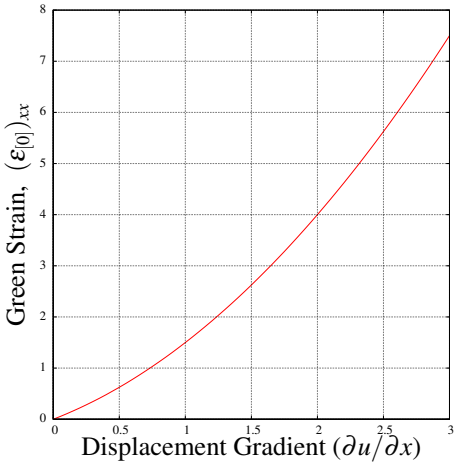

(a) Green Strain versus $\frac{\partial u}{\partial x}$(tension)

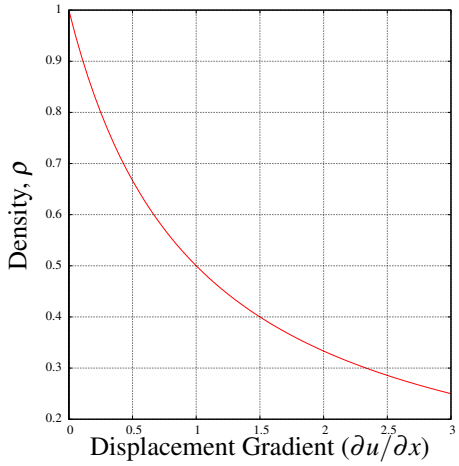

(b) Green Strain versus $\frac{\partial u}{\partial x}$(tension)

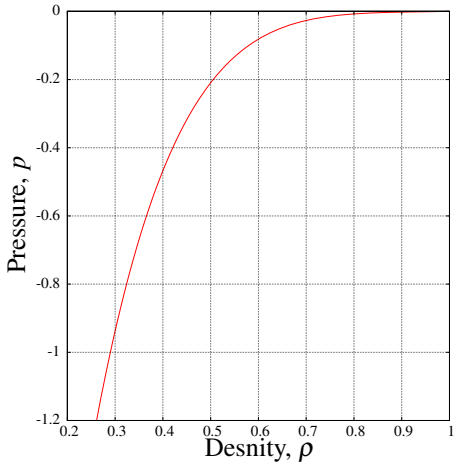

(c) Pressure versus Density(tension)

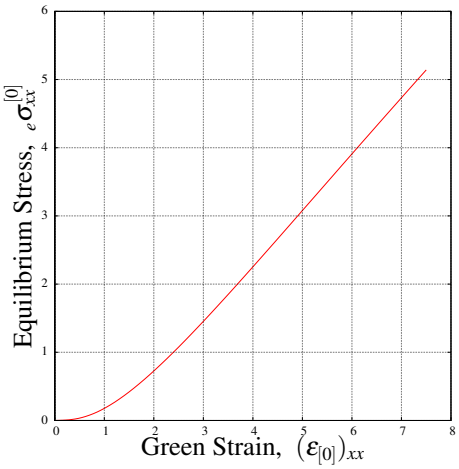

(d) Equilibrium Stress versus Green Strain(tension)

Figure 3.2: Plots of $(\varepsilon_{[0]})_{xx}$ versus $\partial u/\partial x$, ρ versus $\partial u/\partial x$, $p(\rho)$ versus ρ and ${}_e\sigma_{xx}^{[0]}$ versus $(\varepsilon_{[0]})_{xx}$ in tension

5. Using $\sigma_{xx}^{[0]}$ in (3.3) and ${}_e\sigma_{xx}^{[0]}$ in (3.8) for the range of $(\varepsilon_{[0]})_{xx}$ that corresponds to choosen range of $\partial u/\partial x$, ${}_d\sigma_{xx}^{[0]}$ is calculated using (3.7). Plots of $\sigma_{xx}^{[0]}$ and ${}_d\sigma_{xx}^{[0]}$ versus $(\varepsilon_{[0]})_{xx}$ are shown in figure 3.3(a). We note that ${}_d\sigma_{xx}^{[0]}$ versus $(\varepsilon_{[0]})_{xx}$ is highly nonlinear for large range of $(\varepsilon_{[0]})_{xx}$.

6. Modulus ${}^dE$ in ${}_d\sigma_{xx}^{[0]} = {}^dE(\varepsilon_{[0]})_{xx}$ can be determined

$$ {}^dE = \frac{\partial({}_d\sigma_{xx}^{[0]})}{\partial((\varepsilon_{[0]})_{xx})} \tag{3.9} $$

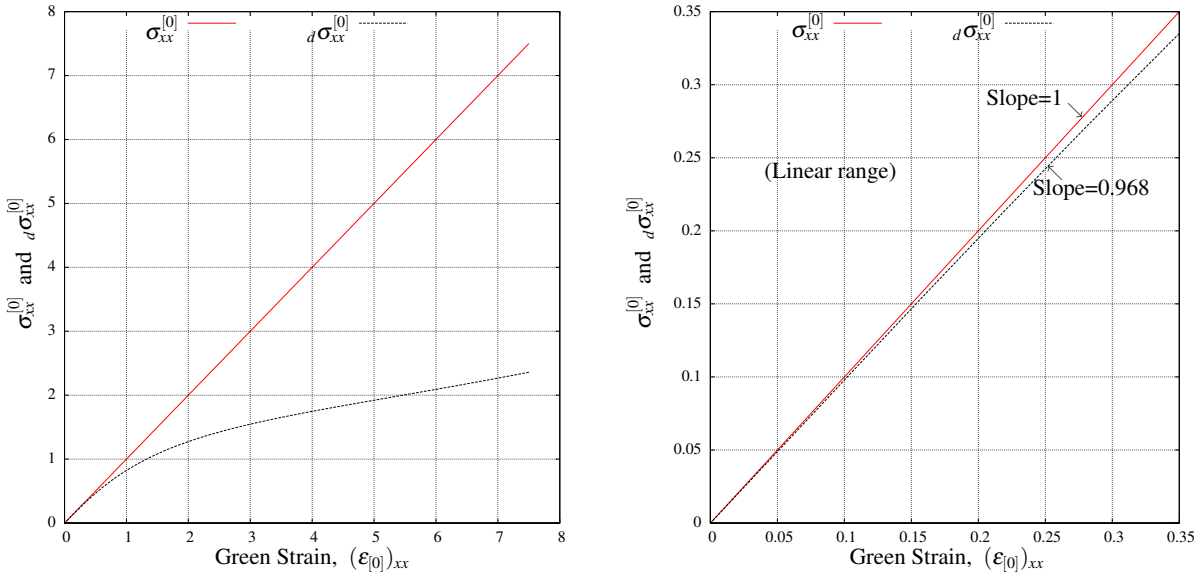

(a) Total and Deviatoric Stress vs Green Strain (Tension) (b) Total and Deviatoric Stress vs Green Strain (Tension)

Figure 3.3: Plots of $\sigma_{xx}^{[0]}$ versus $(\varepsilon_{[0]})_{xx}$ and $_d\sigma_{xx}^{[0]}$ versus $(\varepsilon_{[0]})_{xx}$ in tension for nonlinear and linear range

7. We note that for 1D case $(\varepsilon_{[0]})_{xx}$=$\sqrt{ii_{\varepsilon_{[0]}}}$ in which $ii_{\varepsilon_{[0]}}$=$tr([\varepsilon_{[0]}]^2)$, the second invariant of $\boldsymbol{\varepsilon_{[0]}}$, hence $(\varepsilon_{[0]})_{xx}$ in (1) can be replaced by $\sqrt{ii_{\varepsilon_{[0]}}}$.

8. Figure 3.3(b) show plot of $\sigma_{xx}^{[0]}$ versus $(\varepsilon_{[0]})_{xx}$ and $_d\sigma_{xx}^{[0]}$ versus $(\varepsilon_{[0]})_{xx}$ in the linear range (tension only), the slopes of these are $E = 1$ and $^dE = 0.968$.

9. Plots of $(\varepsilon_{[0]})_{xx}$ versus $\partial u/\partial x$, ρ versus $\partial u/\partial x$, $p(\rho)$ versus ρ and $_e\sigma_{xx}^{[0]}$ versus $(\varepsilon_{[0]})_{xx}$ in compression using the same equation of state (3.6) are shown in figures 3.4(a)-(d)

10. Figures 3.5(a) and 3.5(b) show plots of $\sigma_{xx}^{[0]}$ versus $(\varepsilon_{[0]})_{xx}$, $_d\sigma_{xx}^{[0]}$ versus $(\varepsilon_{[0]})_{xx}$ in the non-linear as well as linear range for compression loading. From figure the slopes yield $E = 1$ and $^dE = 0.954$ (in compression)

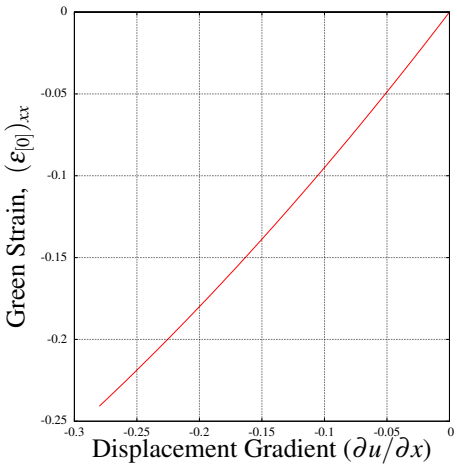

(a) Green Strain vs $\frac{\partial u}{\partial x}$(Compression)

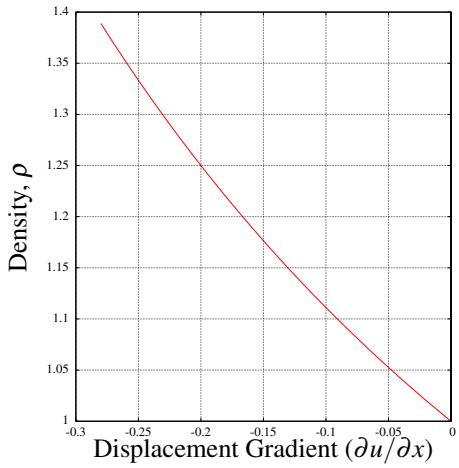

(b) Density vs $\frac{\partial u}{\partial x}$(Compression)

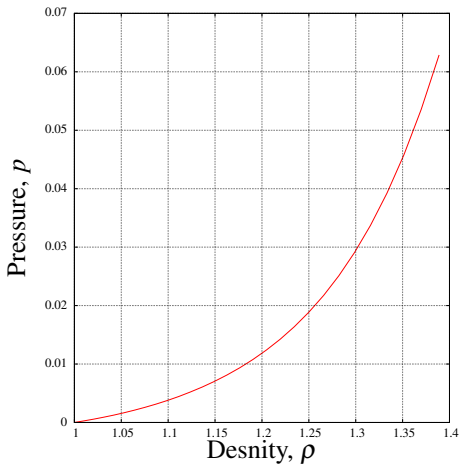

(c) Pressure vs Density(Compression)

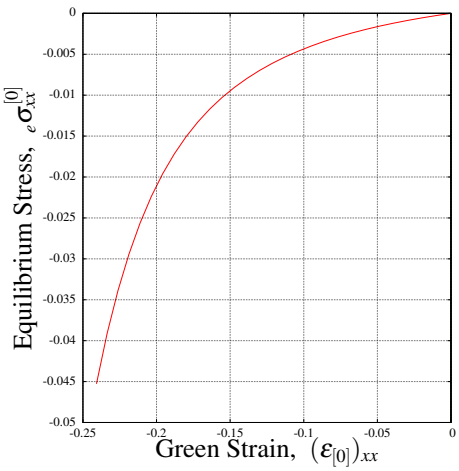

(d) Equilibrium Stress vs Green Strain (Compression)

Figure 3.4: Plots of $(\varepsilon_{[0]})_{xx}$ versus $\partial u/\partial x$, ρ versus $\partial u/\partial x$, $p(\rho)$ versus ρ and ${}_e\sigma_{xx}^{[0]}$ versus $(\varepsilon_{[0]})_{xx}$ in compression

3.4 Computations of Evolutions: Numerical Results

Evolution for pulse and ramp loadings are computed using a space-time strip for a time increment Δt with time marching. We choose the orders of spaces in space and time $(k = (k_1, k_2))$ to be $k_1 = 2$ and $k_2 = 2$. In the mathematical models used the spatial derivative of all dependent variables are of first order, but the time derivative are upto orders two. Thus for (k_1, k_2) =$(2,2)$ the integrals in the LSP over $\bar{\Omega}_{xt}^T$ are Riemann in space but Lebeque in time. However, due to smoothness of evolutions we expect the convergence of the solution of class C^1 in time to solutions of C^2 in time in the weak sense. We note that we have dimensionless wave speed $v = \sqrt{E/\rho_o} = 1$,

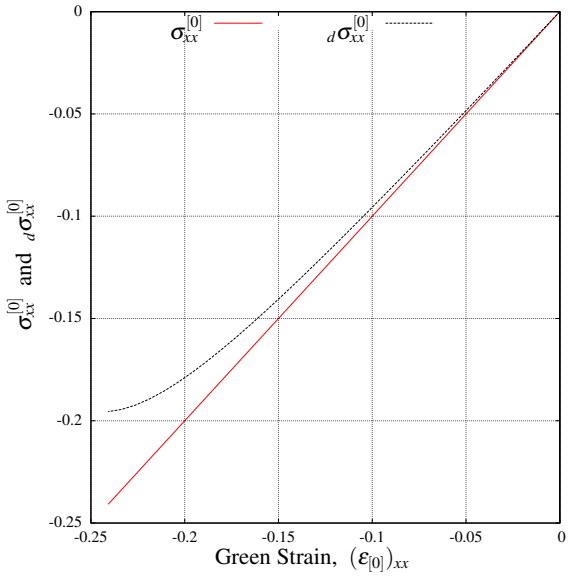

(a) Total and Deviatoric Stress vs Green Strain (Compression)

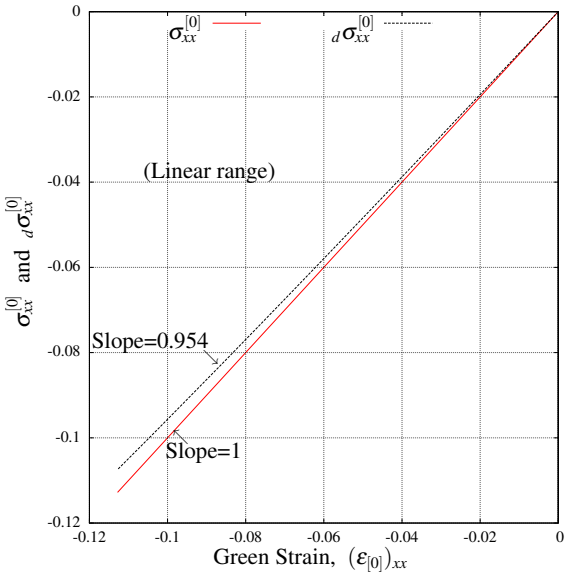

(b) Total and Deviatoric Stress vs Green Strain (Compression)

Figure 3.5: Plots of $\sigma^{[0]}_{xx}$ versus $(\varepsilon_{[0]})_{xx}$ and $_d\sigma^{[0]}_{xx}$ versus $(\varepsilon_{[0]})_{xx}$ in compression for nonlinear and linear range

hence for time increment of Δt the wave will advance a spatial distance of $\Delta x = \Delta x$. We consider a uniform sixteen element discretization for the first space-time (and all subsequent ones) using nine-node p-version hierarchial space-time element with space-time local approximation in $H^{k,p}(\bar{\Omega}_{xt})$; $k = (k_1, k_2) = (2,2)$ space. Uniform p-levels are considered in space and time, p-levels are increased from 3 to 11 in increments of two. Newton's linear method with line search is considered converged when $max|g_i| \leq \Delta$; $\Delta \leq D(10^{-6})$. Generally less than 5-10 iteration have been sufficient for convergence of the iterative solution method.

Convergence Study:

First we consider convergence behaviour of the residual functional I for ${}^1\bar{\Omega}^T_{xt}$, the first space time strip using a fixed sixteen element uniform mesh for ${}^1\bar{\Omega}^T_{xt}$ with p-level from 3-11 in increment of 2. These convergence studies are considered for,

1. 1D wave propagation assuming infinitesimal strain $(f = 0)$ for $\pm = 0.01$

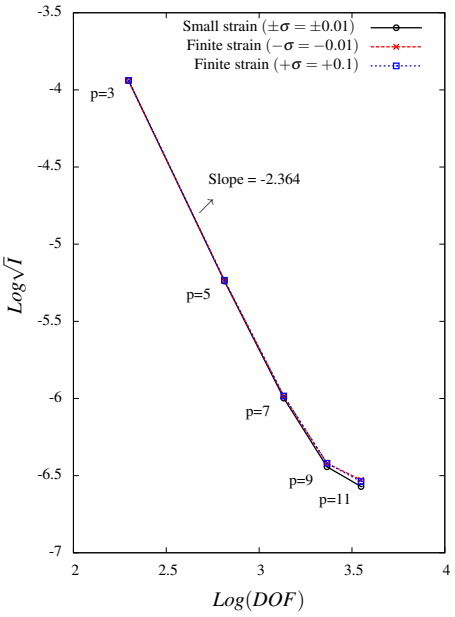

(a) TE

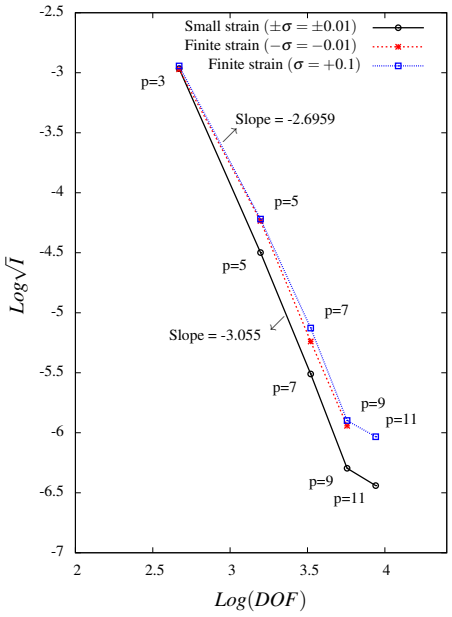

(b) TVE

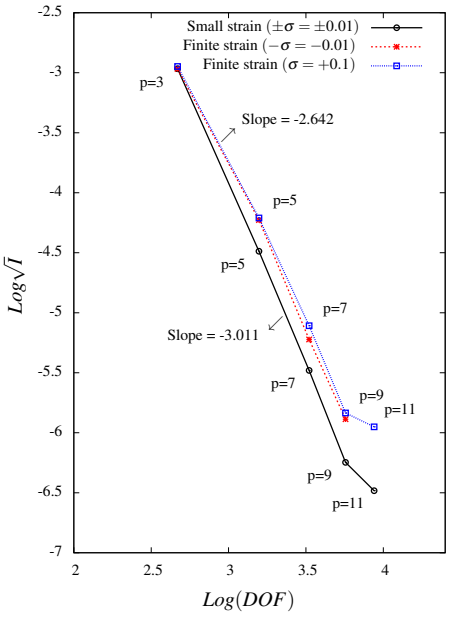

(c) TVEM

Figure 3.6: Convergence of Residual Functional I: $\log\sqrt{I}$ versus $\log dof$

2. 1D wave propagation with finite deformation and finite strain $(f = 1)$ for $-\sigma_1$=0.01 and $\sigma_1 = 0.1$

We conduct studies for TE and TVE solid with and without memory. Figures 3.6(a),(b) and (c) show plots of $log(\sqrt{I})$ versus $log(dof)$ for TE, TVE, TVEM. In all three cases at $p = p_1 = p_2 = 9$, I is of the order of $O(10^{-12})$ or lower confirming good convergence of the computed solution for the first space-time strip to the theoretical solution. In all three cases (TE, TVE, TVM) the asymptotic range is achieved even at $p = 3$. For TE case, both linear and nonlinear studies yield same convergence rate of 2.364. In case of TVE infinitesimal strain slightly higher convergence rate (3.055) is observed compared to finite deformation case ($\pm\sigma_1$ yield nearly same rates) in which case a convergence rate of 2.6959 is achieved. For TVEM the convergence rate for infinitesimal strain is same (3.011) as that for the TVE (3.055). For finite strain rate a slightly lower convergence rate (2.642) is observed compared to infinitesimal strain case.

We observe that for TE, TVE and TVEM convergence rate of 2.364, 2.6859, and 2.642 are observed for the finite deformation case, nearly the same for practical purposes. In all three studies (TE, TVE and TVEM) onset of post asymptotic range is observed indicating that p-levels beyond 9 for this 16 element discretization are unlikely to result in significant improvement in I.

3.4.1 Comparison of Wave Propagation: Thermodynamic Pressure and Mechanical Pressure

In this section we compare the wave propagation results of current work with the published work [1] in which thermodynamic pressure is approximated by mean normal stress. In all the numerical studies that follow in this section, we consider wave propagation in thermoviscoelastic solid without memory and refer to the results of current studies by "TP" (thermodynamic pressure) and those of the published work [1] as "MP" (mechanical pressure).

TVE Solid

Tensile Ramp Loading

We consider a tensile stress ramp applied with $\sigma_1 = 0.25$, $c = 0.006$, and $\Delta t = 0.1$. The plots in figure 3.7(a)-3.7(f) shows the stress wave propagation towards fixed end (x=0) for $t = \Delta t,\ 2\Delta t,\ 4\Delta t$ and getting reflected at the fixed end of the rod at $t = 9\Delta t$. Wave propagation before and after reflection from the free end (x=1) are as shown in $t = 12\Delta t,\ 18\Delta t$. It could be noticed from the graphs that the waves propagate faster with relatively higher velocity for mechanical pressure (MP) case as compared to the material with thermodynamic pressure (TP). This is as a result of the difference in modulus E used in both the studies. In the published work [1], the modulus $E = \frac{3}{2}^d \underset{\sim}{E}$ while in the current work E=$(0.968)^d \underset{\sim}{E}$ is used. Before the reflection, the value of stress is same as applied, $\sigma_1 = 0.25$ in both the cases, but after the reflection for $t = 9\Delta t$ (figure 3.7(d)) from the fixed end, the stress is more for mechanical pressure case ($\sigma_1 = 0.51$), when compared to the current study that incorporates the appropriate equation of state ($\sigma_1 = 0.47$). Figure 3.8(a)-3.8(f) shows the density plots for time steps $t = \Delta t,\ 2\Delta t,\ 4\Delta t, 10\Delta t,\ 12\Delta t$, and $18\Delta t$. Due to the nature of load applied, the density in the material decreases and this decrease at a given point is more in the case of material with mechanical pressure equation (MP) as compared to the decrease in density in the current study with thermodynamic pressure equation. Similar trend could be observed after reflection from the fixed end ($x = 0$) for density where the decrease in density is less for TP compared to MP which is consistent with the speed at which the waves propagate after reflection. Figure 3.9(a)-3.9(f) shows the displacement plot for $t = \Delta t,\ 2\Delta t,\ 4\Delta t, 10\Delta t,\ 12\Delta t$, and $18\Delta t$. The displacement of rod as the stress wave propagates between the ends of rod ($0 \geq x \leq 1$) is always lower in the case of TP compared to MP which is consistent with the stress and density plots that showed relatively slower velocity of stress wave propagation and less reduction in density for TP compared to MP. Thus from the above discussion we can conclude that incorporating mechanical pressure to calculate equilibrium stress in a compressible solid results in over estimation of the speed at which the stress wave propagate and the reduction in density.

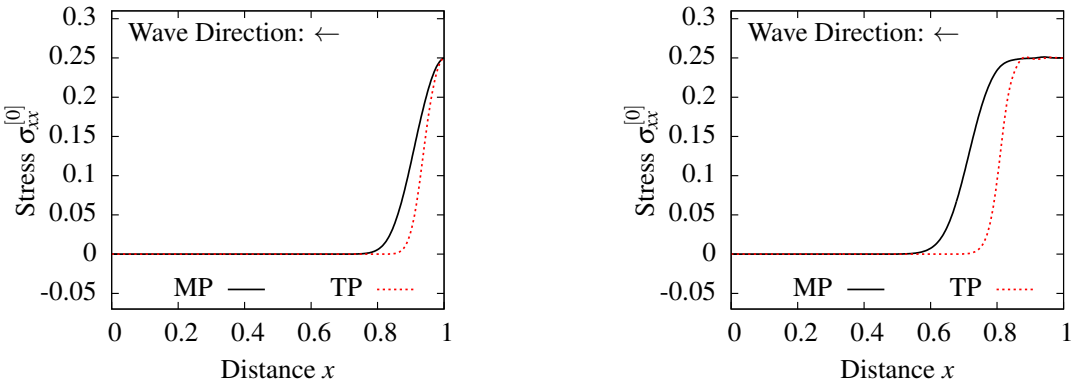

(a) $t = \Delta t$

(b) $t = 2\Delta t$

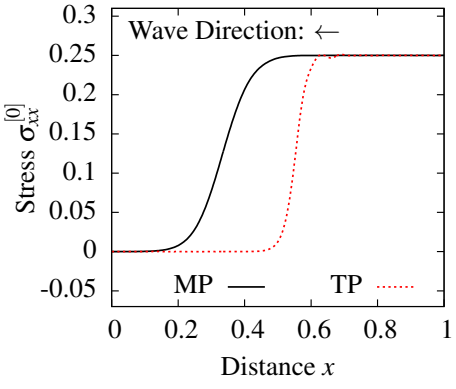

(c) $t = 4\Delta t$

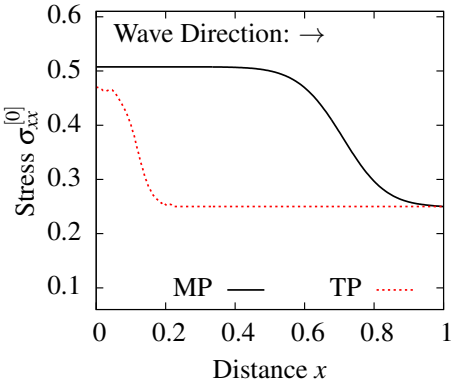

(d) Reflection, $t = 9\Delta t$

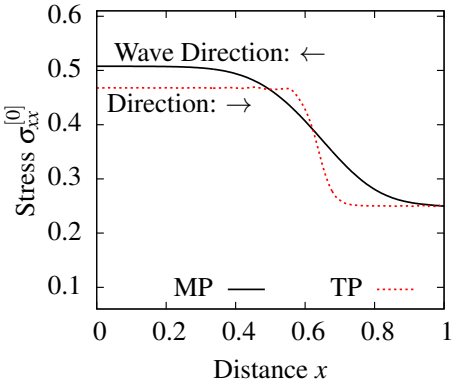

(e) $t = 12\Delta t$

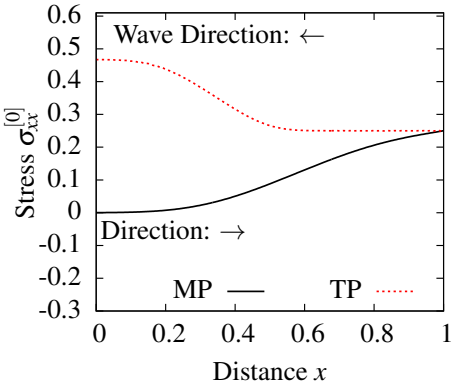

(f) $t = 18\Delta t$

Figure 3.7: Evolution of $\sigma_{xx}^{[0]}$ along the length of the rod in tension ($\sigma_1 = 0.25$, $\Delta t = 0.1$,$c = 0.006$): TVE

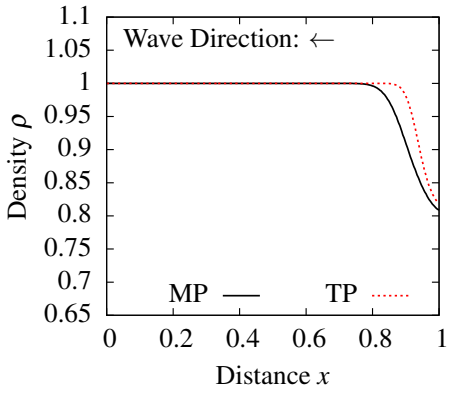

(a) $t = \Delta t$

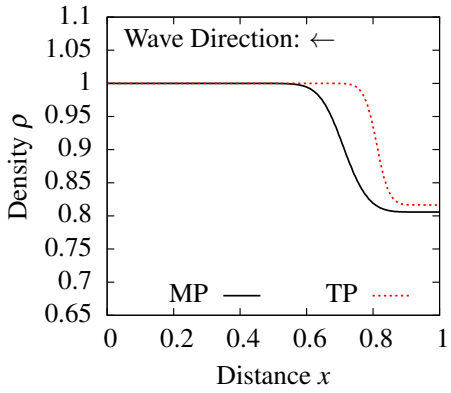

(b) $t = 2\Delta t$

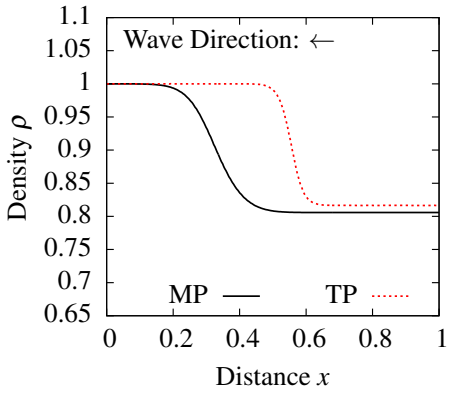

(c) $t = 4\Delta t$

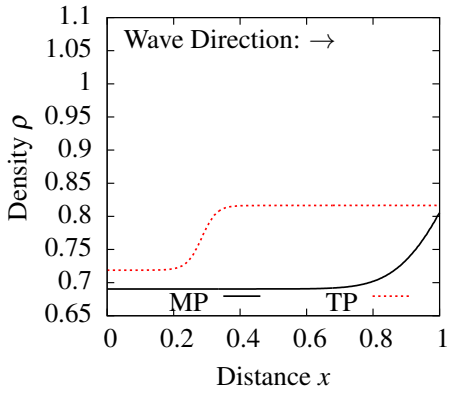

(d) Reflection, $t = 10\Delta t$

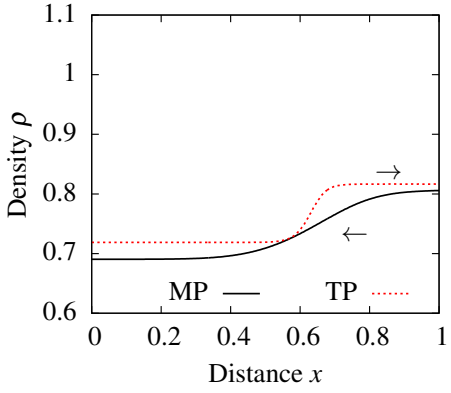

(e) $t = 12\Delta t$

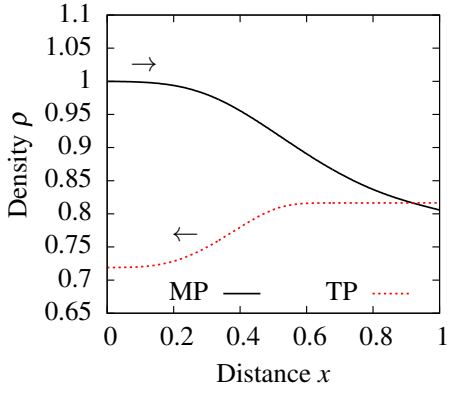

(f) $t = 18\Delta t$

Figure 3.8: Evolution of *Density*(ρ) along the length of the rod in tension ($\Delta t = 0.1$, $\sigma_1 = 0.25$)

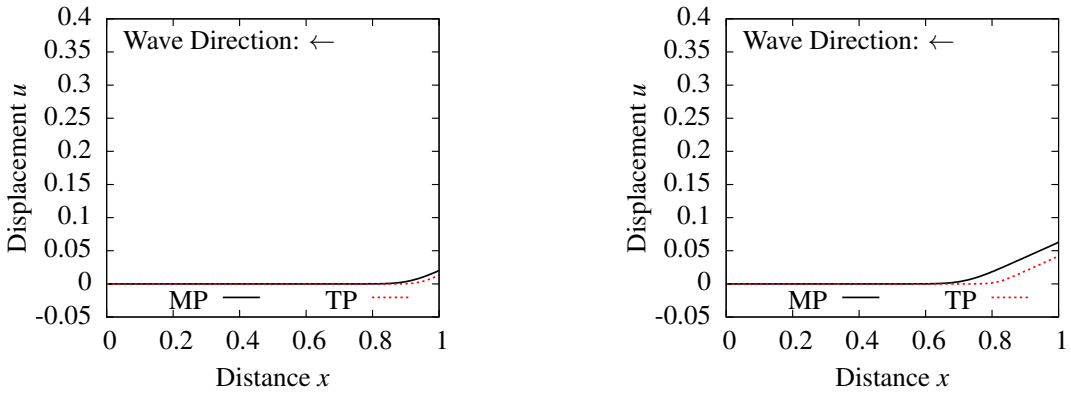

(a) $t = \Delta t$

(b) $t = 2\Delta t$

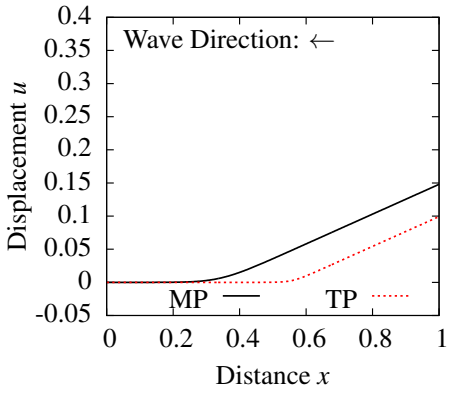

(c) $t = 4\Delta t$

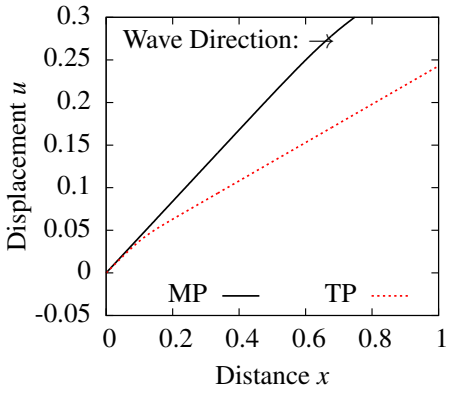

(d) Reflection, $t = 9\Delta t$

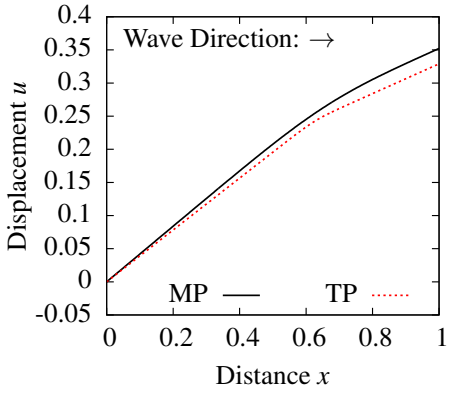

(e) $t = 12\Delta t$

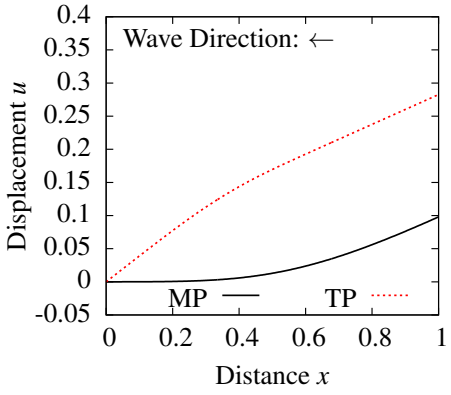

(f) $t = 18\Delta t$

Figure 3.9: Evolution of displacement u along the length of the rod in tension ($\Delta t = 0.1$, $\sigma_1 = 0.25$)): TVE

Compressive Ramp Loading

In this section we consider a compressive ramp loading of $\sigma_1 = -0.01$, $c = 0.006$ and $\Delta t = 0.1$. The plots in figure 3.10(a)-3.10(f) shows the stress wave propagation between ends of the rod (($0 \geq x \leq 1$). Figure 3.10(a),(b) and (c) shows the wave propagation towards the fixed end and figure 3.10(d) shows wave reflection at the fixed end ($x = 0$) of the rod at $t = 10\Delta t$. Wave propagation before and after reflection from the free end (x=1) are as shown in $t = 12\Delta t,\ 18\Delta t$. Here also it is evident from the stress plots (figure 3.10(a)-(f)) that the speed at which the wave propagate is overestimated in the case of material using mechanical pressure (MP) compared to the material modelled with thermodynamic pressure(TP) for ${}_e\sigma_{xx}^{[0]}$. This is again due to the difference in modulus value. Figure 3.11(a)-3.11(f) shows the change in density for MP and TP case for $t = \Delta t,\ 2\Delta t, 4\Delta t, 10\Delta t, 12\Delta t$ and $15\Delta t$. For all the time steps it is observed that the increase in density of the rod subjected to compressive load is more for mechanical pressure (MP) compared to the change in the case of thermodynamic pressure. And the displacements plots shown in figure 3.12(a)-3.12(f) is consistent with the trend observed in stress and density plots, since at each time step, the displacement at a point for MP is higher than that of TP.

Thus from the above discussions it could well be concluded that in order to represent the correct physics involved in the response of a compressible material like hard rubber, in terms of the speed of wave propagation, density change in the material and the displacement the material particles undergo, it is required that we incorporate the right equation of state for thermodynamic pressure, to account for the ${}_e\sigma_{xx}^{[0]}$ in the material. Following this conclusion it is now required to further study the material with the appropriate mathematical model in comparison with thermoelastic solid with no dissipation and also linear and nonlinear cases to better understand and illustrate the influence of using the actual equation of state to model a homogenous isotropic compressible solid. In the following sections we consider thermo elastic (TE) solid with no dissipation and compare their results with TVE and TVEM solid for two different loading conditions. And also study linear and Nonlinear cases for TVE and TVEM solid.

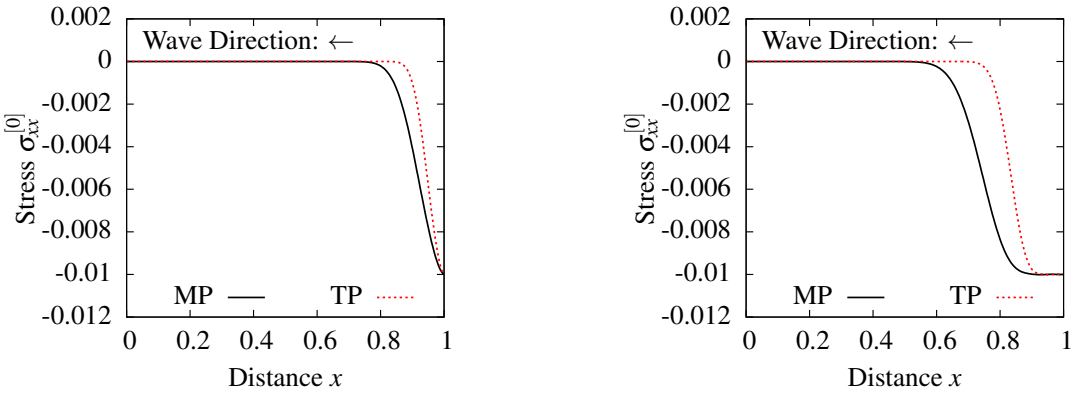

(a) $t = \Delta t$

(b) $t = 2\Delta t$

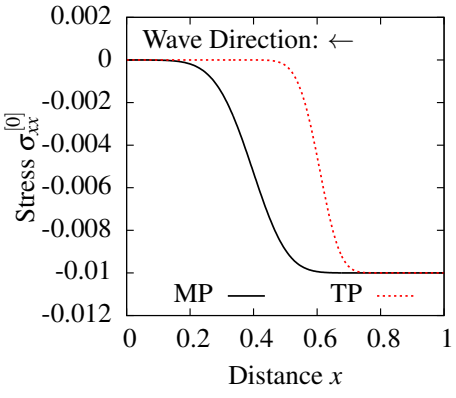

(c) $t = 4\Delta t$

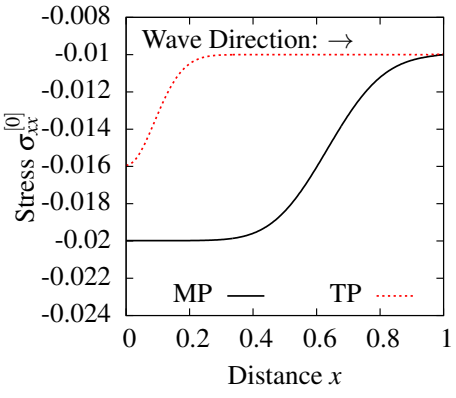

(d) Reflection, $t = 10\Delta t$

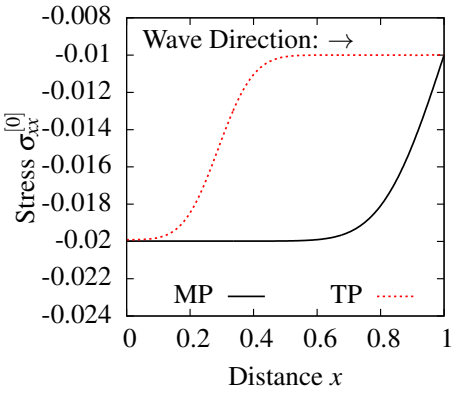

(e) $t = 12\Delta t$

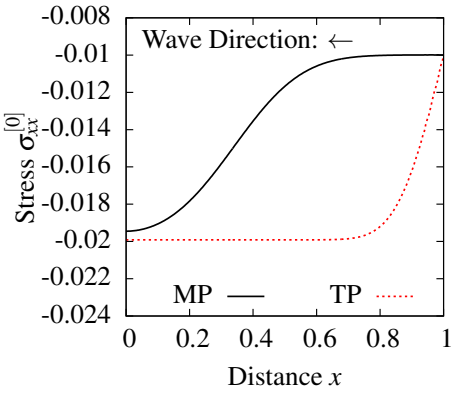

(f) $t = 18\Delta t$

Figure 3.10: Evolution of $\sigma_{xx}^{[0]}$ along the length of the rod in compression ($\sigma_1 = -0.01$, $\Delta t = 0.1$, $c = 0.006$): TVE

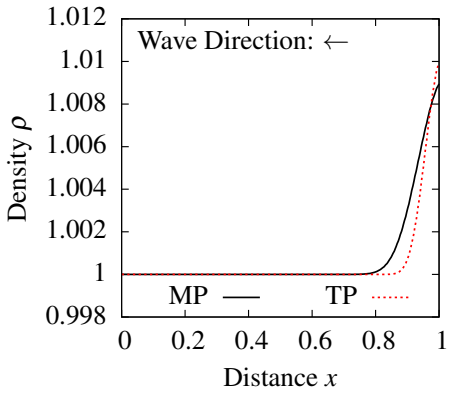

(a) $t = \Delta t$

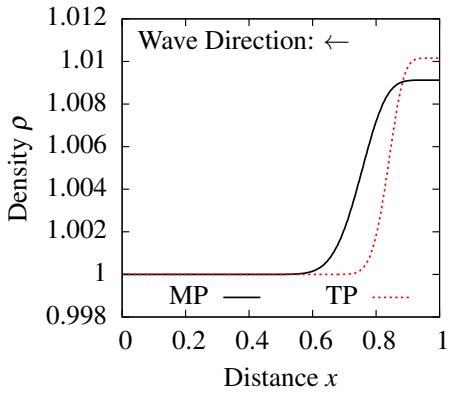

(b) $t = 2\Delta t$

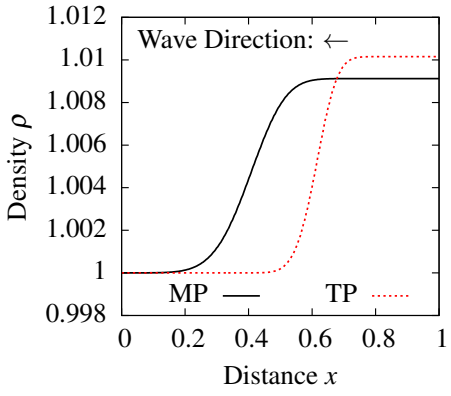

(c) $t = 4\Delta t$

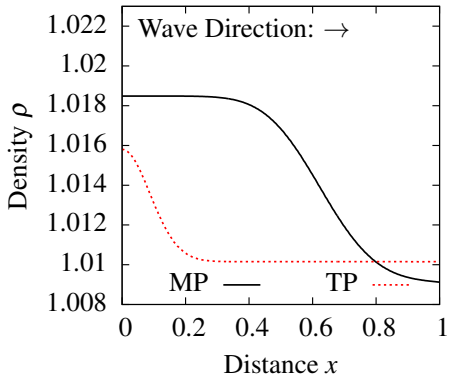

(d) Reflection, $t = 10\Delta t$

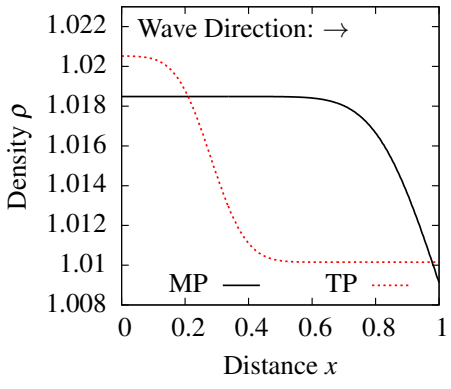

(e) $t = 12\Delta t$

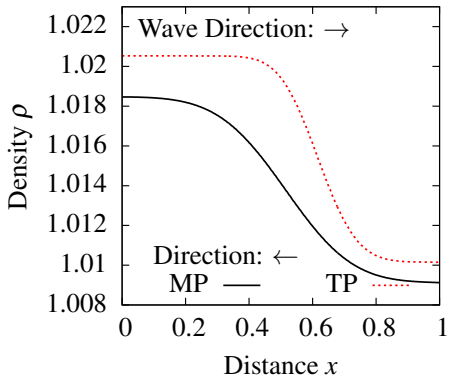

(f) $t = 15\Delta t$

Figure 3.11: Evolution of *Density*(ρ) along the length of the rod in compression ($\sigma_1 = -0.01$, $\Delta t = 0.1$, $c = 0.006$): TVE

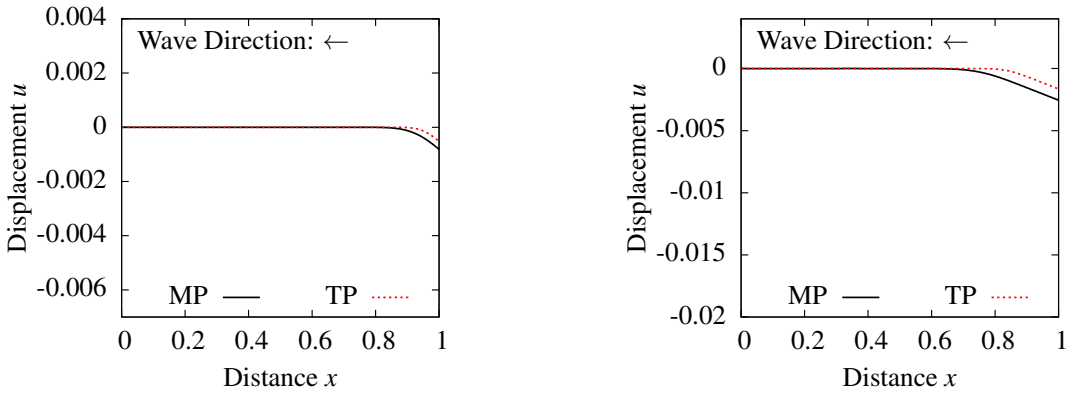

(a) $t = \Delta t$

(b) $t = 2\Delta t$

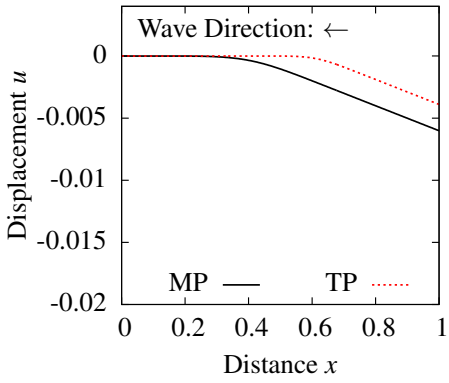

(c) $t = 4\Delta t$

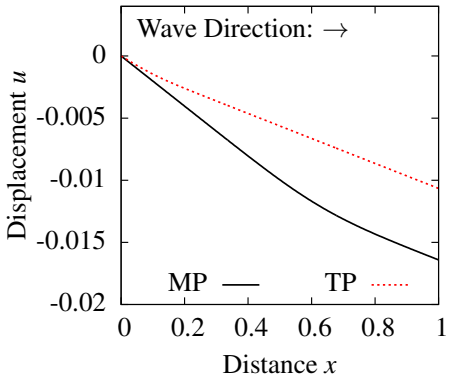

(d) Reflection, $t = 10\Delta t$

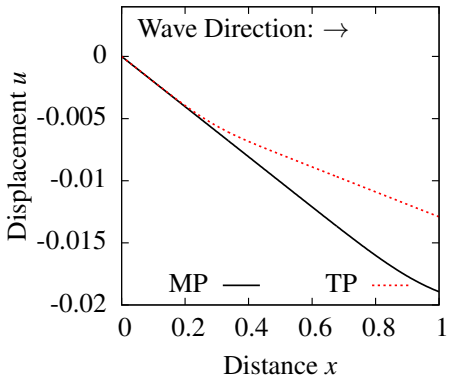

(e) $t = 12\Delta t$

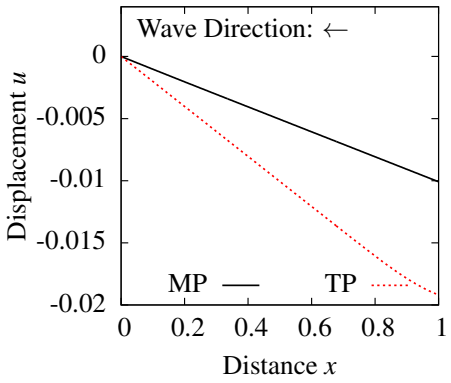

(f) $t = 18\Delta t$

Figure 3.12: Evolution of displacement u along the length of the rod in compression ($\sigma_1 = -0.01$, $\Delta t = 0.1$, $c = 0.006$): TVE

3.4.2 TE and TVE Solid

In this section we present computed evolutions for TE and TVE solid for nonlinear cases. When considering compressive $\sigma_{xx}^{[0]}$ at $x = 1$, caution should be exercised regarding the magnitude of $-\sigma_1$ as for this case for some value of $-\sigma_1$ the stiffness due to $\sigma_{xx}^{[0]}$ will become equal to the nonlinear siffness of the rod causing instability, hence failure of computations [32]- [34]. This will occur at the fixed end during reflection when the magnitude of the stress momentarily jumps (double in linear case). Hence in the present study involving TE solid, we choose $\sigma_1 = \pm 0.01$ for loading L1 as well as loading L2, well below the stress value that causes instability. In all computations, constant $\Delta t = 0.1$ is maintained.

Loading L1: Pulse

(a) Compressive

We consider a compressive stress pulse with $\sigma_1 = -0.0127$ with $f = 1$ and c = 0.006 for TVE. As seen from the graphs 3.13(a)-(f) stress pulse for TE solid propagates without any amplitude decay and base elongation as expected due to reversibility of the deformation process, where as in the case of TVE solid there is significant amplitude decay and base elongation as a result of dissipation caused due to damping which is influenced by the value of the damping co-efficient in the mathematical model. Figure 3.13 shows stress wave propagation over $0 \geq x \leq 1$ for $t = \Delta t,\ 2\Delta t,\ 6\Delta t,\ 10\Delta t,\ 15\Delta t$ and $25\Delta t$. At $t = 10\Delta t$, the stress pulse is reflecting from the impermeable boundary at $x = 0$. Upon reflection, the reflected pulse propagates back toward the right end of the rod $(x = 1.0)$ and reflects from the free boundary at $x = 1.0$. This reflected stress pulse now propagates toward the left end of the rod (figure 3.13 (f) at $t = 18\Delta t$). We observe that the amplitude of the stress pulse and its base are maintained during propagation and repeated reflections as expected in case of TE solid and amplitude slowly dying out in the case of TVE solid. Also the figures show that the stress waves in the case of TVE solid leading TE wave because of the higher increase in density in TE solid as compared to TVE in the deformed portion of the rod. This results in the decrease in wave propagation velocity in TE solid.

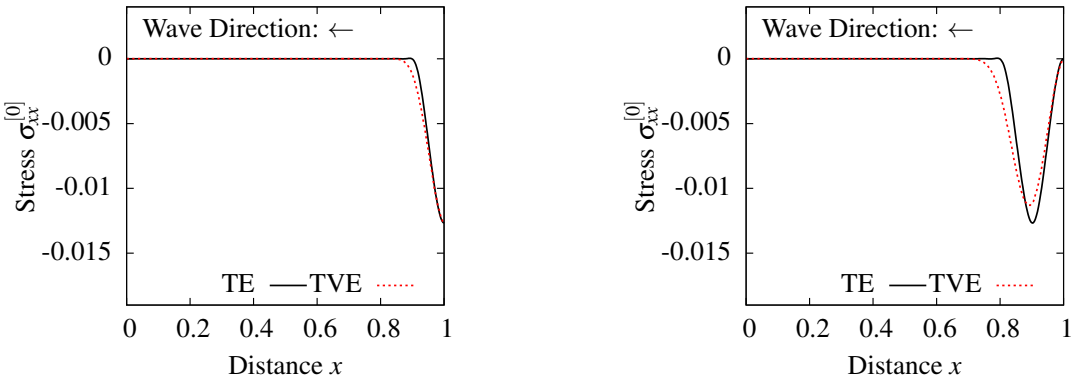

(a) $t = \Delta t$

(b) $t = 2\Delta t$

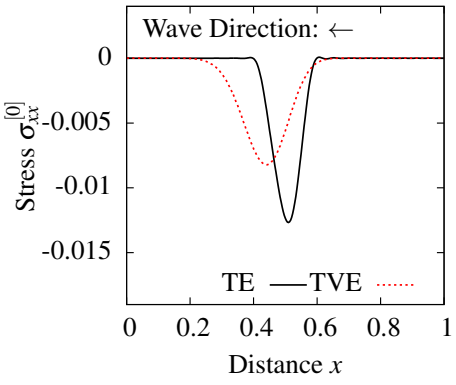

(c) $t = 6\Delta t$

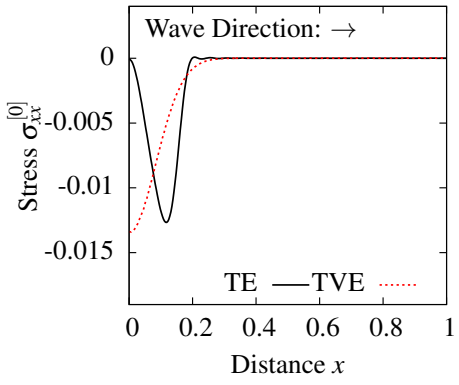

(d) Reflection, $t = 10\Delta t$

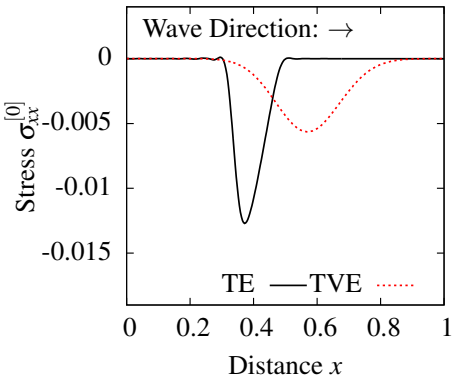

(e) $t = 15\Delta t$

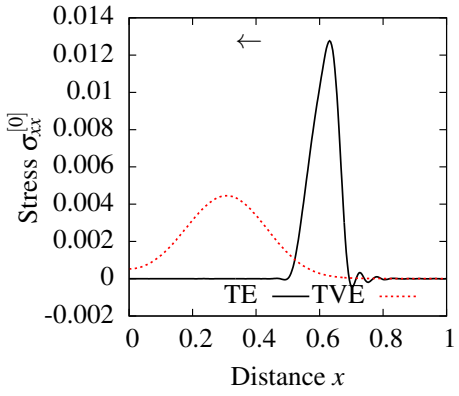

(f) $t = 25\Delta t$

Figure 3.13: Evolution of $\sigma_{xx}^{[0]}$ along the length of the rod in compression ($\sigma_1 = -0.0127$, $\Delta t = 0.1$, $c = 0.006$): TE , TVE

(b) Tensile

In this study, we choose a tensile stress pulse with $\sigma_1 = 0.0124$ applied at $x = 1.0$. Computed evolutions for TE and TVE solid are shown in figure 3.14 (a)-(f) for the same values of time, t, as used in figures 3.13(a)-(f). For both TE and TVE cases, the wave shape is preserved during propagation and the reflections from the boundaries at $x = 0$ and $x = 1$ take place as expected. In case of TVE the material density reduction due to elongation at the deformed region of the rod is more than the density decrease in TE, hence increasing the local wave speed in TVE solid. Thus, in figures 3.14(a)-(f) we observe that the wave in TVE solid leads the TE wave throughout the evolution. The significantly different behaviors of TE and TVE of the pulses at reflection from the boundary at $x = 0$ is observed here also. This is quite similar to the reflection shown in figure 3.13 (d), hence not repeated.

Loading L2: Ramp

(a) Compressive

In this study, we consider loading L2 with $\sigma_1 = -0.0127$, a ramp loading over $0 \leq t \leq \Delta t$. Here also we consider $f = 1$ (nonlinear case) and $c = 0.006$ as well. The magnitude of σ_1 remains constant in TE and the difference in amplitude decay and base elongation could be observed for TE and TVE solid. Figures 3.15(a)-(f) show propagation of stress wave over $0 \leq x \leq 1$ for $t = \Delta t,\ 4\Delta t,\ 7\Delta t,\ 10\Delta t,\ 14\Delta t,\ 23\Delta t$. At $t = 10\Delta t$, the stress wave is reflecting from the impermeable boundary at $x = 0$. Upon reflection, the reflected stress wave propagates back toward the right end boundary at $x = 0.0$ and reflects from the free boundary at $x = 1.0$. The reflected stress wave now propagates back toward the left end of the rod at $x = 0.0$ (figure 3.15(f) at $t = 23\Delta t$). We observe that the amplitude of the stress wave and its support (base) are maintained during propagation and after reflection as expected in the thermoelastic solid and the decay of the amplitude and base elongation in thermoviscoelastic solid. Due to compression, the density increases in the deformed portion of the medium for TE solid compared to TVE, hence the wave speed is reduced in TE solid. The stress wave reflecting from the impermeable boundary at $x = 0$ are similar to figures 3.13 (d)) are not reported here for the sake of brevity. Also it is evident that there is contin-

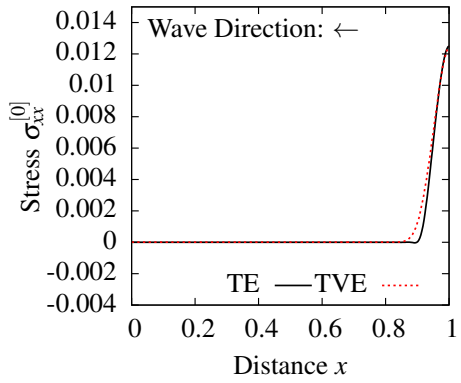

(a) $t = \Delta t$

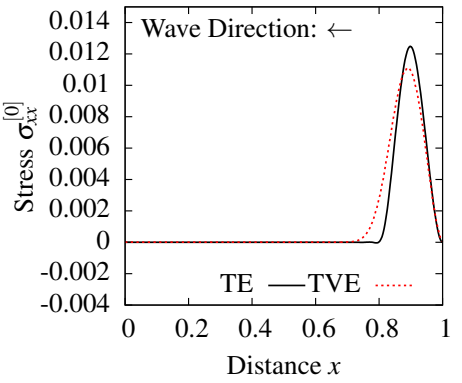

(b) $t = 2\Delta t$

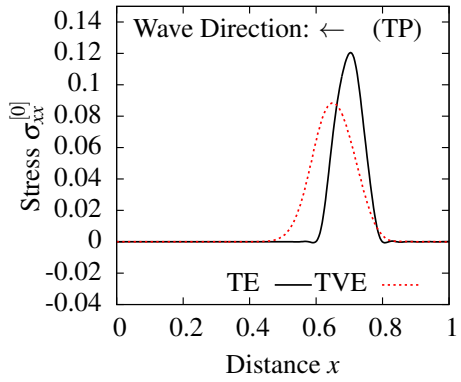

(c) $t = 4\Delta t$

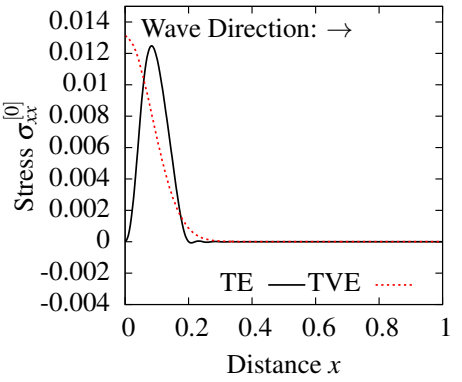

(d) Reflection, $t = 10\Delta t$

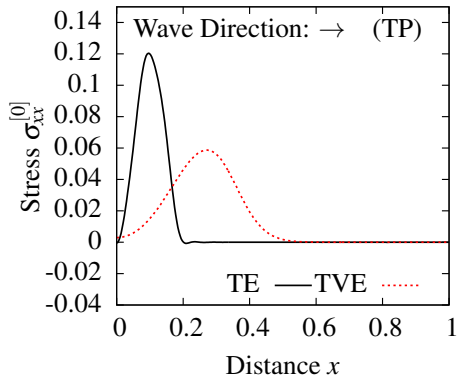

(e) $t = 12\Delta t$

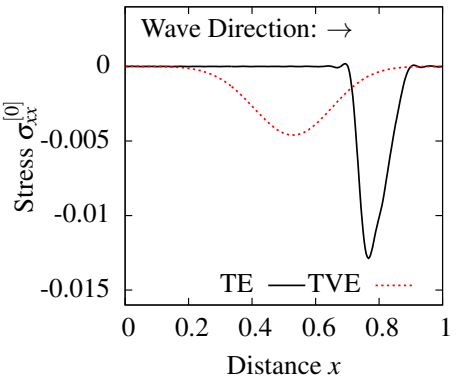

(f) $t = 23\Delta t$

Figure 3.14: Evolution of $\sigma_{xx}^{[0]}$ along the length of the rod in tension ($\sigma_1 = 0.0124$, $\Delta t = 0.1$, $c = 0.006$): TE , TVE

ued temperature rise within the TVE material due to sustained load at the free end $(x = 1.0)$ and associated dissipation mechanism converting mechanical energy into entropy.

(b) Tensile

In this study, we consider tensile stress loading with $\sigma_1 = 0.0124$ applied at $x = 1.0$ over Δt. Computed evolutions for TE and TVE cases are shown in figure 3.16(a)-(f) for the same values of time t as used in figures 3.16(a)-(f). For both TE and TVE cases the wave shape is preserved during evolution i.e. propagation and reflections. For the tensile stress wave in TVE solid, the material density reduces locally more during deformation (due to elongation) compared to TE, which results in increasing local wave speed in TVE. Hence, in figures 3.16(a)-(f) we observe that the nonlinear wave in TVE leads the wave in TE throughout the evolution. The results for the reflection and propagation from the boundaries and velocity of wave are not presented for brevity.

3.4.3 Linear and Nonlinear Waves in TVE Solids

In this section, we consider linear and nonlinear waves in TVE solid. These solids have elasticity, mechanism of dissipation which results in heat, hence influences specific internal energy. The dissipation mechanism is obviously present in linear (small strain) as well as nonlinear cases (Green's strain). In the current work the use of linear and nonlinear waves in all the studies imply wave propagation simulated using linear and nonlinear mathematical models. For linear case, (f=0), with $\frac{\partial u}{\partial x} \ll 1$, hence ρ_0=$\rho(x,t)$ holds during evolution and for nonlinear case $f = 1$. In the case of tensile load applied for TVE solid, we can take more liberty with the magnitude of stress σ_1 due to not being restricted by the instability issues. We consider dimensionless damping coefficient $c = 0.006$ in all numerical studies presented in this section.

Loading L1: Pulse

(a) Compressive

Evolutions are computed for compressive pulse of $\sigma_1 = -0.1$ over $0 \leq t \leq 2\Delta t$. Figures 3.17(a)-

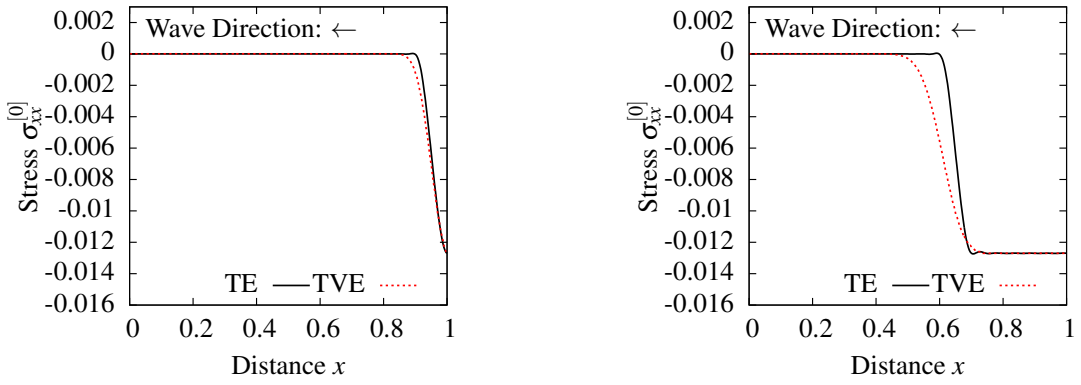

(a) $t = \Delta t$

(b) $t = 4\Delta t$

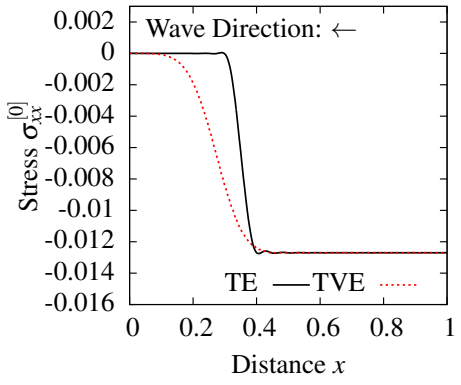

(c) $t = 7\Delta t$

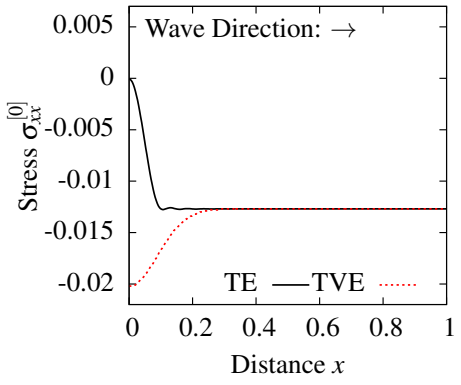

(d) Reflection, $t = 10\Delta t$

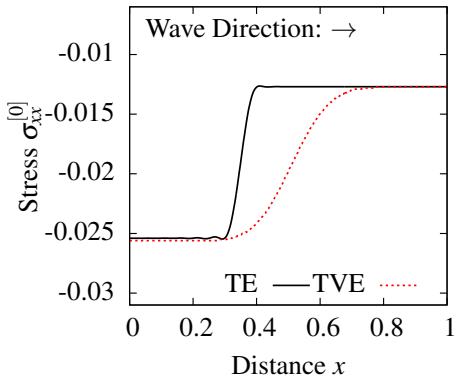

(e) $t = 14\Delta t$

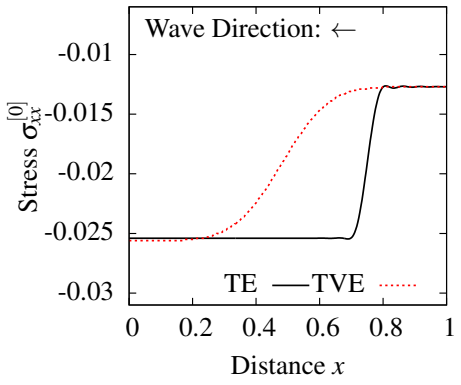

(f) $t = 23\Delta t$

Figure 3.15: Evolution of $\sigma_{xx}^{[0]}$ along the length of the rod in compression:($\Delta t = 0.1$, $\sigma_1 = -0.0127$, $c = 0.006$) TE , TVE

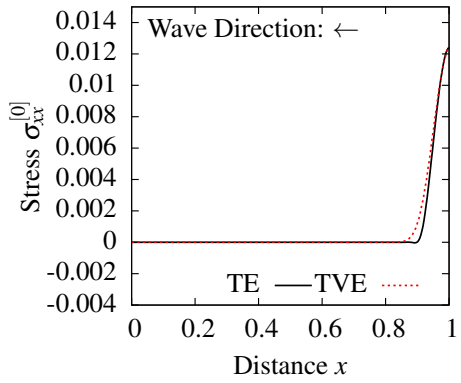

(a) $t = \Delta t$

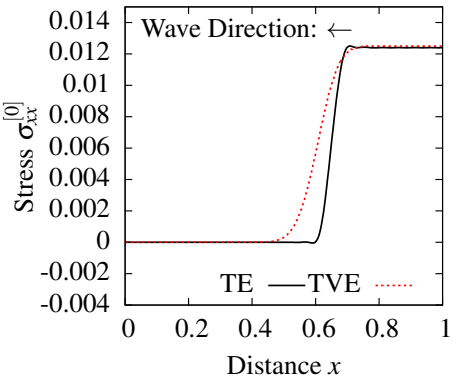

(b) $t = 4\Delta t$

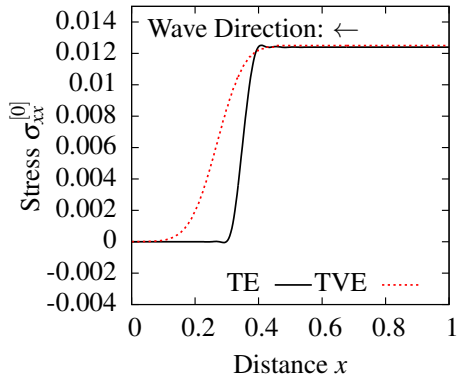

(c) $t = 7\Delta t$

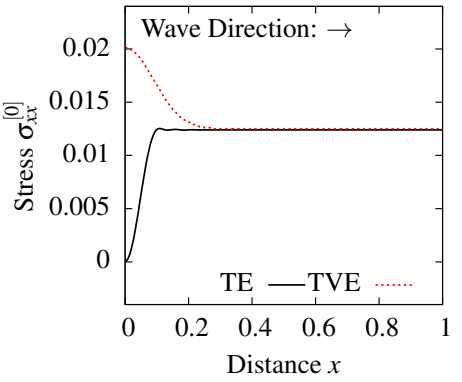

(d) Reflection, $t = 10\Delta t$

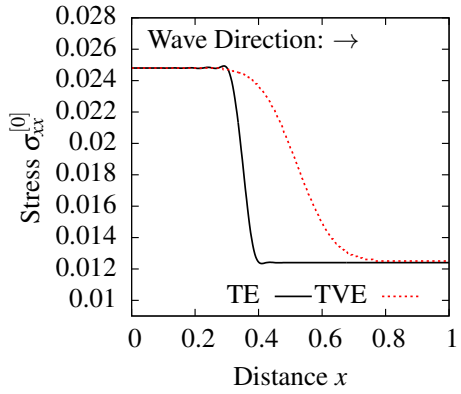

(e) $t = 14\Delta t$

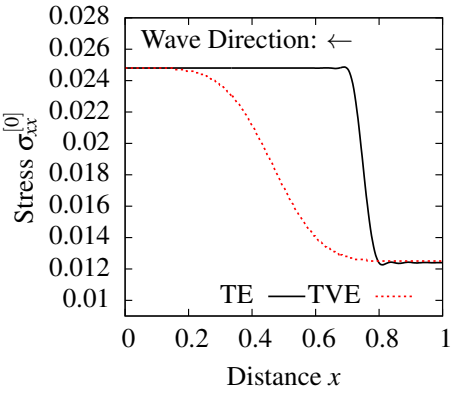

(f) $t = 23\Delta t$

Figure 3.16: Evolution of $\sigma_{xx}^{[0]}$ along the length of the rod in tension ($\Delta t = 0.1$, $\sigma_1 = 0.0124$, $c = 0.006$): TE , TVE

(f) show evolutions of waves for $t = \Delta t,\ 2\Delta t,\ 4\Delta t,\ 10\Delta t,\ 15\Delta t$ and $23\Delta t$. In both linear and nonlinear cases, the amplitudes of the waves progressively decays and the support elongates as the evolution proceeds. At $t = 23\Delta t$ (figure 3.17(e)) the peak value is only 40% of the peak of the original wave initiated at the commencement of the evolution. Due to local increase in density for the nonlinear case, the evolution for the nonlinear wave lags the evolution for the linear case. Also since in TVE solid, there is entropy production due to rate of mechanical work, hence heat generation due to mechanical work, this would result in temperature changes along the length of the rod during evolution. In the studies conducted here, the initial dimensionless temperature at time $t = 0$ is considered to be 1 i.e. $\theta = 1$ is used as initial condition. Figures 3.19(a)-(f) show temperature distributions along the rod for the same values of time as in figure 3.17. Even in temperature distribution graphs we observe that the nonlinear case lags the linear case, lower peak values for nonlinear case and quite complex temperature distribution along $0 \leq x \leq 1$ after wave reflection from $x = 0.0$ boundary (figures 3.19(e) and (f)).

(b) Tensile

When $\sigma_1 = 0.1$ for loading L1, we have a tensile pulse. Computed evolutions for same values of time t as in the case of compressive loading are shown in figures 3.20(a)-(f). Due to dissipation, the wave peaks are reduced for both linear and nonlinear cases. The evolution for linear waves lags the evolution of nonlinear waves due to a decrease in density (because of tension), hence increased wave speed in the locally deformed region occupied by the wave. Reflection of the wave at $x = 0.0$ (figures 3.20(d) at $t = 10\Delta t$) and from the $x = 1.0$ boundary (figure 3.20(f) at $t = 23\Delta t$) are smooth and present no problems. Evolution of temperature is shown in figures 3.22(a)-(f). Evolution of temperature for the nonlinear wave leads the linear wave. This is consistent with the evolution of stress wave in figures 3.20(a)-(f). Complex temperature distribution in figures 3.22 (e) and (f) after reflection are simulated accurately (I of the order of $O(10^{-13})$ or lower for each space-time strip).

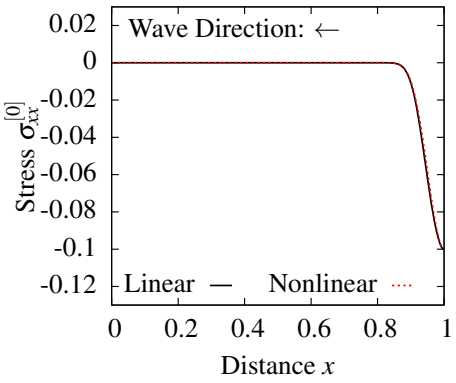

(a) $t = \Delta t$

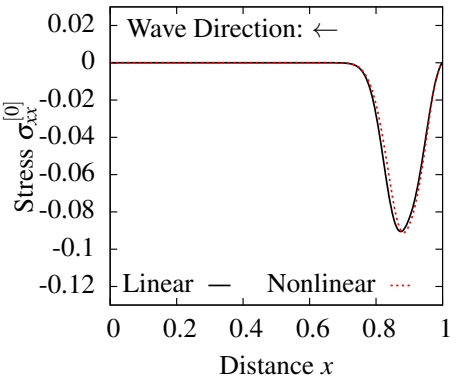

(b) $t = 2\Delta t$

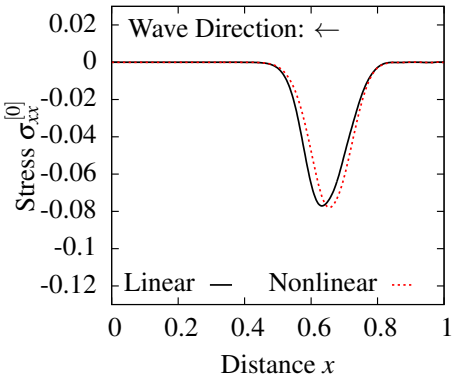

(c) $t = 4\Delta t$

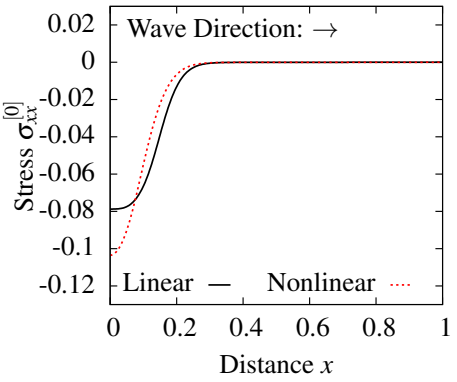

(d) Reflection, $t = 10\Delta t$

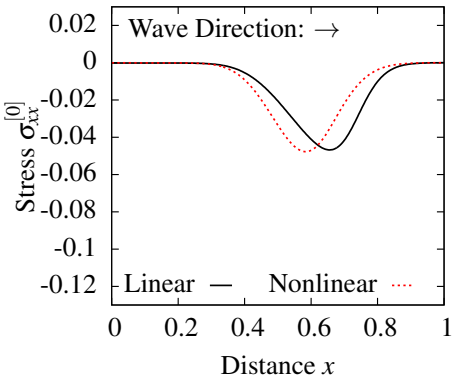

(e) $t = 15\Delta t$

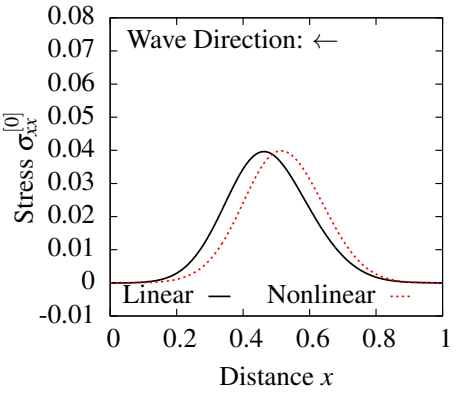

(f) $t = 23\Delta t$

Figure 3.17: Evolution of $\sigma_{xx}^{[0]}$ along the length of the rod in compression($\Delta t = 0.1$, $\sigma_1 = -0.1$, $c = 0.006$): TVE

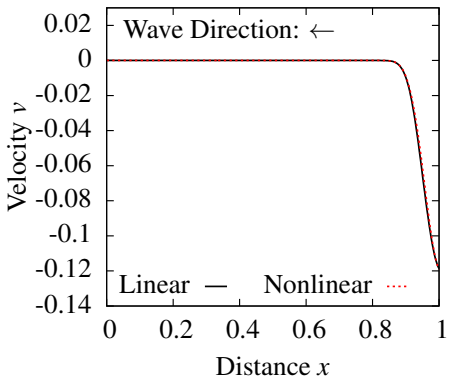

(a) $t = \Delta t$

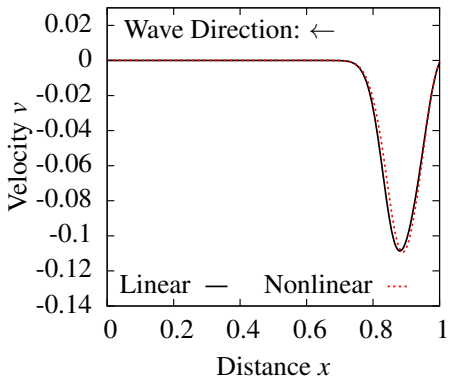

(b) $t = 2\Delta t$

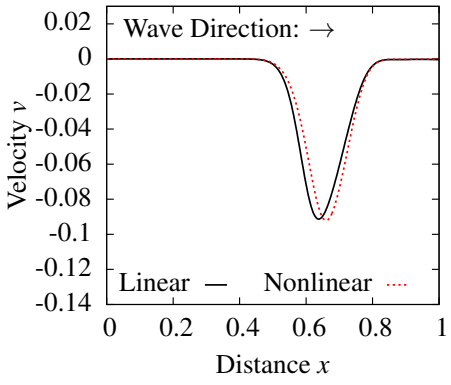

(c) $t = 4\Delta t$

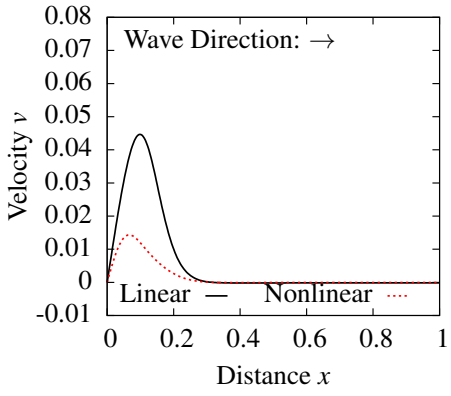

(d) Reflection, $t = 10\Delta t$

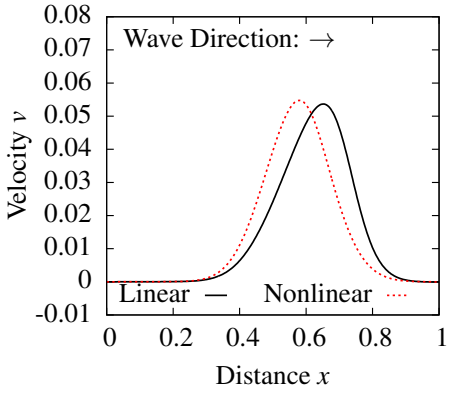

(e) $t = 15\Delta t$

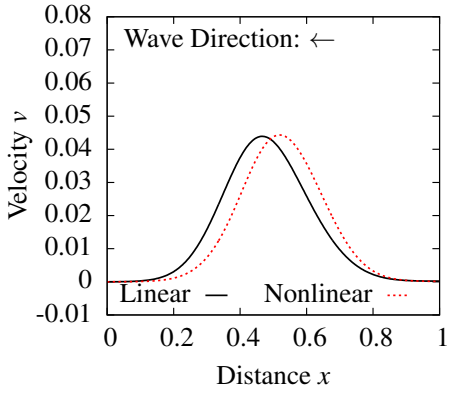

(f) $t = 23\Delta t$

Figure 3.18: Evolution of $Velocity(v)$ along the length of the rod in compression($\Delta t = 0.1$, $\sigma_1 = -0.1$, $c = 0.006$): TVE

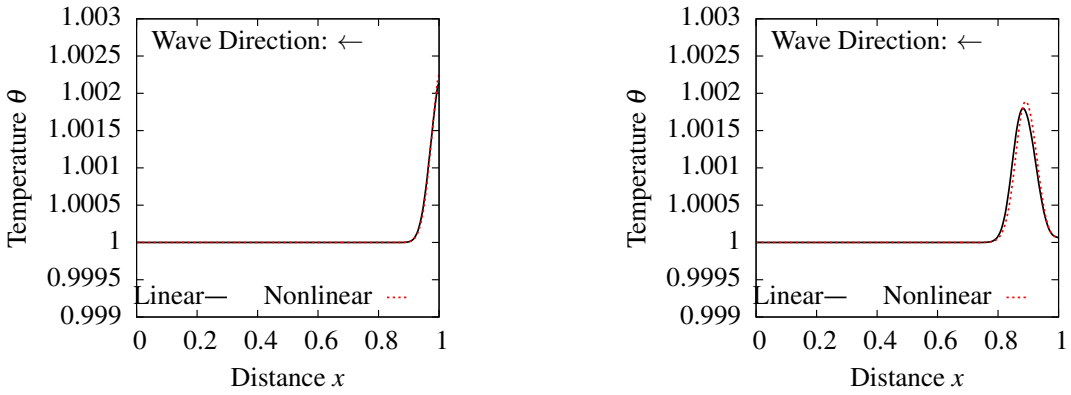

(a) $t = \Delta t$

(b) $t = 2\Delta t$

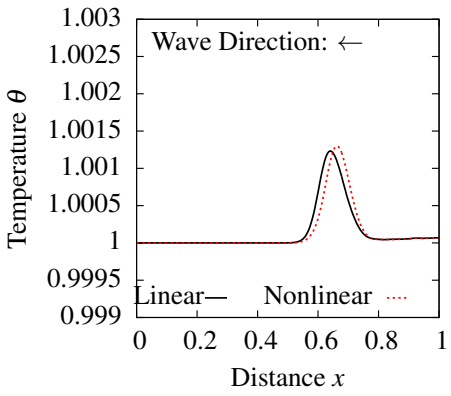

(c) $t = 4\Delta t$

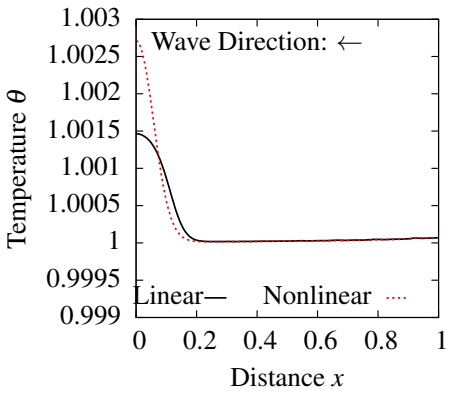

(d) Reflection, $t = 10\Delta t$

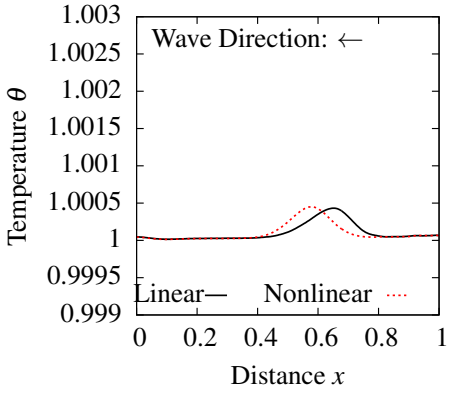

(e) $t = 15\Delta t$

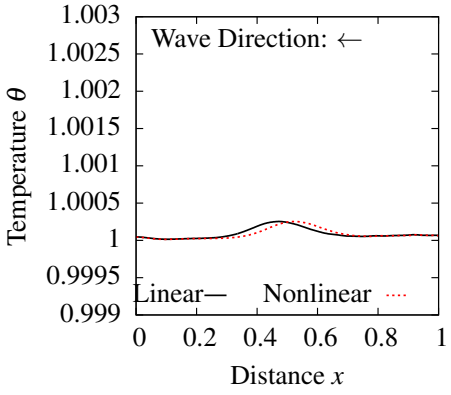

(f) $t = 23\Delta t$

Figure 3.19: Evolution of θ along the length of the rod in compression($\Delta t = 0.1$, $\sigma_1 = -0.1$, $c = 0.006$): TVE

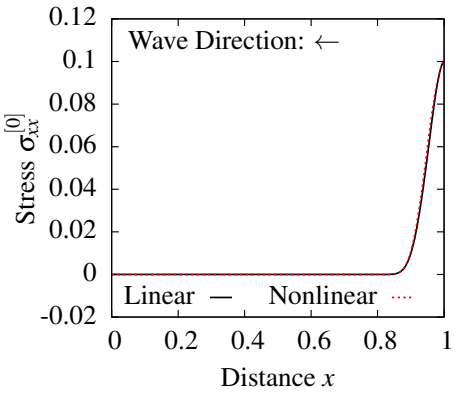

(a) $t = \Delta t$

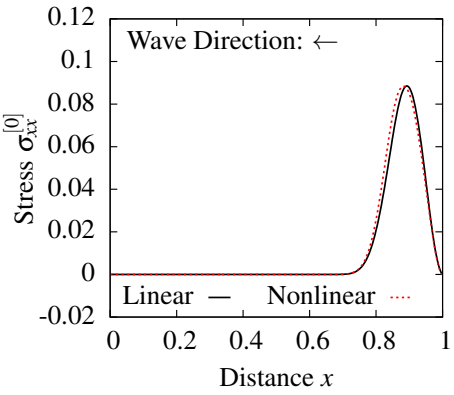

(b) $t = 2\Delta t$

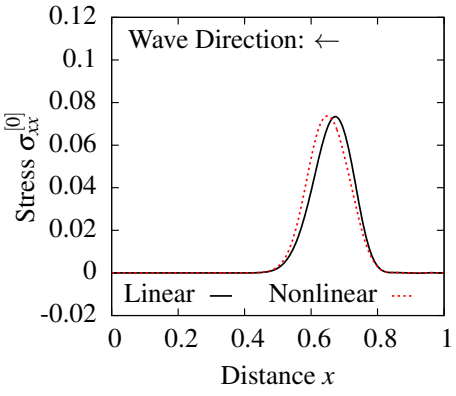

(c) $t = 4\Delta t$

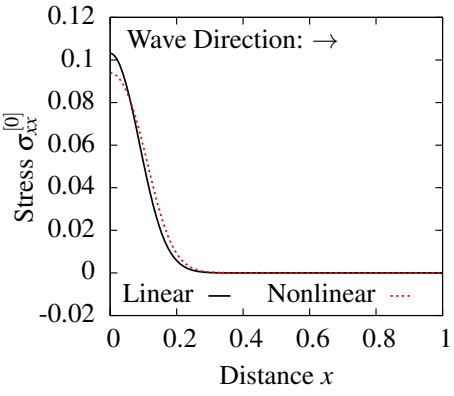

(d) Reflection, $t = 10\Delta t$

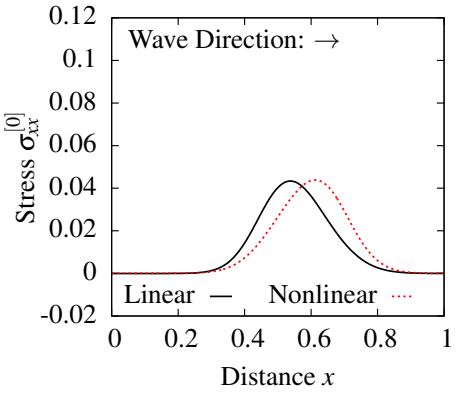

(e) $t = 15\Delta t$

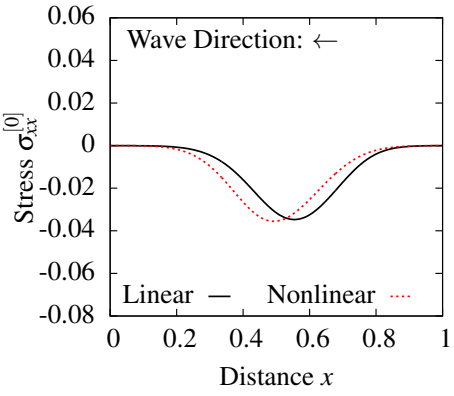

(f) $t = 23\Delta t$

Figure 3.20: Evolution of $\sigma_{xx}^{[0]}$ along the length of the rod in tension ($\Delta t = 0.1$, $\sigma_1 = 0.1$, $c = 0.006$): TVE

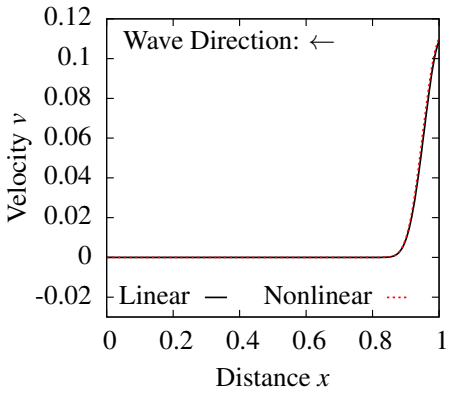

(a) $t = \Delta t$

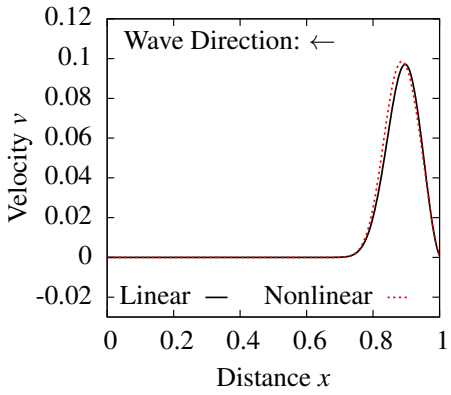

(b) $t = 2\Delta t$

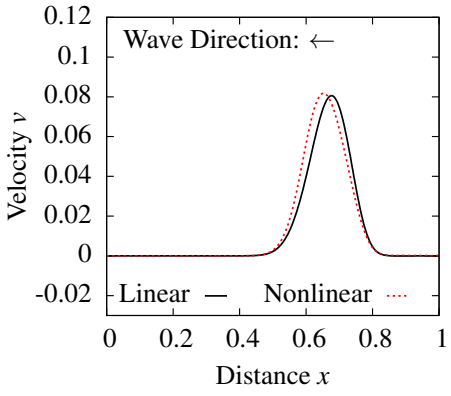

(c) $t = 4\Delta t$

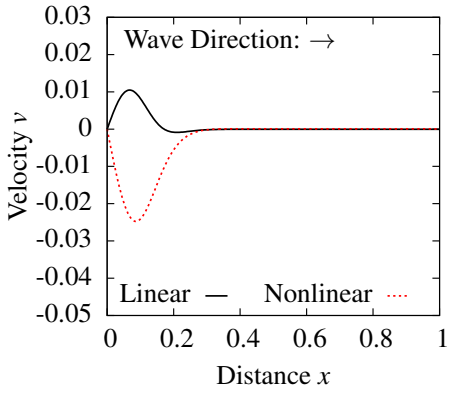

(d) Reflection, $t = 10\Delta t$

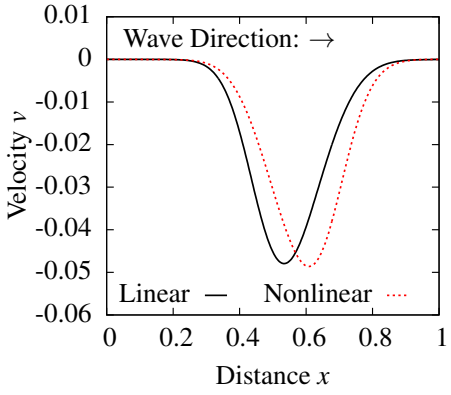

(e) $t = 15\Delta t$

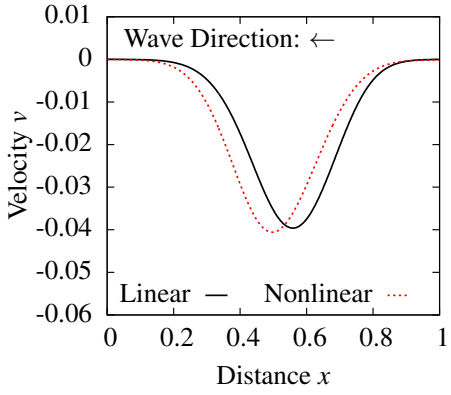

(f) $t = 23\Delta t$

Figure 3.21: Evolution of $Velocity(v)$ along the length of the rod in tension ($\Delta t = 0.1$, $\sigma_1 = 0.1$, $c = 0.006$): TVE

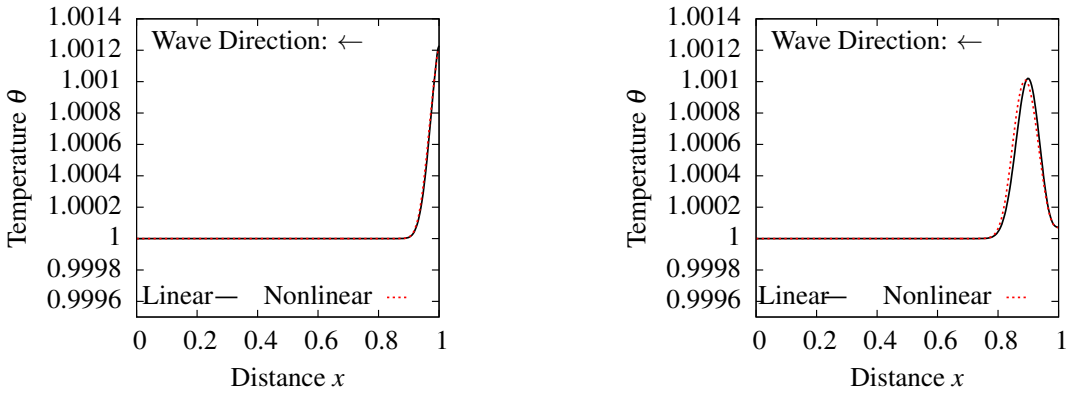

(a) $t = \Delta t$

(b) $t = 2\Delta t$

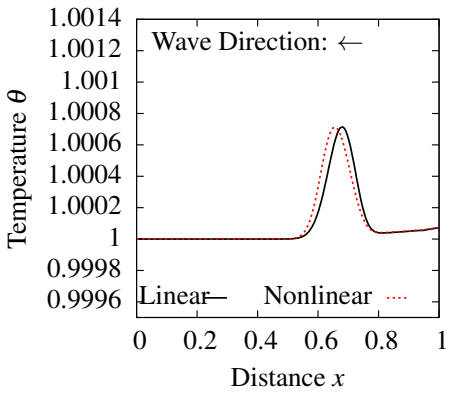

(c) $t = 4\Delta t$

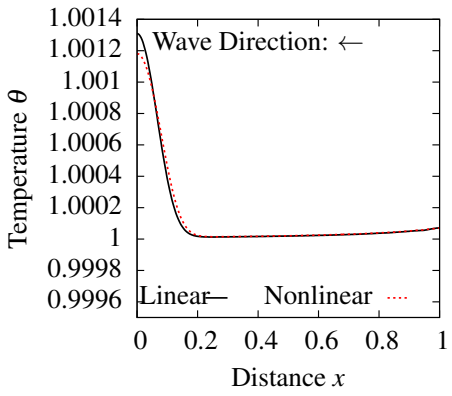

(d) Reflection, $t = 10\Delta t$

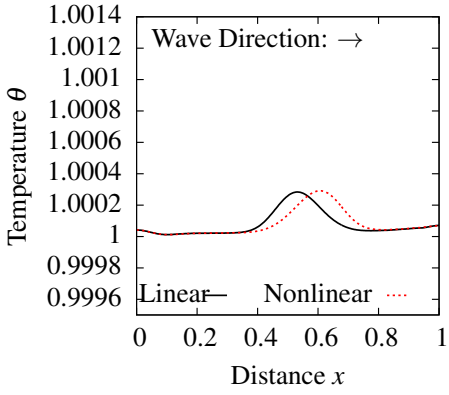

(e) $t = 15\Delta t$

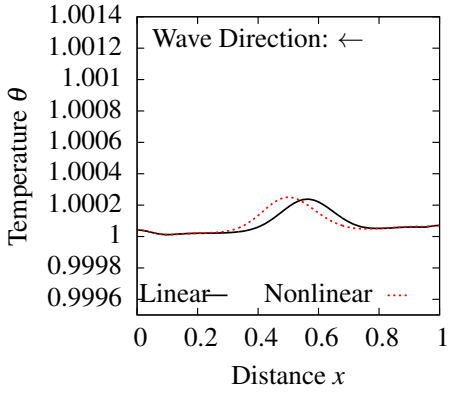

(f) $t = 23\Delta t$

Figure 3.22: Evolution of θ along the length of the rod in tension ($\Delta t = 0.1$, $\sigma_1 = 0.1$, $c = 0.006$): TVE

Loading L2: Ramp

(a) Compressive

In this study, we consider a compressive ramp of $\sigma_1 = -0.1$ over $0 \leq t \leq \Delta t$. Figures 3.23(a)-(f) show evolutions for linear and nonlinear waves at $t = \Delta t,\ 2\Delta t,\ 6\Delta t,\ 10\Delta t,\ 12\Delta t$ and $19\Delta t$.

Due to the nature of the loading, a progressive increase in density will result for the nonlinear case. This increase in density should result in slower wave speeds for the nonlinear case. At $t = 6\Delta t$ in figure 3.23(a) the nonlinear wave already lags the linear. The nonlinear reflection naturally occurs after the linear due to the slower speed of nonlinear wave. Reflections are smooth and wave shapes recover as seen in figure 3.23(e). Figure 3.23(f), at $t = 19\Delta t$, dramatically illustrates the differences in wave speeds. Figures 3.25(a)-(f) show the temperature evolutions for the same values of time as in figures 3.23(a)-(f).

The behavior of the temperature evolutions is similar to what is observed for the stress wave in figures 3.23(a)-(f). The nonlinear waves propagate more slowly than the linear waves; again, this is clearly seen in figure 3.25(f). There is a continued temperature rise within the material due to sustained load at the free end ($x = 1.0$) and the associated dissipation mechanism converting mechanical energy into entropy.

Loading L2: Tensile

In this case we consider tensile ramp loading with $\sigma_1 = 0.25$. We consider such high values of σ_1 to demonstrate more clearly the shock formation in case of nonlinear waves. In tension, such high values of σ_1 can be used as in tension we do not have the problem of instability. Dimensionless damping coefficient c is choosen to be 0.006, same as in loading L1. Because of high value of σ_1, large elongation and significant progressive reduction in density will occur. This results in substantial and progressively increased wave speed. As a consequence, the waves behind the waves are moving at faster speeds resulting in "piling up" of the waves which ultimately results in a sharp front referred to as a shock. Figures 3.26(a)-(f) show evolution of stress for both linear and nonlinear cases at times $t = \Delta t,\ 4\Delta t,\ 6\Delta t,\ 9\Delta t,\ 12\Delta t$, and $18\Delta t$. From figure 3.26(c), we

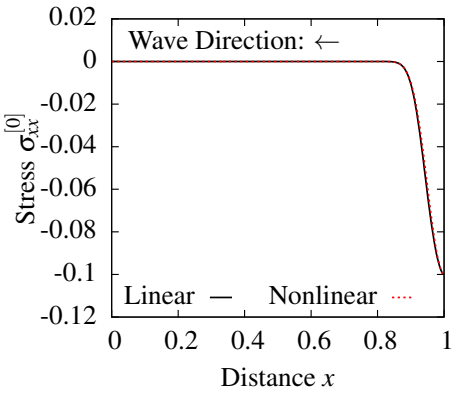

(a) $t = \Delta t$

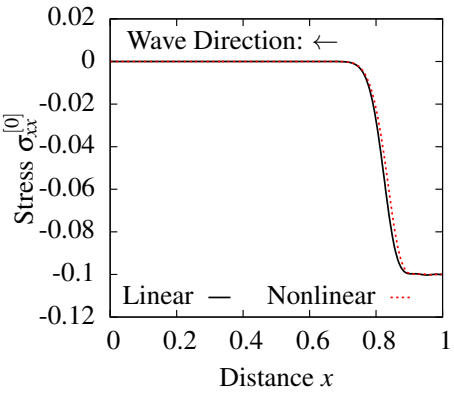

(b) $t = 2\Delta t$

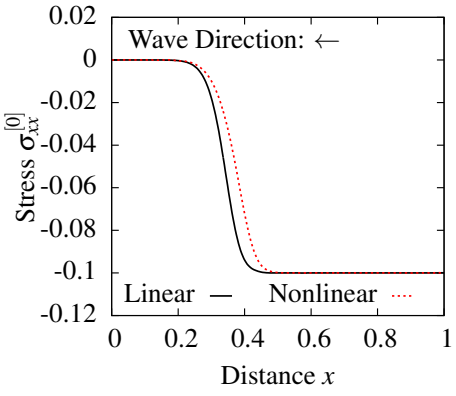

(c) $t = 6\Delta t$

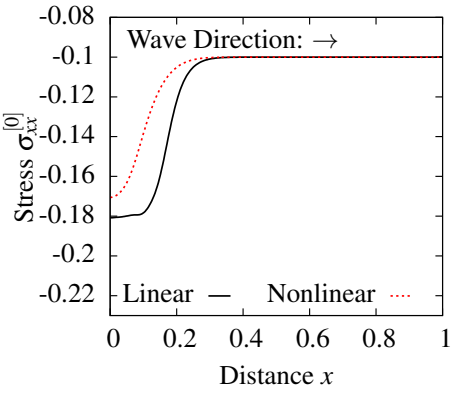

(d) Reflection, $t = 10\Delta t$

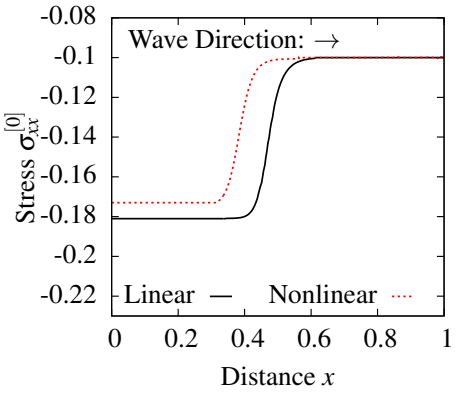

(e) $t = 12\Delta t$

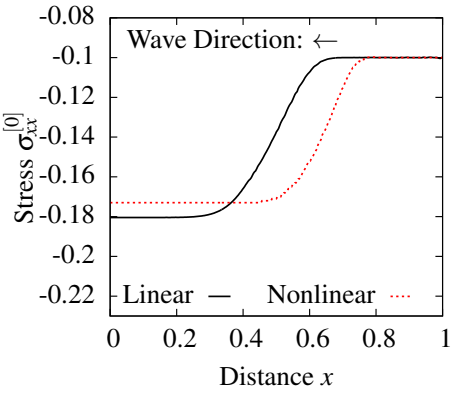

(f) $t = 19\Delta t$

Figure 3.23: Evolution of $\sigma_{xx}^{[0]}$ along the length of the rod in compression ($\Delta t = 0.1$, $\sigma_1 = -0.1$, $c = 0.006$): TVE

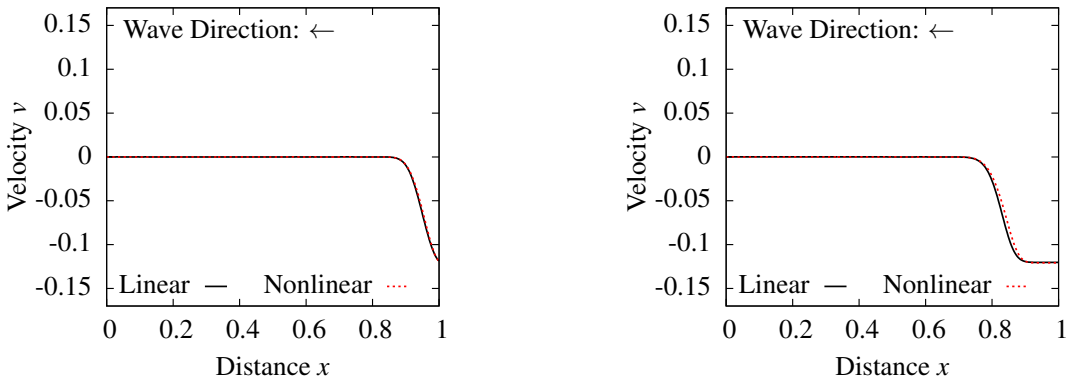

(a) $t = \Delta t$

(b) $t = 2\Delta t$

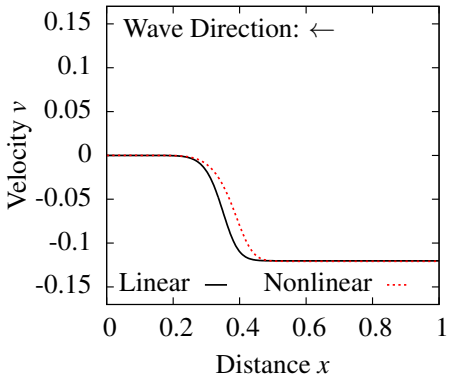

(c) $t = 6\Delta t$

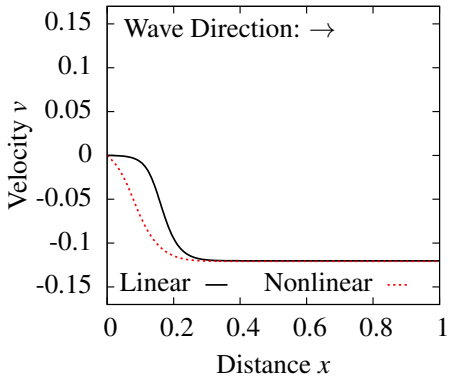

(d) Reflection, $t = 10\Delta t$

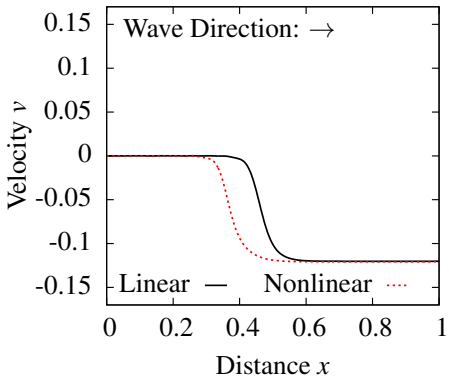

(e) $t = 12\Delta t$

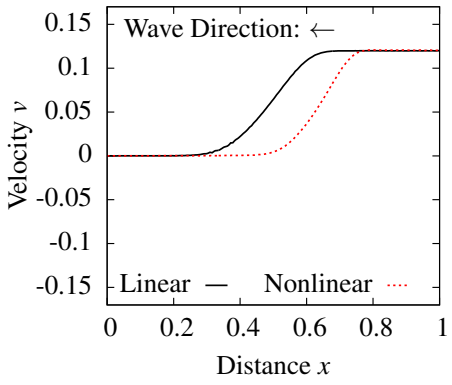

(f) $t = 19\Delta t$

Figure 3.24: Evolution of $Velocity(v)$ along the length of the rod in compression ($\Delta t = 0.1$, $\sigma_1 = -0.1$, $c = 0.006$): TVE

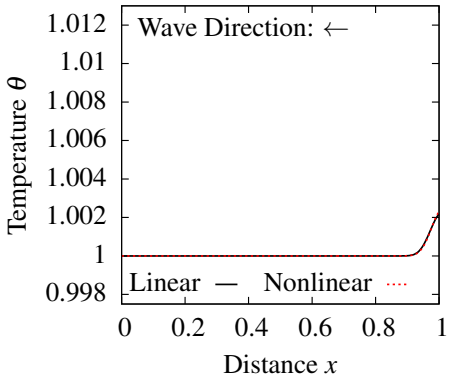

(a) $t = \Delta t$

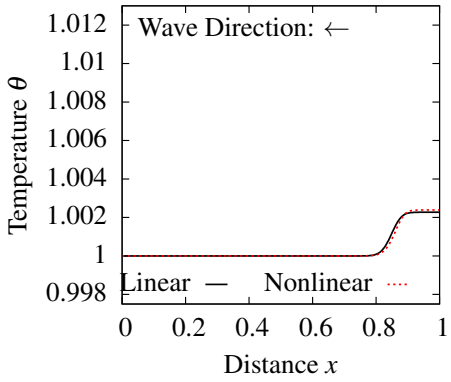

(b) $t = 2\Delta t$

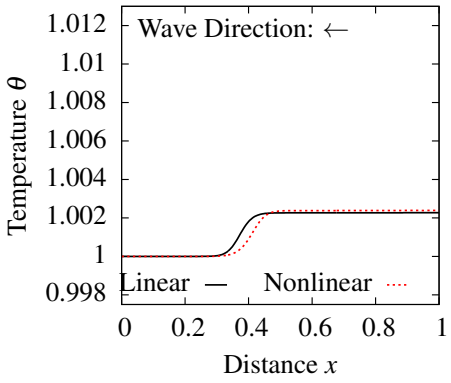

(c) $t = 6\Delta t$

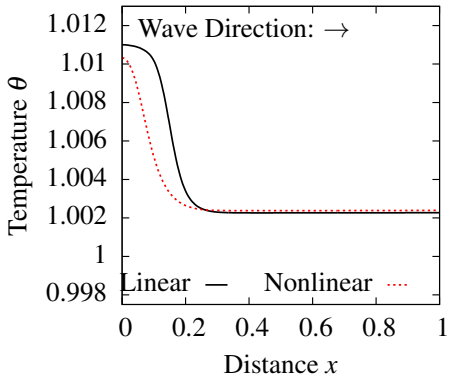

(d) Reflection, $t = 10\Delta t$

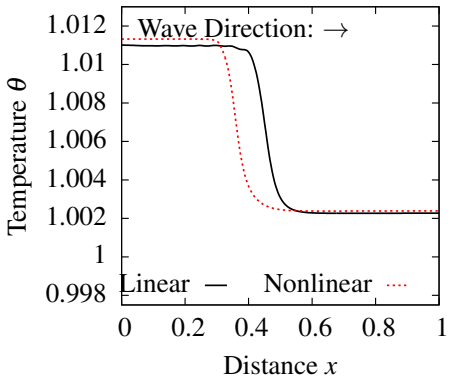

(e) $t = 12\Delta t$

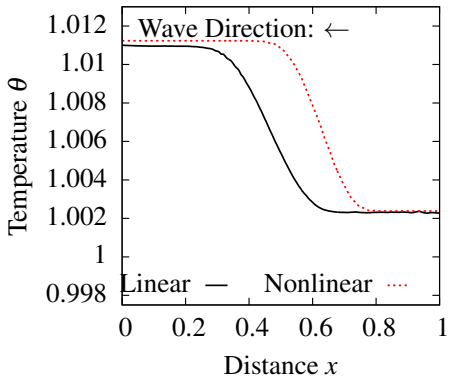

(f) $t = 19\Delta t$

Figure 3.25: Evolution of θ along the length of the rod in compression ($\Delta t = 0.1$, $\sigma_1 = -0.1$, $c = 0.006$): TVE

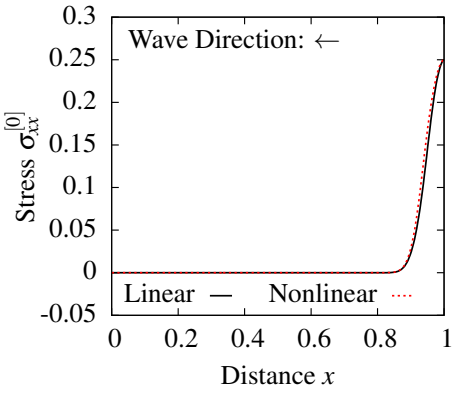

(a) $t = \Delta t$

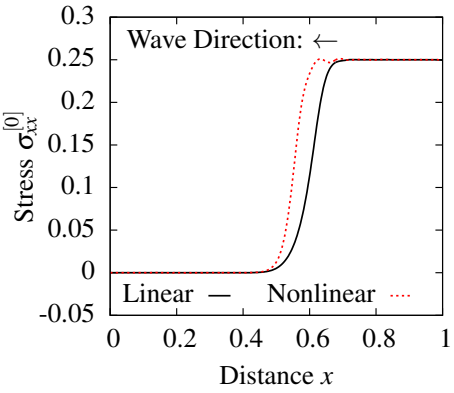

(b) $t = 4\Delta t$

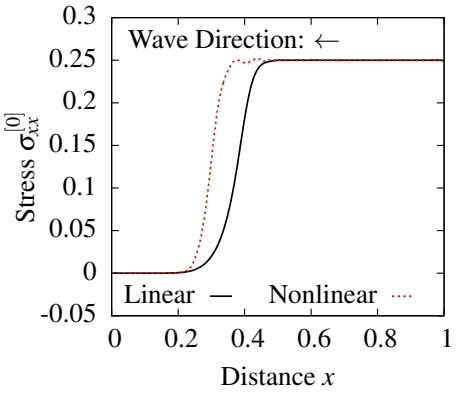

(c) $t = 6\Delta t$

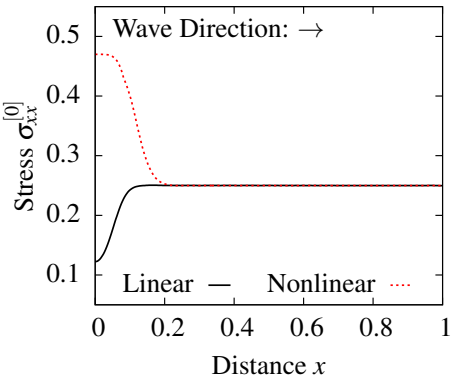

(d) Reflection, $t = 9\Delta t$

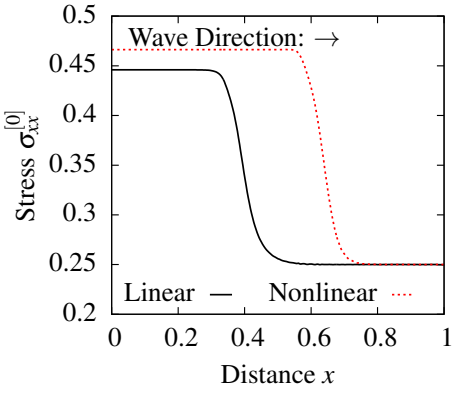

(e) $t = 12\Delta t$

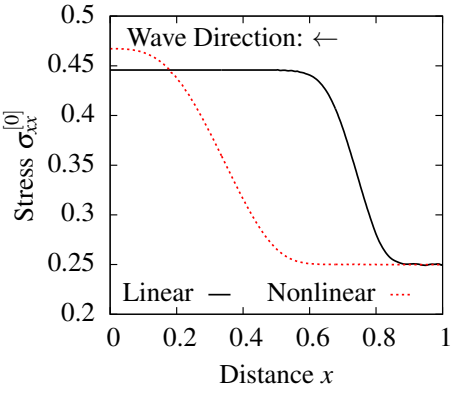

(f) $t = 18\Delta t$

Figure 3.26: Evolution of $\sigma_{xx}^{[0]}$ along the length of the rod($\Delta t = 0.1$, $\sigma_1 = 0.25$, $c = 0.006$): TVE

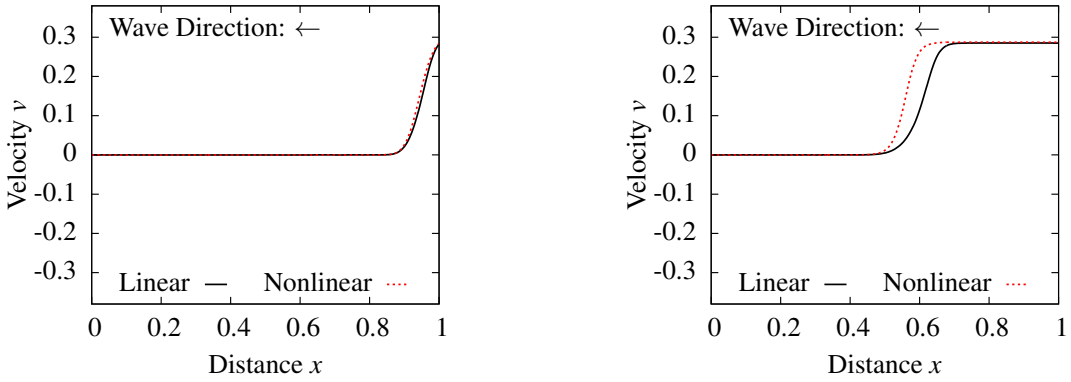

(a) $t = \Delta t$

(b) $t = 4\Delta t$

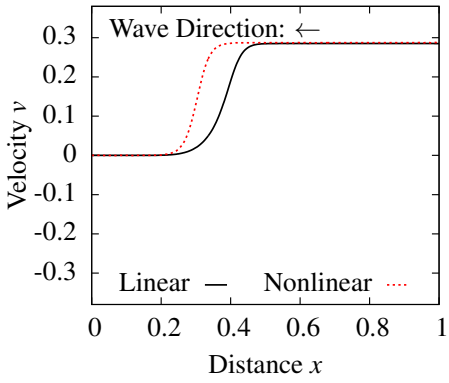

(c) $t = 6\Delta t$

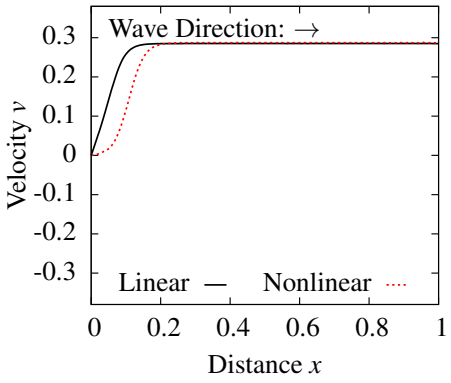

(d) Reflection, $t = 9\Delta t$

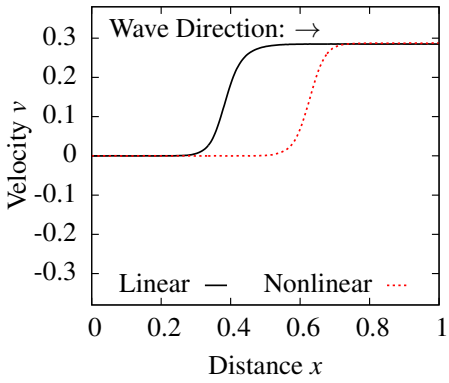

(e) $t = 12\Delta t$

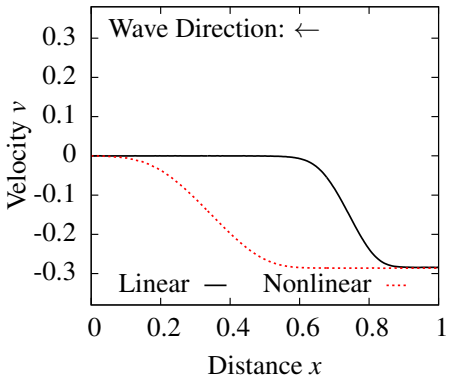

(f) $t = 18\Delta t$

Figure 3.27: Evolution of *Velocity* along the length of the rod($\Delta t = 0.1$, $\sigma_1 = 0.25$, $c = 0.006$): TVE

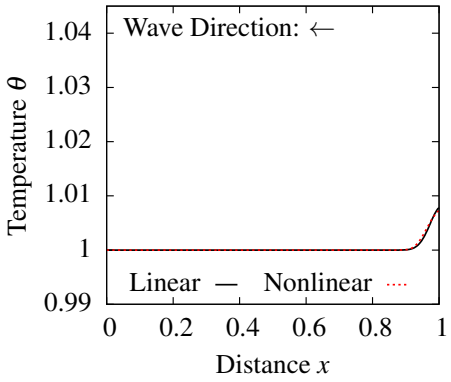

(a) $t = \Delta t$

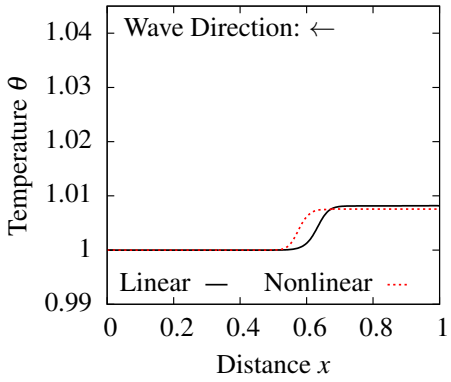

(b) $t = 4\Delta t$

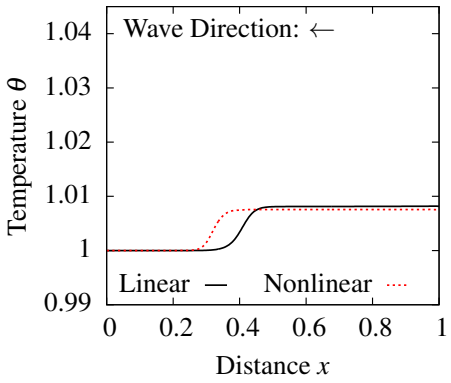

(c) $t = 6\Delta t$

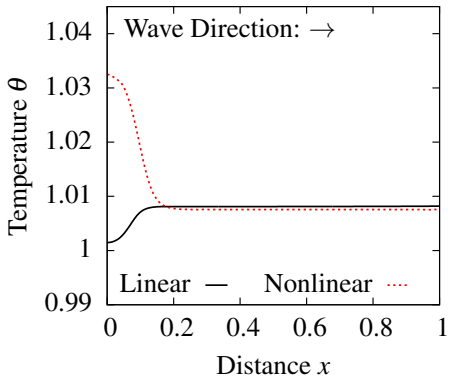

(d) Reflection, $t = 9\Delta t$

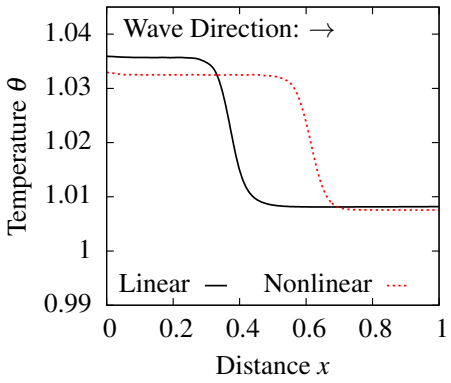

(e) $t = 12\Delta t$

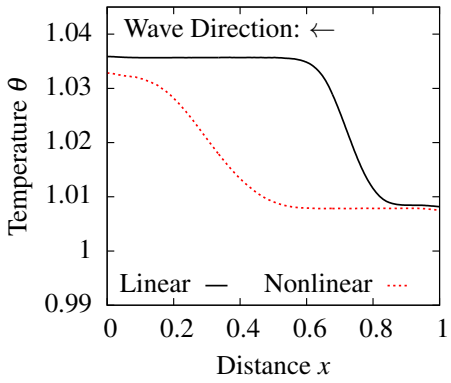

(f) $t = 18\Delta t$

Figure 3.28: Evolution of θ along the length of the rod($\Delta t = 0.1$, $\sigma_1 = 0.25$, $c = 0.006$): TVE

note that even at $t = 6\Delta t$, the nonlinear wave has steepened significantly compared to linear wave confirming shock formation. Comparing evolutions of the linear and the nonlinear waves in figures 3.26(b) and (c) for $t = 4\Delta t$ and at $t = 6\Delta t$, we note that between time $t = 4\Delta t$ to time $t = 6\Delta t$, the right portion of the wave is traveling faster than the lower left portion of the wave resulting in further steepening of the nonlinear wave in figure 3.26(c). Reflection in figures 3.26(d) are smooth and present no problem. The nonlinear waves are travelling much faster than the linear waves, hence the nonlinear waves are always ahead of the linear waves throughout the evolution. This is dramatically illustrated in figures 3.26(e) and (f). The evolution of the temperature for the same time values as in figures 3.26(a)-(f) is shown in figures 3.28(a)-(f). Shock formation in the temperature evolution and its speed of propagation are similar to the stress wave evolutions shown in figures 3.26(a)-(f). Due to the nature of the applied stress wave (ramp), the influence of dissipation can only be observed in the temperature evolution and not the stress evolution. Without dissipation, there would have been no change in temperature along the length of the rod.

3.4.4 Nonlinear Waves in TVE and TVEM

TVEM are solid with dissipation and memory (rheology). If the damping coefficient is same in TVE and TVEM, then the dissipation remains the same in both. Thus for the same damping coefficient in TVE and TVEM, the only difference in the behavior of stress wave in TVEM compared to TVE solid is due to rheology i.e. stress relaxation. In the current section comparison of nonlinear stress waves for TVE and TVEM are studied to illustrate the effect of rheology.

Loading L1: Compressive and Tensile

In this section we consider pulse loading $\sigma_1 = \pm 0.1$ with damping co-efficient $c = 0.006$ in both TVE and TVEM and $De = 0.002$ for TVEM. Figures 3.29(a)-(f) show plots of the stress pulse propagation and reflection for TVE solid and TVEM for $\sigma_1 = -0.1$ at times $t = \Delta t,\ 2\Delta t,\ 6\Delta t, 10\Delta t,$ $15\Delta t$, and $24\Delta t$. Due to damping, the wave magnitudes progressively diminish along with base elongation as evolution proceeds. For TVEM, the peak values of pulse are consistently higher due

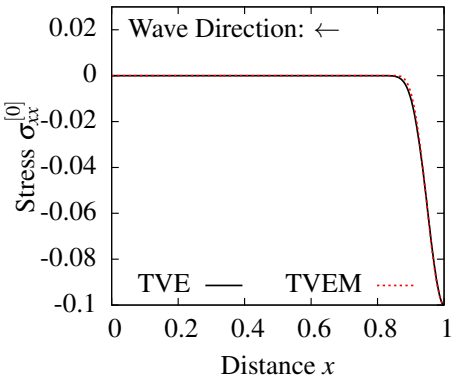

(a) $t = \Delta t$

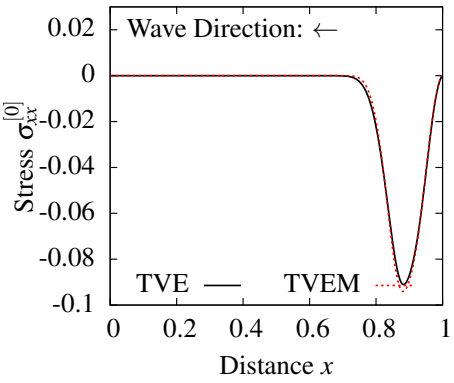

(b) $t = 2\Delta t$

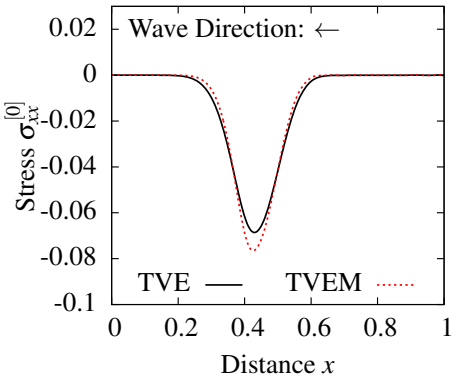

(c) $t = 6\Delta t$

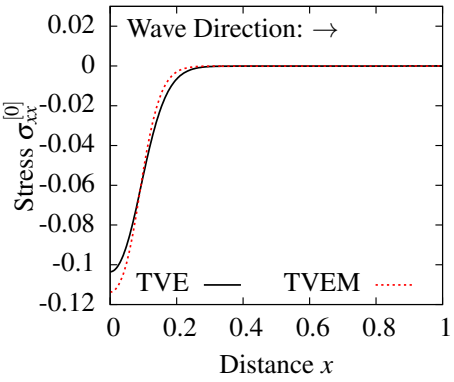

(d) Reflection, $t = 10\Delta t$

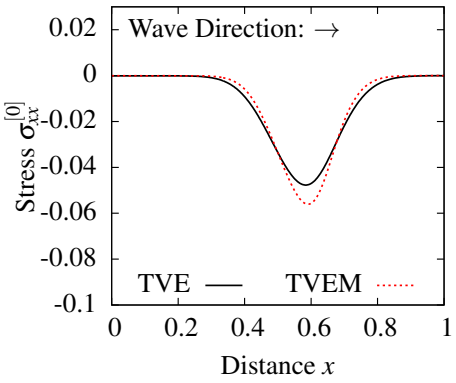

(e) $t = 15\Delta t$

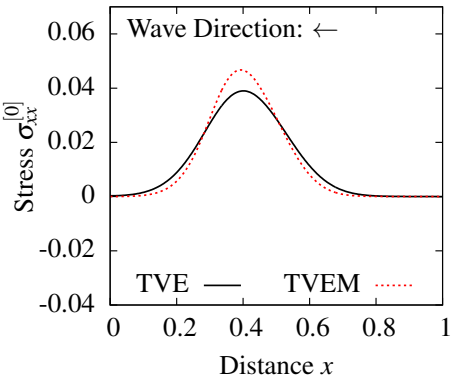

(f) $t = 24\Delta t$

Figure 3.29: Evolution of $\sigma_{xx}^{[0]}$ along the length of the rod in compression($\Delta t = 0.1$, $\sigma_1 = -0.1$, $c = 0.006$, $De = 0.002$):TVE , TVEM

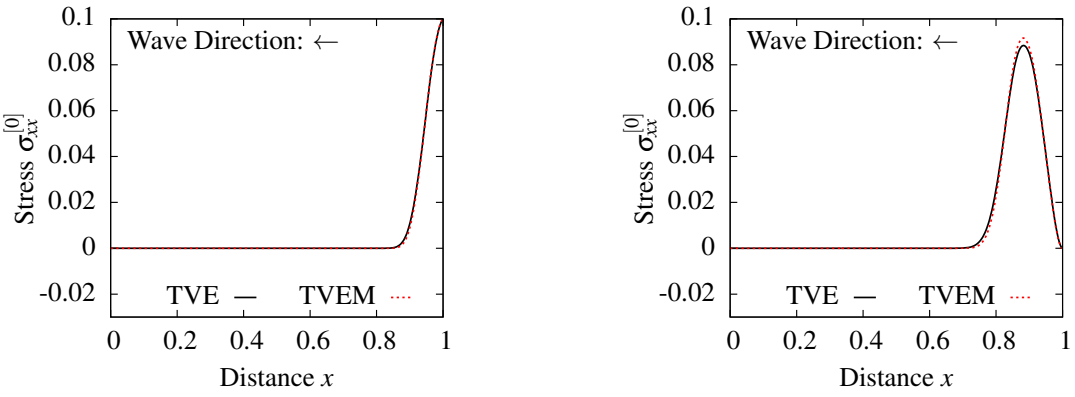

(a) $t = \Delta t$

(b) $t = 2\Delta t$

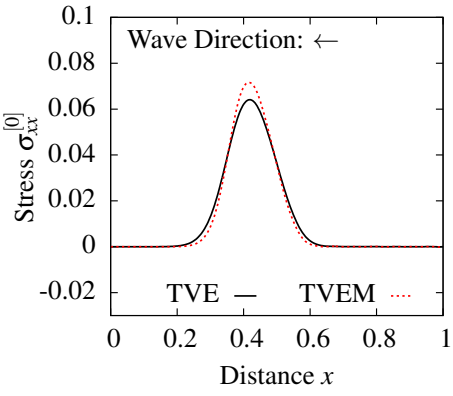

(c) $t = 6\Delta t$

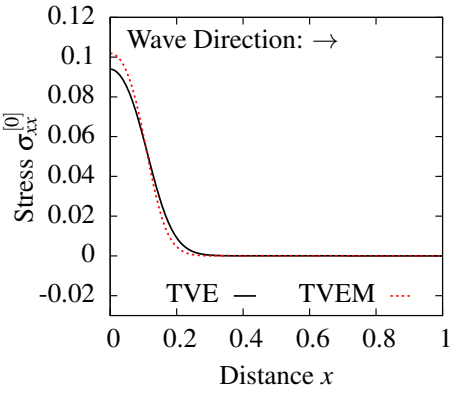

(d) Reflection, $t = 10\Delta t$

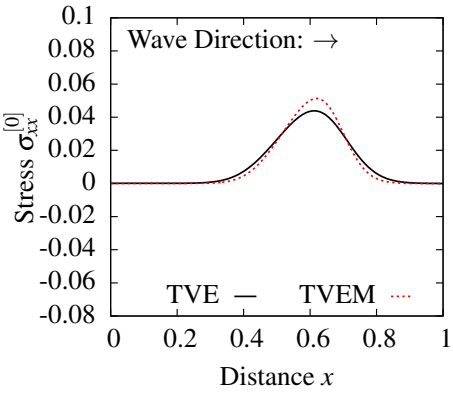

(e) $t = 15\Delta t$

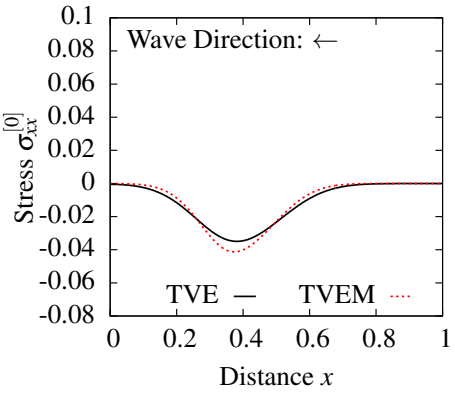

(f) $t = 24\Delta t$

Figure 3.30: Evolution of $\sigma_{xx}^{[0]}$ along the length of the rod in tension($\Delta t = 0.1$, $\sigma_1 = 0.1$, $c = 0.006$, $De = 0.002$):TVE , TVEM

to rheology, i.e. stress relaxation. In this case, the relaxation time (De) controls the relaxed state and hence additional time is required to achieve the same lower peak values as for TVE solid. For example, in figures 3.29(a), (b), (e), and (f), the peaks corresponding to TVEM (dashed line) will achieve the same lower values as the corresponding peaks for TVE solid (solid lines) if more time was allowed to elapse. Secondly, we note that the supports of the stress waves for TVEM are shorter than those of the corresponding TVE solid.

Similar results are presented in figures 3.30(a)-(f) for $\sigma_1 = 0.1$ i.e. tensile wave. The behavior of the stress wave in TVE solid and TVEM is similar to what has been described for compressive stress wave.

Loading L2: Compressive and Tensile

In this case we consider ramp loading of magnitude $\sigma_1 = -0.05$ in compression and $\sigma_1 = 0.1$ in tension. The damping co-efficient is choosen to be $c = 0.006$ and $De = 0.004$. Figure 3.31(a), (b), (c), (d), (e), and (f) shows the comparison of wave propagation in TVE and TVEM for $t = \Delta t,\ 2\Delta t,\ 6\Delta t, 9\Delta t,\ 12\Delta t$, and $23\Delta t$. Here we note that given the nature of loading (ramp), the amplitude of the wave is always the same in both TVE and TVEM, but the relaxation effect due to the relaxation time (De) results in the wave being more steep in TVEM at a given instant compared to the wave in TVE where the slope of ramp progressively decreases with time. Due to the relaxation effect in TVEM, the wave will require additional time to reach the same slope as TVE at any given instant of time. Similar results are presented in figures 3.32(a)-(f) for $\sigma_1 = 0.1$ i.e. tensile wave. The behavior of the stress wave in TVE solid and TVEM is similar to what has been described for compressive stress wave.

3.4.5 Linear and Nonlinear Waves in TVEM

In this section we consider the study for linear and nonlinear waves in TVEM for L2 loading i.e. ramp loading. The results in this section are similar to the results shown for TVE, but including the relaxation effect that was studied in section 3.4.3. For loading L2 we consider $c = 0.006$,

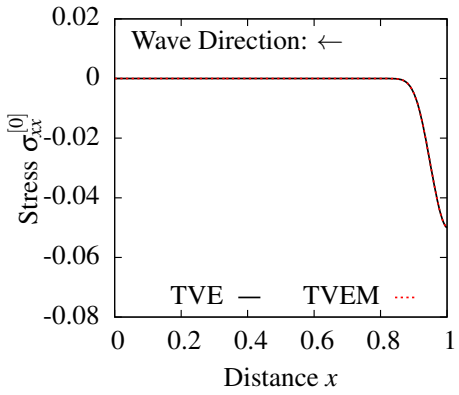

(a) $t = \Delta t$

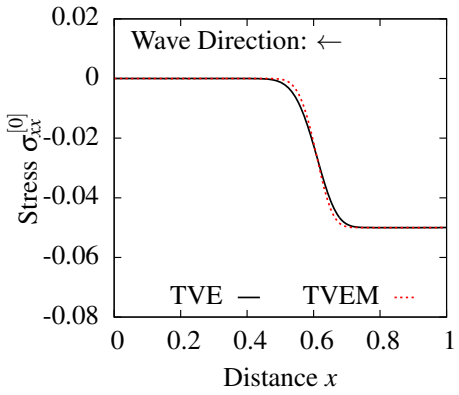

(b) $t = 4\Delta t$

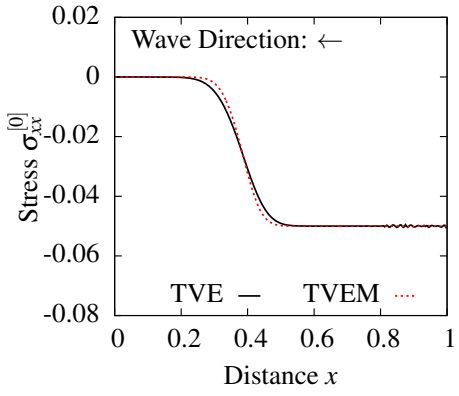

(c) $t = 6\Delta t$

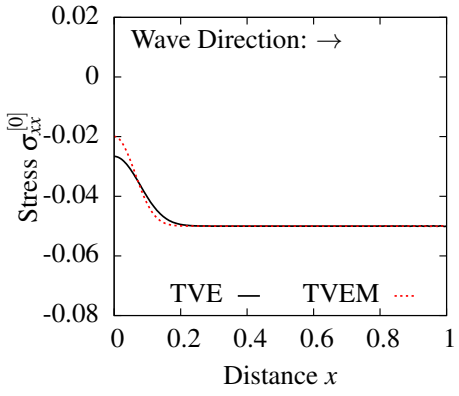

(d) Reflection, $t = 9\Delta t$

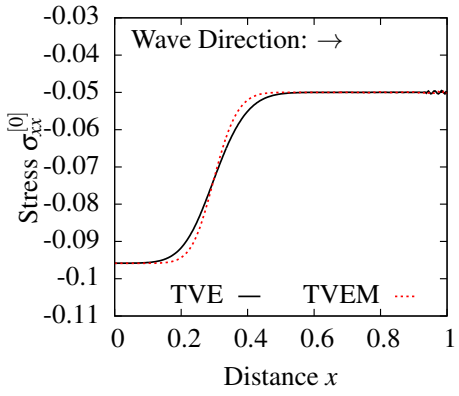

(e) $t = 12\Delta t$

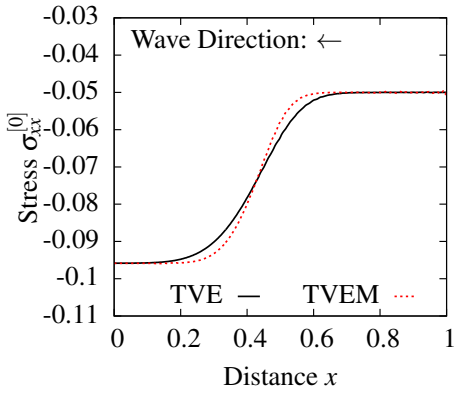

(f) $t = 23\Delta t$

Figure 3.31: Evolution of $\sigma_{xx}^{[0]}$ along the length of the rod in compression($\Delta t = 0.1$, $\sigma_1 = -0.05$, $c = 0.006$, $De = 0.004$):TVE , TVEM

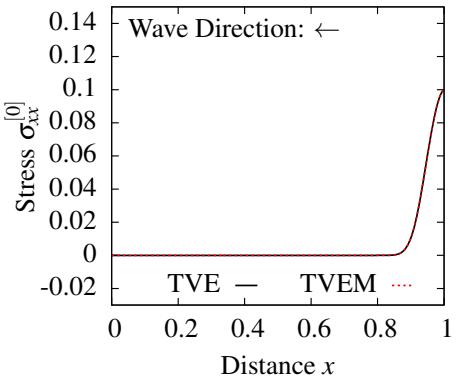

(a) $t = \Delta t$

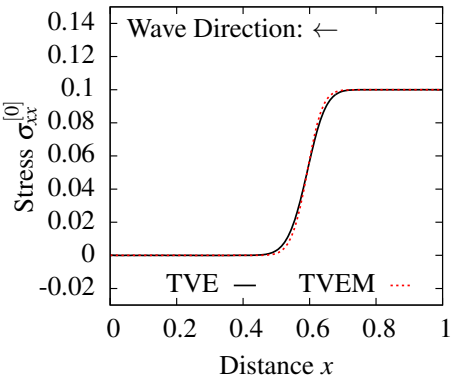

(b) $t = 4\Delta t$

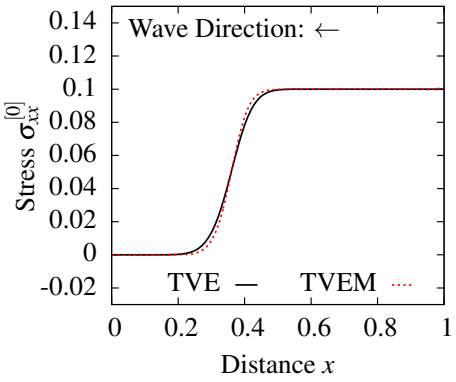

(c) $t = 6\Delta t$

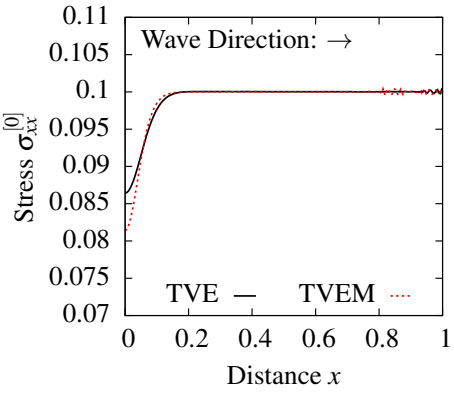

(d) Reflection, $t = 8\Delta t$

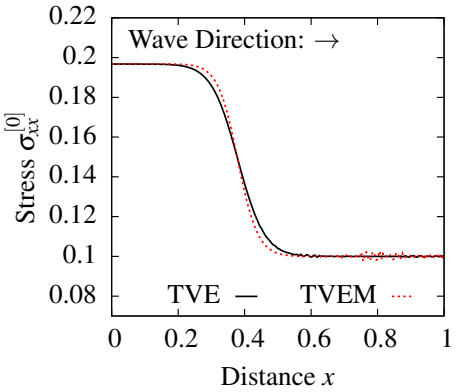

(e) $t = 12\Delta t$

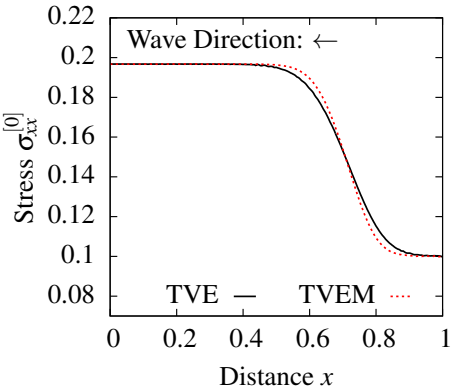

(f) $t = 19\Delta t$

Figure 3.32: Evolution of $\sigma_{xx}^{[0]}$ along the length of the rod in tension($\Delta t = 0.1$, $\sigma_1 = 0.1$, $c = 0.006$, $De = 0.004$):TVE , TVEM

$De = 0.002$, $\sigma_1 = 0.25$ (tension) and $\sigma_1 = 0.1$ (compression). Computed evolution for linear and nonlinear cases are shown in figures 3.33(a)-(f) for stress in tension and figures 3.34(a)-(f) for stress in compression. We observe that the behavior is similar to L2 tensile and compressive loading for TVE figure 3.26(a)-(f) and figure 3.23(a)-(f) and hence not repeated for brevity.

3.4.6 Evolution for Large Values of Time: Tensile

In this section we present studies for evolution of tensile ramp loading in TVE and TVEM for large values of time. We study evolutions computed for 4000 time steps i.e. 400 units of time that corresponds to 2.8 seconds as t_0 in this case is 0.007 seconds. We choose tensile load $\sigma_1 = 0.3$, damping coefficient $c = 0.006$, $\Delta t = 0.1$. The space-time strip element discretization for these studies are the same as the previous studies with $k_1 = k_2 = 2$, $p = 9$ for both TVE solid and TVEM.

Figure 3.35 shows plots of displacement u at $x = 1.0$ versus time t for $0 \leq t \leq 400$ for TVE solid for $f = 0$ (linear case) and $f = 1$ (nonlinear case). Similar plots for linear and nonlinear cases for TVEM at $De = 0.0008$ are shown in figure 3.36. From these figures , we observe that linear and nonlinear responses are drastically different for TVE as well as for TVEM in terms of peak negative and positive displacement values and mean values of displacements. The residual functional I values for each space-time strip are $O(10^{-7})$ or lower confirming the time accuracy of the evolution. Thus, the results reported for TVE solid and TVEM are free of numerical dispersion. Upon further evolution, the stationary states for TVE solid and TVEM evolution studies are obtained. The displacement values $({}^s u|_{x=1.0})$ corresponding to the stationary states are

TVE Solid:

$$ {}^s u|_{x=1.0} = 0.3077 \quad \text{(linear)} $$

$$ {}^s u|_{x=1.0} = 0.2650 \quad \text{(nonlinear)} $$

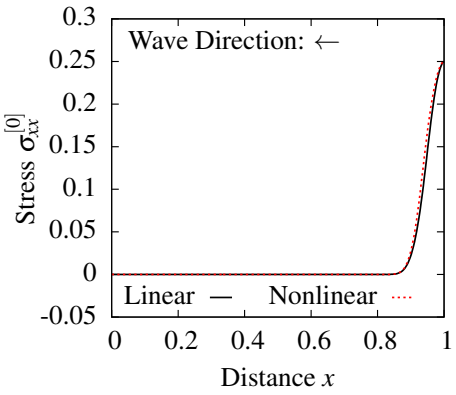

(a) $t = \Delta t$

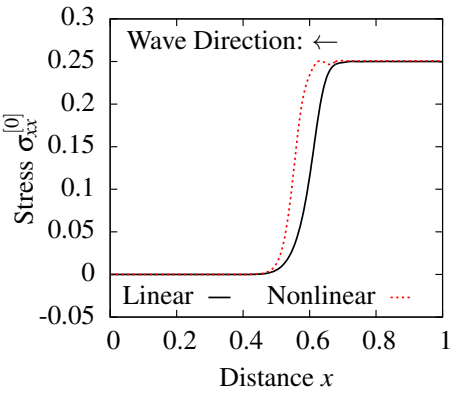

(b) $t = 4\Delta t$

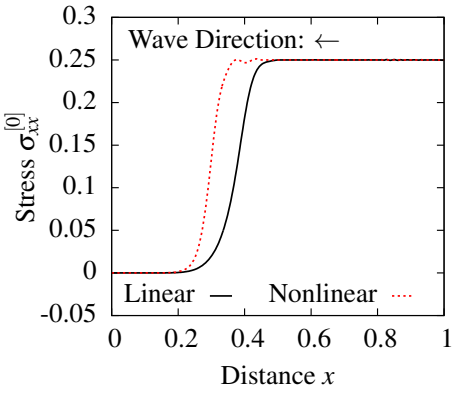

(c) $6\Delta t$

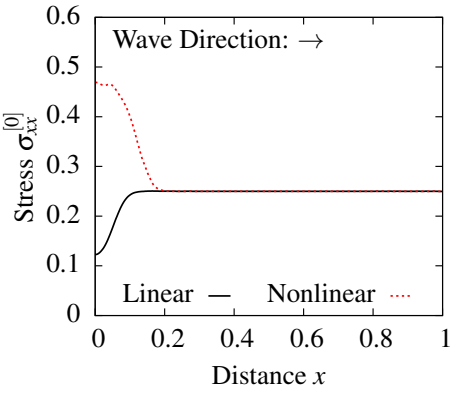

(d) Reflection, $9\Delta t$

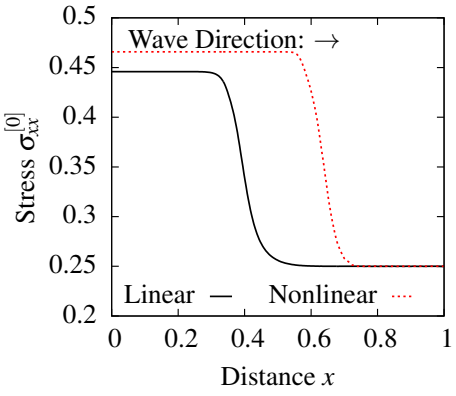

(e) $t = 12\Delta t$

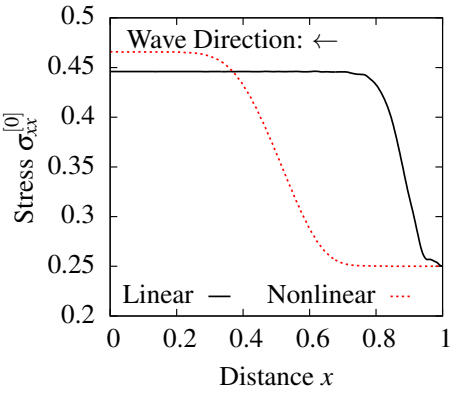

(f) $t = 17\Delta t$

Figure 3.33: Evolution of $\sigma_{xx}^{[0]}$ along the length of the rod in tension($\Delta t = 0.1$, $\sigma_1 = 0.25$, $c = 0.006$, $De = 0.002$): TVEM

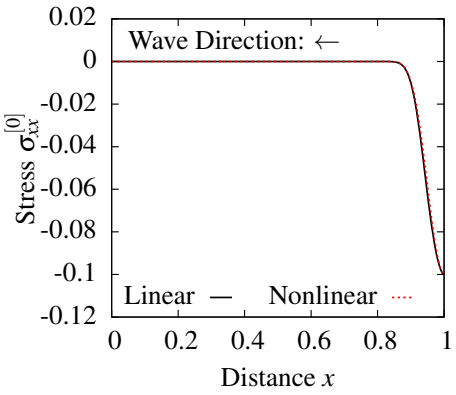

(a) $t = \Delta t$

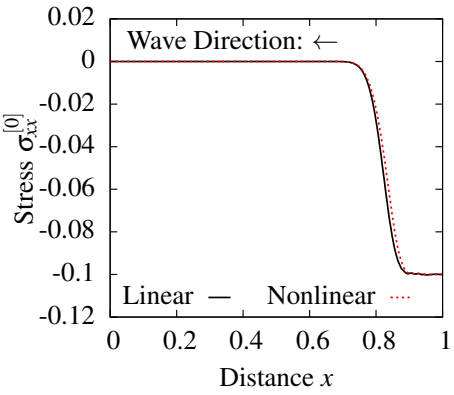

(b) $t = 2\Delta t$

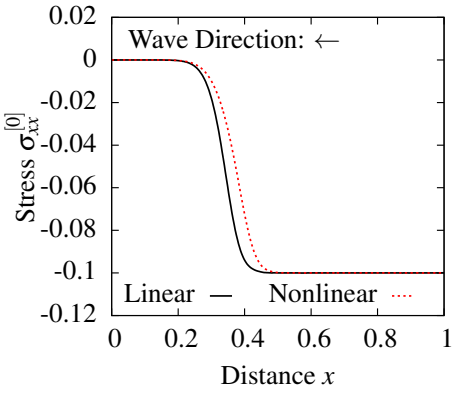

(c) $6\Delta t$

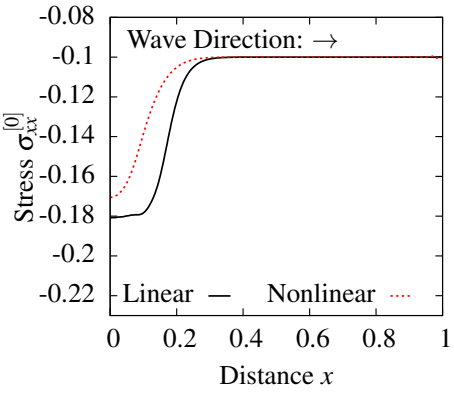

(d) Reflection, $10\Delta t$

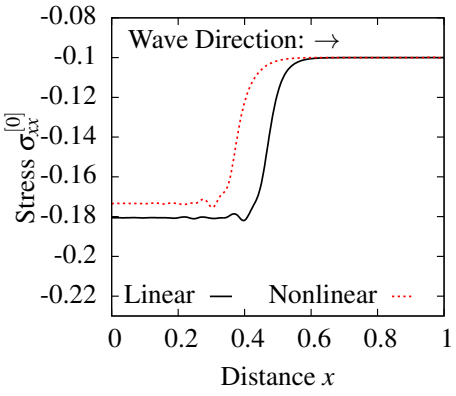

(e) $t = 12\Delta t$

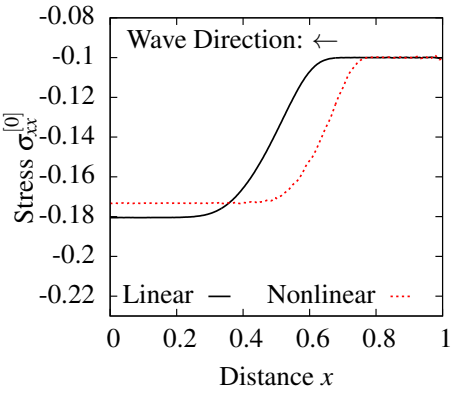

(f) $t = 19\Delta t$

Figure 3.34: Evolution of $\sigma_{xx}^{[0]}$ along the length of the rod in compression($\Delta t = 0.1$, $\sigma_1 = -0.1$, $c = 0.006$, $De = 0.002$): TVEM

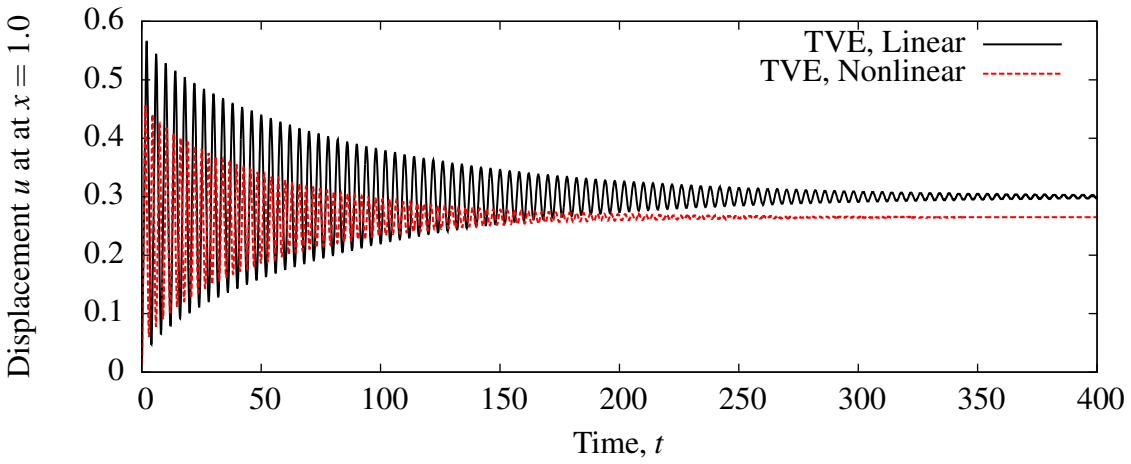

Figure 3.35: Displacement u at $x = 1.0$: TVE, L2, $\Delta t = 0.1$, $\sigma_1 = 0.3$

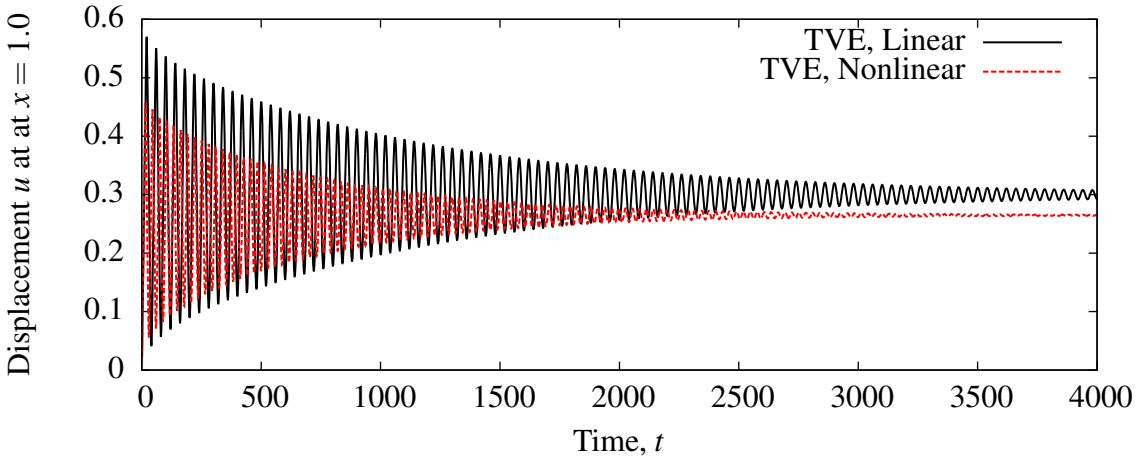

Figure 3.36: Displacement u at $x = 1.0$: TVEM, L2, $\Delta t = 0.1$, $\sigma_1 = 0.3$

TVEM Solid:

$$^{s}u|_{x=1.0} = 0.3077 \quad \text{(linear)}$$

$$^{s}u|_{x=1.0} = 0.2657 \quad \text{(nonlinear)}$$

These values of displacements at $x = 1.0$ are almost the same as the mean values of the displacements in figures 3.35 and 3.36. We observe that: (i) displacement ($^{s}u|_{x=1.0}$) for the nonlinear case is lower than linear case as expected due to increase of stiffness caused by tensile stress field which results in lower values of displacement. This holds true in figures 3.35 and 3.36 as well during the

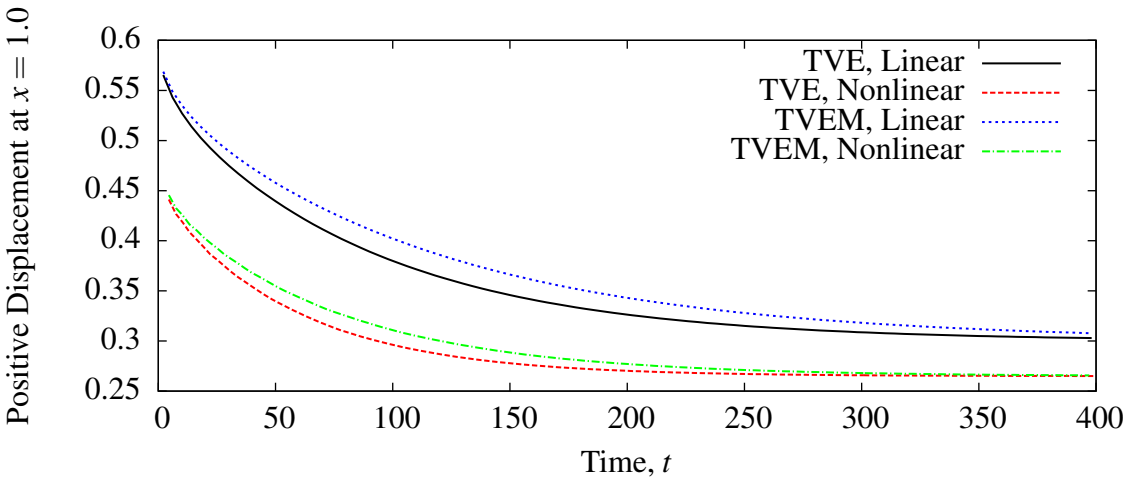

Figure 3.37: Peak Positive Displacement of Free End $(u|_{x=1.0})$: TVE and TVEM, L2, $\Delta t = 0.1$, $\sigma_1 = 0.3$

evolution. (*ii*) In the case of TVEM, the displacement values for ${}^s u|_{x=1.0}$ are exactly the same as those for TVE solid. This is due to the fact that upon complete stress relaxation the TVEM behavior is the same as the behavior of TVE solid. However, the peak values in figure 3.36 for linear as well as nonlinear cases are not the same as the corresponding values in figure 3.35. Figure 3.37 shows plots of peak positive displacement of the free end $(u|_{x=1.0})$ as a function of time t for TVE solid and TVEM for both linear and nonlinear cases.

The differences in the displacement values for TVE solid and TVEM solid for linear case ($f = 0$) are obviously due to rheology in TVEM. The same is true for TVE solid and TVEM for the nonlinear case. Drastically different values of displacements at $x = 1.0$ for linear and nonlinear cases for both TVEM and TVE solid are quite obvious from figure 3.37 as well as figures 3.35 and 3.36.

Remarks

For all the numerical performed for TVEM, the value of the Deborah used is quite small. The values considered for the studies were based on realistic judgement depending on the material choosen for the studies. Higher value of deborah number's can be used for material's like memory foam that is characterized with high value of relaxation time.

Chapter 4

Summary and Conclusions

This work presents 1D wave propagatioon studies usiing experimentally determined thermodynamic pressure $p(\rho)$ for hard rubber as equation of state. Mathematical models in R^3 and R^1 are presented with complete details for compressible TE, TVE and TVEM solids. The second Piola-Kirchhoff stress and Green's strain tensors are used as conjugate pairs in the conservation and balance laws. The constitutive theory for the second Piola-Kirchhoff stress tensor is assumed to be linear function of Green's strain tensor for TE. For TVE and TVEM the constitutive theories are assumed to be linear in strain tensor, its material derivative, and the material derivative of the second Piola-Kirchhoff stress tensor. The constitutive theory used for heat vector is simple Fourier heat conduction law with constant thermal conductivity.

The space-time integral formulation based on space-time residual functional for a space-time strip with time marching is highly meritorious in (a) reducing the problem size (b) ensuring accurate evolution for the current space-time strip before time marching is commenced. When the space-time residual functional is $O(10^{-6})$ or lower only then time marching is commenced. This ensures time accurate evolution during the entire range of time. The orders of the scalar product approximation space in space and time (k_1, k_2) are chosen to be 2 so that the space-time integrals over the discretization of the space-time strip are Riemann in space and Lebeque in time. However, due to smoothness of evolutions we expect the convergence of the solution of class C^1 in time to

solutions of C^2 in time in the weak sense

From the numerical studies we observe the following.

(1) With the incorporation of the actual equation of state in the mathematical models it can be shown that the assumption of mean normal stress for equilibrium stress assumed in [1] over predicts the speed of stress waves propagation. This is as a result of the difference in modulus E used in both the studies. In the published work [1], the modulus $E = \frac{3}{2}^d \underset{\sim}{E}$ while in the current work E=$(0.968)^d \underset{\sim}{E}$ in tension and E= $(0.954)^d \underset{\sim}{E}$ in compression is used.

(2) Additionally the assumption of mechanical pressure in the published work [1] over estimates the density change in the rod when subjected to tensile load and under predicts the density change when subjected to compressive loading which also effects the speed at which the waves propagate.

(3) In thermoelastic solid nonlinear waves maintain their amplitude and support for all space-time strips as well as for extended time evolution confirming that the computational process utilized here is relatively free of numerical dispersion.

(4) In thermoviscoleastic material the compressive nonlinear waves lag the linear waves due to increased density, hence reduced wave speed. And the tensile nonlinear waves lead the linear waves because of reduced density, hence increased wave speed.

(5) The difference in the speed of wave propagatioon for linear and nonlinear cases and the change in density for tensile and compressive load for thermoviscoelastic material without memory applies for thermoviscoelastic material with memory.

(6) In both thermoviscoelastic solid with memory as well as the thermoviscoelastic solids without memory, the wave amplitude decays and the wave base elongates as evolution proceeds due to dissipation i.e. conversion of mechanical energy into entropy which results in temperature rise along the length of the rod. Complex temperature distribution due to dissipation

is free of oscillations and is simulated without any difficulty together with the deformation field.

(7) Progressively changing density due to compressibility or elongation results in progressively changing wave speed which finally results in piling up of waves forming a shock. This phenomenon exists in compressive as well as tensile nonlinear waves when the matter is compressible. Compared to linear waves, in the case of nonlinear compressive waves the shock formation occurs behind the linear wave. Whereas in the case of tensile wave the shocks are formed ahead of the linear wave. Since in tension, large values of σ_1 can be used without occurance of instability, the studies shown in figures 3.33(a)-(f) for L2 loading with $\sigma_1 = 0.25$ clearly show the formation of shock wave ahead of the linear wave.

(8) In the case of TVEM, the results are similar to TVE solid except that in case of TVEM momentarily higher stress magnitudes are observed during evolutions because of rheology.

(9) From the extended time evolutions shown in figures 3.35 and 3.36 for TVE and TVEM (for L2 loading) for 4000 time steps we make some remarks

   (1) Transient response has dramatically higher displacements than the static response. A rod of length one unit is elongated as much as 0.58 units during evolution.

   (2) Evolutions are smooth and free of numerical dispersion and are time accurate. This is confirmed by I valules $O(10^{-6})$ or lower for each space-time strip.

   (3) Linear and nonlinear responses differ significantly. Tension increases the effective stiffness value as compression reduces it.

   (4) Peak positive displacement for linear and nonlinear cases for TVE and TVEM shown in figure 3.37 show the differences in linear and nonlinear responses quite clearly.

Thus this work demonstrates the significance of using thermodynamic pressure $p(\rho)$ by including the actual equation of state of the material to account for equilibrium stress that is responsible for the change in volume of the material. The studies presented also illustrate the significance of

nonlinearity due to Green's strain and the need for incorporating it in wave propagation studies involving finite deformation. These studies presented here can not be performed in a time accurate manner without using the mathematical models presented here and without using the space-time variationally consistent space-time finite element formulations, [22]- [31], based on space-time residual functional as used here.

Bibliography

[1] Surana, K. , Knight, J. and Reddy, J. (2015) Nonlinear Waves in Solid Continua with Finite Deformation. American Journal of Computational Mathematics, 5, 345-386. doi: 10.4236/ajcm.2015.53032

[2] Surana, Karan S. (2014) Advanced Mechanics of Continua. CRC Press, Boca Raton, FL.

[3] Engelbrecht, J. (1983) Nonlinear Wave Processes of Deformation in Solids. Pitman Publishing, London.

[4] Graham, R.A. (1993) Solids Under High-Pressure Shock Compression. Springer-Verlag, New York.

[5] Zarembo, L.K. and Krasil'nikov, V.A. (1970) Nonlinear Phenomena in the Propagation of Elastic Waves in Solids. *Soviet Physics Uspekhi*, 13(6), 778-797.

[6] Fosdick, R., Ketema, Y. and Yu, J.H. (1997) A Non-linear Oscillator with History Dependent Force. *Int. J. Non-Linear Mechanics*, 33(3), 447-459.

[7] Lima, W.J.N. de and Hamilton, M.F. (2003) Finite-Amplitude Waves in Isotropic Elastic Plates. *J. of Sound and Vibration*, 265, 819-839.

[8] Gei, M., Bigoni, D. and Franceschini, G. (2004) Thermoelastic Small-Amplitude Wave Propagation in Nonlinear Elastic Multilayers. *Mathematics and Mechanics of Solids*, 9, 555-568.

[9] Lima, W.J.N. de and Hamilton, M.F. (2005) Finite Amplitude Waves in Isotropic Elastic Waveguides with Arbitrary Constant Cross-Sectional Area. *Wave Motion*, 41, 1-11.

[10] Renton, J.D. (1987) Applied Elasticity: Matrix and Tensor Analysis of Elastic Continua. Ellis Horwood, Chichester.

[11] Landau, L.D. and Lifshitz, E.M. (1986) Theory of Elasticity. Pergamon Press, New York.

[12] Engelbrecht, J., Berezovski, A. and Salupere, A. (2007) Nonlinear Deformation Waves in Solds and Dispersion. *Wave Motion*, 44, 493-500.

[13] Shariyat, M., Lavasani, S.M.H. and Khaghani, M. (2010) Nonlinear Transient Thermal Stress and Elastic Wave Propagation Analyses of Thick Temperature-Dependent FGM Cylinders, using a Second-Order Point-Collocation Method. *Applied Mathematicl Modeling*, 34, 898-918.

[14] Yu, S.T.J., Yang, L., Lowe, R. and Bechtel, S.E. (2010) Numerical Simulation of Linear and Nonlinear Waves in Hypoelastic Solids by the CESE Method. *Wave Motion*, 47, 168-182.

[15] Berezovski, A., Berezovski, M. and Engelbrecht, J. (2006) Numerical Simulation of Nonlinear Elastic Wave Propagation in Piecewise Homogeneous Media. *Materials Science and Engineering A*, 418, 364-369.

[16] Shariyat, M., Khaghani, M. and Lavasani, S.M.H. (2010) Nonlinear Thermoelasticity, Vibration, and Stress Wave Propagation Analyses of Thick FGM Cylinders with Temperature-Dependent Material Properties. *European Journal of Mechanics A/Solids*, 29, 378-391.

[17] Li, Y., Vandewoestyne, B. and Abeele, K.V.D. (2012) A Nodal Discontinuous Galerkin Finite Element Method for Nonlinear Elastic Wave Propagation. *J. Acoust. Soc. Am.*, 131(5), 3650-3663.

[18] Shariyat, M. (2012) Nonlinear Transient Stress and Wave Propagation Analyses of the FGM Thick Cylinders, Employing a Unified Generalized Thermoelasticity Theory. *Internationl Journal of Mechanical Sciences*, 65, 24-37.

[19] Yu, Y.M. and Lim, C.W. (2013) Nonlinear Constitutive Model for Axisymetric Bending of Annular Graphene-Like Nanoplate with Gradient Elasticity Enhancement Effects. *J. of Engineering Mechanics*, 139(8), 1025-1035.

[20] Nucera, C. and di Scalea, F.L. (2014) Nonlinear Semianalytical Finite-Element Algorithm for the Analysis of Internal Resonance Conditions in Complex Waveguides. *J. of Engineering Mechanics*, 140(3), 502-522.

[21] Surana, K.S., Maduri, R. and Reddy, J.N. (2006) One Dimensional Elastic Wave Propagation in Periodically Laminated Composites Using h; p; k Framework and STLS Finite Element Processes. *Mechanics of Advanced Materials and Structures*, 13, 161-196.

[22] Surana, K.S. and Reddy, J.N. (2015) Mathematics of Computations and the Finite Element Method for Initial Value Problems.

[23] Surana, K.S., Ahmadi, A.R. and Reddy, J. (2002) The k-version of Finite Element Method for Self-Adjoint Operators in BVP. *International Journal of Computational Engineering Science*, 3(2), 155-218.

[24] Surana, K.S., Ahmadi, A.R. and Reddy, J. (2003) The k-version of Finite Element Method for Non-Self-Adjoint Operators in BVP. *International Journal of Computational Engineering Science*, 4(4), 737-812.

[25] Surana, K.S., Ahmadi, A.R. and Reddy J. (2004) The k-version of Finite Element Method for Nonlinear Operators in BVP. *International Journal of Computational Engineering Science*, 5(1), 133-207.

[26] Winterscheidt, D. and Surana, K.S. (1993) p-Version Least-Squares Finite Element Formulation for Convection-Diffusion Problems. *International Journal for Numerical Methods in Engineering*, 36(1), 111-133.

[27] Winterscheidt, D. and Surana, K.S. (1994) p-Version Least Squares Finite Element Formulation for Two-Dimensional, Incopressible Fluid Flow. *International Journal for Numerical Methods in Fluids*, 18(1), 43-69.

[28] Bell, B.C. and Surana, K.S. (1994) A Space-Time Coupled p-Version Least-Squares Finite Element Formulation for Unsteady Fluid Dynamics Problems. *International Journal for Numerical Methods in Engineering*, 37(20), 3545-3569.

[29] Bell, B.C. and Surana, K.S. (1996) A Space-Time Coupled p-Version Least Squares Finite Element Formulation for Unsteady Two-Dimensional Navier-Stokes Equations. *International Journal for Numerical Methods in Engineering*, 39(15), 2593-2618.

[30] Surana, K.S., Reddy, J.N. and Allu, S. (2007) The k-Version of Finite Element Method for Initial Value Problems: Mathematical and Computational Framework. *International Journal of Computational Methods in Engineering Science and Mechanics*, 8, 123-136.

[31] Surana, K.S., Allu, S., Reddy, J.N. and Tenpas, P.W. (2008) Least Squares Finite Element Processes in hpk Mathematical Framework for Non-Linear Conservation Law. *International Journal of Numerical Methods in Fluids*, 57(10), 1545-1568.

[32] Reddy, J.N. (2004) An Introduction to Nonlinear Finite Element Analysis. Oxford University Press, New York.

[33] Bathe, K.J. (1996) Finite Element Procedures. Prentice Hall, New Jersey.

[34] Riks, E. (1979) An incremental Approach to the Solution of Snapping and Buckling Problems. *International Journal of Solids and Structures*, 15, 529-551.

[35] Kumari, Mithlesh and Dass, Narsingh (1991) An equation of state applied to plastics, rubbers, glasses, and polymers. Journal of Applied Physics 1991 70:3, 1863-1865